

**SYNTHESIS AND CHARACTERIZATION OF LEAD SULPHIDE
NANOPARTICLES FROM LEAD ALKYL XANTHATE SINGLE SOURCE
PRECURSORS USING A SOLVENTLESS METHOD**



**BY
SELINA AMA SAAH
BSc. (Hons) Chemistry, KNUST**

**A Thesis submitted to the Department of Chemistry, College of Science,
Kwame Nkrumah University of Science and Technology in partial fulfilment of
the requirements for the degree of MPhil in Polymer Science and Technology**

June, 2013

ABSTRACT

Xanthates have been successfully investigated as single source precursors for producing metal sulphide nanoparticles. These offer advantages over other precursors because they have low decomposition pathways, they are cheap, they are clean and they have pre-formed M-S bond. Although ethyl xanthates have been investigated with much success, there are few or no reports on the syntheses of higher alkyl xanthates. In this work a series of lead alkyl xanthates have been synthesized with the alkyl groups being ethyl, n-butyl, 1-hexyl and 1-octyl. The purities of the precursors were confirmed by micro-elemental analyses. Infra-red, ^1H NMR, ^{13}C NMR, melting point, and mass spectroscopy were also used to characterize the precursors. The thermal behaviours of the precursors were determined by TGA and DSC. The crystal structure of lead hexyl xanthate was determined. The low melting points recorded for the precursors confirmed that the lead alkyl xanthates could be used as single source precursors in low thermal decomposition for the syntheses of lead sulphide nanoparticles. The PbS nanoparticles were then produced using the melt method which is a rapid, less toxic and cheap process. The as-prepared lead sulphide nanoparticles were characterized by XRD and TEM which confirmed a growth towards cubic PbS phases. The calculated particle sizes from the Debye Scherer equation were 26.45, 25.17, 24.79 and 23.32 nm for the PbS nanoparticles obtained from the decomposition of ethyl, butyl, hexyl and lead octyl xanthate respectively. SEM and EDX were also used to determine the morphology and purity of the as-prepared PbS nanoparticles respectively.

DEDICATION

This work is dedicated to Madam Grace Owusu-Antwi for her motherly love throughout my research.

KNUST



ACKNOWLEDGEMENT

First and foremost, I would like to thank the Almighty God for guiding me through my research period.

Secondly, I would like to thank the Leverhulme Trust - Royal Society Africa Awards Scheme for funding this work. I am very grateful to Prof. Paul O'Brien (POB) for allowing this research to be carried out in his laboratory at the School of Chemistry, University of Manchester.

I thank Prof Paul O'Brien of the School of Chemistry, University of Manchester and Dr. J. A. M. Awudza of Chemistry Department, KNUST for their advice and direction throughout my research and for being outstanding examples of successful research supervisors. I also thank Dr. M. A. Malik for guidance in carrying out the research.

I want to acknowledge the important contributions to this work made by Mr. Nathaniel Owusu Boadi and Dr. Godfred Darko, who collaborated closely with me on many aspects of this research, and Prof. Victor Nana Berko-Boateng who advised me throughout the period.

I am grateful to have been part of such a supportive, hardworking, and inspiring group of research associates, graduate students and post doctoral fellows in POB group at the University of Manchester. Over the course of my research I have been fortunate enough to work with a truly outstanding group.

I would like to thank Dr. Chris Wilkins for spending long hours assisting me with SEM and EDX analyses, and for his patience, encouragement and support.

Finally, I would like to thank my family and course mates in KNUST for their continuing love and support. I am eternally grateful to them.

TABLE OF CONTENTS

ABSTRACT	ii
DECLARATION	iii
DEDICATION	iv
ACKNOWLEDGEMENT	v
TABLE OF CONTENTS	vi
LIST OF FIGURES	x
LIST OF TABLES	xii
LIST OF FREQUENTLY USED ABBREVIATIONS	xiii
CHAPTER ONE.....	1
INTRODUCTION.....	1
1.1 Background to Single Source Precursors (SSP).....	1
1.2 Single Source Precursors for PbS Nanoparticles	1
1.2.1 Lead Dithioacarbamate Complexes	2
1.2.2 Lead Dialkyldithiophosphinato Complexes.....	2
1.2.3 Lead Dithioimidodiphosphinato Complexes	3
1.2.4 Lead Dithiocarbonato Complexes (Xanthates).....	4
1.3 Nanoparticles.....	4
1.3.1 Quantum Dots	6
1.3.2 Lead Sulphide (PbS) Quantum Dots.....	7
1.3.3 Properties of Lead Sulphide (PbS) Quantum Dots	7
1.3.4 Applications of PbS Quantum Dots.....	9
1.4 Synthetic Routes to PbS Nanoparticles	9
1.5 Aims and Objectives of the Project.....	11
1.5.1 Main Aim	11
1.5.2 Specific Objectives	12
1.6 Justification of Objectives	12
CHAPTER TWO.....	13
LITERATURE REVIEW.....	13
2.1 Single Source Precursors (SSP)	13
2.2 Lead Xanthate as a Single Source Precursor for PbS Nanoparticles	14

2.2.1 Background to Xanthates	14
2.2.2 Chemical Properties of Xanthates.....	15
2.2.3 Uses of Xanthates	18
2.3 Other Metal Sulphides from Metal Xanthate Single Source Precursors	20
2.4. Other Uses of Xanthate Ligand	23
2.5 Other Single Source Precursors for the Syntheses of PbS Nanoparticles	24
2.5.1 Lead Dithioacarbamate Complexes	24
2.5.2 Lead Dialkyldithiophosphinato Complexes.....	26
2.5.3 Lead Dithioimidodiphosphinato Complexes	26
2.6 Routes from Single Source Precursors to Nanomaterials	27
2.6.1 Solution Phase Thermal Decomposition.....	27
2.6.2 Synthesis of Thin Films at the Water–Toluene Interface	27
2.6.3 Chemical Vapour Deposition (CVD)	29
2.6.3.1 Low-Pressure Metal–Organic Chemical Vapour Deposition (LP- MOCVD)	30
2.6.3.2 Metal–Organic Chemical Vapour Deposition (MOCVD)	30
2.6.3.3 Aerosol-Assisted Chemical Vapour Deposition (AACVD).....	31
2.6.4 Solventless Method	32
2.7 Application of Nanoparticles in Novel Solar Cells.....	36
2.7.1 Background to Solar Cells	36
2.7.2 Hybrid Solar Cells	37
2.7.3 The use of PbS in Hybrid Solar Cells.....	39
CHAPTER THREE	41
MATERIALS AND METHODS.....	41
3.1 Chemicals	41
3.2 Synthesis of Lead Alkyl Xanthate Precursors.....	41
3.2.1 Synthesis of Lead Ethyl Xanthates [Pb(S ₂ COEt) ₂].....	41
3.2.2 Synthesis of Lead Butyl Xanthates [Pb(S ₂ COBu) ₂].....	42
3.2.3 Synthesis of Lead Hexyl Xanthates [Pb(S ₂ COHex) ₂].....	42
3.2.4 Synthesis of lead octyl xanthates [Pb(S ₂ COOct) ₂].....	42
3.3 Characterization of Lead Xanthate Precursors	42
3.3.1 Nuclear Magnetic Resonance (NMR)	43
3.3.2 Melting Point.....	43

3.3.3 Infra-red Spectroscopy (IR)	43
3.3.4 Micro-elemental Analyses.....	43
3.3.5 Mass Spectroscopy (MS)	44
3.3.6 Thermogravimetry Analysis (TGA).....	44
3.3.7 Differential Scanning Calorimetry (DSC).....	44
3.3.8 X-ray Crystallography.....	44
3.4 Synthesis of PbS from Lead Xanthate Precursors.....	45
3.5 Characterization of PbS Nanoparticles	45
3.5.1 X-ray Diffraction (XRD).....	45
3.5.2 Scanning Electron Microscopy (SEM)	46
3.5.3 Energy Dispersive X-ray Spectroscopy (EDX)	46
3.5.4 Transmission Electron Microscopy (TEM).....	46
CHAPTER FOUR	47
RESULTS AND DISCUSSIONS	47
4.1 Physical Appearance of Lead Xanthate Precursors.....	47
4.2 NMR of Lead Xanthate Precursors	47
4.2.1 ¹ H NMR	48
4.2.2 ¹³ C NMR.....	51
4.3 Melting Points of Lead Xanthate Precursors.....	56
4.4 Infra-red (IR) of Lead Xanthate Precursors	56
4.5 Micro-elemental Analyses of Lead Xanthate Precursors.....	58
4.6 Mass Spectrometric (MS) Analyses of Lead Xanthate Precursors	60
4.7 Thermogravimetric Analyses (TGA) of Lead Xanthate Precursors.....	61
4.8 Differential Scanning Calorimetry (DSC) of Lead Xanthate Precursors.....	63
4.9 Crystal Structure of Lead Hexyl Xanthate ([Pb(S ₂ COHex) ₂].....	67
4.9.1 Crystal Structure Data for [Pb(S ₂ COHex) ₂]	67
4.10 X-ray Diffraction (XRD) of the as-prepared PbS Nanoparticles	69
4.10.1 Effect of Temperature on the as-prepared PbS Nanoparticles.....	69
4.10.2 Effect of Time on the as-prepared PbS Nanoparticles.....	74
4.11 Scanning Electron Microscopy (SEM) of the as-prepared PbS Nanoparticles.....	78
4.12 Energy Dispersive X-ray (EDX) of the as-prepared PbS Nanoparticles	81
4.13 Transmission Electron Microscopy (TEM) of the as-prepared PbS Nanoparticles	84

CHAPTER FIVE	86
CONCLUSIONS AND RECOMMENDATIONS	86
5.1 Conclusions	86
5.2 Recommendations	87
REFERENCES	88
APPENDICES	105

KNUST



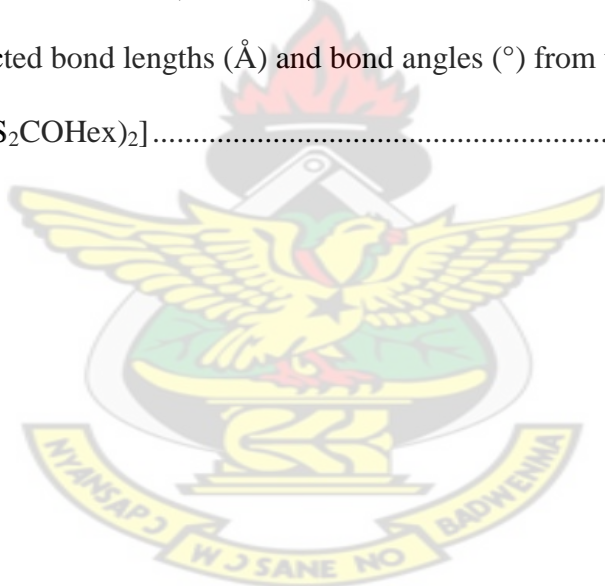
LIST OF FIGURES

Figure 1: Schematic representation of the energy diagram for the strong quantum-confined PbS colloids	9
Figure 2: Setup for Aerosol assisted chemical vapour deposition	31
Figure 4.1: ¹ H NMR for lead ethyl xanthate (normalized intensity against chemical shift)	48
Figure 4.2: ¹ H NMR for lead butyl xanthate (normalized intensity against chemical shift)	49
Figure 4.3: ¹ H NMR for lead hexyl xanthate (normalized intensity against chemical shift)	50
Figure 4.4: ¹ H NMR for lead octyl xanthate (normalized intensity against chemical shift)	51
Figure 4.5: ¹³ C NMR for lead ethyl xanthate (normalized intensity against chemical shift)	52
Figure 4.6: ¹³ C NMR for lead butyl xanthate (normalized intensity against chemical shift)	53
Figure 4.7: ¹³ C NMR for lead hexyl xanthate (normalized intensity against chemical shift)	54
Figure 4.8: ¹³ C NMR for lead octyl xanthate (normalized intensity against chemical shift)	55
Figure 4.9: IR spectra of the lead xanthate precursors	57
Figure 4.10: TGA graphs of lead xanthate precursors	61
Figure 4.11: DSC of lead ethyl xanthate	63
Figure 4.12: DSC of lead butyl xanthate	64
Figure 4.13: DSC of lead hexyl xanthate	65
Figure 4.14: DSC of lead octyl xanthate	66
Figure 4.15: Crystal structure of lead hexyl xanthate	68
Figure 4.16: XRD patterns of PbS nanoparticles obtained from the decomposition of lead ethyl xanthate at (a) 150, (b) 175 and (c) 200 °C.	70
Figure 4.17: XRD patterns of PbS nanoparticles obtained from the decomposition of lead butyl xanthate at (a) 150, (b) 175 and (c) 200 °C.	71
Figure 4.18: XRD patterns of PbS nanoparticles obtained from the decomposition of lead hexyl xanthate at (a) 150, (b) 175 and (c) 200 °C.	72

Figure 4.19: XRD patterns of PbS nanoparticles obtained from the decomposition of lead octyl xanthate at (a) 150, (b) 175 and (c) 200 °C.	73
Figure 4.20: XRD patterns of PbS nanoparticles obtained from the decomposition of lead ethyl xanthate at 175 °C at (a) 5, (b) 15, (c) 30 and (d) 60 minutes.	74
Figure 4.21: XRD patterns of PbS nanoparticles obtained from the decomposition of lead butyl xanthate at 175 °C at (a) 5, (b) 15, (c) 30 and (d) 60 minutes.	75
Figure 4.22: XRD patterns of PbS nanoparticles obtained from the decomposition of lead hexyl xanthate at 175 °C at (a) 5, (b) 15, (c) 30 and (d) 60 minutes.	76
Figure 4.23: XRD patterns of PbS nanoparticles obtained from the decomposition of lead octyl xanthate at 175 °C at (a) 5, (b) 15, (c) 30 and (d) 60 minutes.	77
Figure 4.24: SEM images of PbS obtained from lead ethyl xanthate at (a) 50,000 (b) 20,000 (c) 10,000 and (d) 1,000 X magnifications	78
Figure 4.25: SEM images of PbS obtained from lead butyl xanthate at (a) 50,000 (b) 20,000 (c) 10,000 and (d) 1,000 X magnifications	79
Figure 4.26: SEM images of PbS obtained from lead hexyl xanthate at (a) 50,000 (b) 20,000 (c) 10,000 and (d) 1,000 X magnifications	80
Figure 4.27: SEM images of PbS obtained from lead octyl xanthate at (a) 50,000 (b) 20,000 (c) 10,000 and (d) 1,000 X magnifications	81
Figure 4.28: EDX for PbS obtained from lead ethyl xanthate	82
Figure 4.29: EDX for PbS obtained from lead butyl xanthate	82
Figure 4.30: EDX for PbS obtained from lead hexyl xanthate	83
Figure 4.31: EDX for PbS obtained from lead octyl xanthate	83
Figure 4.32: TEM images of PbS obtained from (a) lead octyl xanthate (b) HR-TEM of (a), (c) lead hexyl xanthate and (d) HR-TEM of (c).....	84

LIST OF TABLES

Table 4.1: Physical appearance of the lead xanthate precursors	47
Table 4.2: Melting points of lead xanthate precursors (average).....	56
Table 4.3: Micro-elemental analyses for the lead ethyl xanthate.....	58
Table 4.4: Micro-elemental analyses for lead butyl xanthate	58
Table 4.5: Micro-elemental analyses for lead hexyl xanthate.....	59
Table 4.6: Micro-elemental analyses for lead octyl xanthate.....	59
Table 4.7: Mass spectra of lead xanthate precursors.....	60
Table 4.8: TGA data for lead xanthate precursors	62
Table 4.9: Crystal data for $[\text{Pb}(\text{S}_2\text{COHex})_2]$	67
Table 4.10: Selected bond lengths (\AA) and bond angles ($^\circ$) from the single crystal structure of $[\text{Pb}(\text{S}_2\text{COHex})_2]$	68



LIST OF FREQUENTLY USED ABBREVIATIONS

TGA	-	Thermogravimetric analysis
DSC	-	Differential scanning calorimetry
SEM	-	Scanning electron microscopy
TEM	-	Transmission electron microscopy
SSP	-	Single source precursor
PbS	-	Lead sulphide
CVD	-	Chemical vapour deposition
AACVD	-	Aerosol-assisted chemical vapour deposition
MOCVD	-	Metal-organic chemical vapour deposition
LP-MOCVD	-	Low-pressure metal-organic chemical vapour deposition
Pb(S ₂ COEt) ₂	-	Lead ethyl xanthate
Pb(S ₂ COBu) ₂	-	Lead butyl xanthate
Pb(S ₂ COHex) ₂	-	Lead hexyl xanthate
Pb(S ₂ COOct) ₂	-	Lead octyl xanthate
NMR	-	Nuclear magnetic resonance
IR	-	Infra-red spectroscopy
MS	-	Mass spectroscopy
XRD	-	X-ray diffraction
EDX	-	Energy dispersive X-ray spectroscopy
UV	-	Ultraviolet

CHAPTER ONE

INTRODUCTION

1.1 Background to Single Source Precursors (SSP)

The use of single source precursors for the syntheses of thin films and nanoparticles have been an area of interest to many researchers (Akhtar *et al.*, 2010; Fan *et al.*, 2007; Lazell and O'Brien, 1999; Malik *et al.*, 2010). Single source precursors are precursors containing two or more of the constituent elements in a single molecule (Malik *et al.*, 2010). Many researches on single source precursors have revealed them as efficient route to high quality, crystalline monodispersed nanoparticles of semiconducting materials (Akhtar *et al.*, 2010; Akhtar *et al.*, 2011). Single source precursors provide several key advantages over other routes (Fan *et al.*, 2007). These advantages include:

- (i) appreciable volatility and stability to moisture (Barreca *et al.*, 2005).
- (ii) existence of preformed bonds that can lead to the synthesis of a material with fewer defects and/or better stoichiometry (Ritch *et al.*, 2010).
- (iii) easy to handle and characterize (Akhtar *et al.*, 2010).
- (iv) potential to reduce the environmental impact of material processing (Fan *et al.*, 2007).
- (iv) easy purification as there is only one precursor involved.

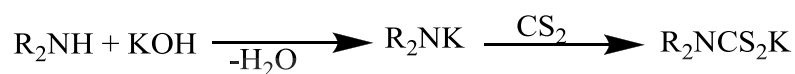
1.2 Single Source Precursors for PbS Nanoparticles

Although there are a number of single source precursors, only a few have been used to synthesize PbS nanoparticles. The unique characteristics about these precursors are the existence of S-donor atom and also the existence of a pre-formed M-S bond (Fan *et al.*, 2007; Jain, 2006). These single source precursors include, lead dithioacarbamate

complexes, lead dialkyldithiophosphinato complexes, lead dithioimidodiphosphinato complexes and lead dithiocarbonato complexes (Jain, 2006).

1.2.1 Lead Dithioacarbamato Complexes

Dithiocarbamates are the half-amides of dithiocarbonic acids. The synthesis of dithiocarbamates can be represented as follows:

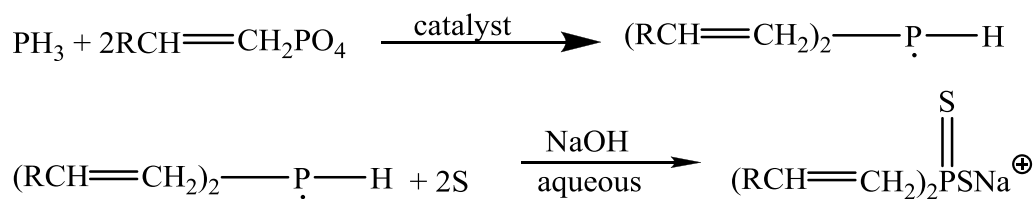
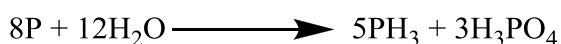


Scheme 1: Reaction for the synthesis of dithiocarbamates

The parent compound dithiocarbamic acid can be obtained as colourless needles from its sodium or ammonium salt by treating with cold water or strong mineral acid. The acids are quite unstable, decomposing to thiocyanic acid and hydrogen sulphide, but can be kept below 5°C for a short time. However, the stability of metal dithiocarbamate complexes is pH dependent (Sharma, 1986).

1.2.2 Lead Dialkyldithiophosphinato Complexes

Dithiophosphinates are produced by hydrolysis of elemental phosphorus to phosphine at high temperature. Phosphine is reacted with isobutylene to form a secondary phosphine intermediate. The product of this reaction is then reacted with sulphur in alkaline solution to give di-isobutyl dithiophosphinate (Nyamekye, 1991). The reaction processes are shown below:

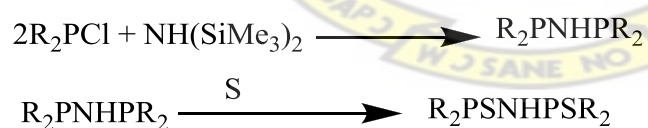


Scheme 2: Reaction for the synthesis of dithiophosphinates

The above approach offers a great deal of control of the size and the size distribution of the particles and facilitates their production at relatively low temperatures under ambient conditions, without glovebox practices (Güler, 2005; Maspero *et al.*, 2003).

1.2.3 Lead Dithioimidodiphosphinato Complexes

The synthetic process for imidodiphosphinic acid derivatives $\text{R}_2\text{P}(\text{S})\text{NH}(\text{S})\text{PR}_2'$ involves two steps: a simple condensation reaction of R_2PCl with $\text{NH}(\text{SiMe}_3)_2$ to give a phosphorus(III) compound, followed by oxidation with S to give the desired product. The equations are shown below:

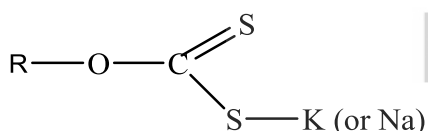


Scheme 3: Reaction for the synthesis of dithioimidodiphosphinate

The deprotonation of the amine (N-H) bond in $\text{R}_2\text{P}(\text{S})\text{NH}(\text{S})\text{PR}_2$ derivative leads to bidentate chelating ligand that can form neutral complexes of the type $\text{M}[(\text{N}(\text{R}_2\text{PS})_2)]_n$ with transition or main group metals (Boadi *et al.*, 2012).

1.2.4 Lead Dithiocarbonato Complexes (Xanthates)

The alkyl derivatives of dithiocarbonic acid are often referred to as xanthates (Garje and Jain, 2003). The name xanthate is derived from the Greek word “xanthos” meaning blond or yellow, because most xanthate complexes have a characteristic yellow colour (NICNAS, 2000). Xanthates are usually prepared by the reaction between potassium or sodium salt, alcohol and carbon disulfide. Their properties can be suitably modified by the appropriate choice of the O bound substituents (Singhal *et al.*, 2007). They have the general structure:



Scheme 4: Structure of xanthates

Although Pb(II)-xanthate complexes have significant importance in mining and reducing environmental pollution, they are also potential single source precursors for the syntheses of lead sulphide nanoparticles. Lead ethyl xanthates have been well investigated into, but little attention has been paid to longer alkyl chain lead xanthate complexes (Boadi *et al.*, 2012; Drake *et al.*, 1991; Fan *et al.*, 2007).

1.3 Nanoparticles

Nanoparticles are materials which have at least one of their dimensions ranging from 1 – 100 nm (Fan *et al.*, 2007; Soppimath *et al.*, 2001). Nanomaterials promise to unravel the secrets behind fundamental principles of chemistry and physics. Further, numerous applications have been investigated for nanomaterials in physical, chemical and biological sciences. This explains why nanoscience and nanotechnology have attracted practitioners from different disciplines (Fan *et al.*, 2007).

Synthetic methods for the production of nanoparticles are typically grouped into two categories namely, “top–down” and “bottom–up”. The “top–down” method involves division of a massive solid into smaller portions whereas the “bottom–up” method of nanoparticle fabrication involves the condensation of atoms and molecular entities in a gas phase or a solution. Also integration of nanoscale building blocks into functional assemblies and further into multifunctional devices can be achieved through the “bottom–up” method. This is by far a more popular route for the synthesis of nanoparticles as compared to the “top–down” method (Lee *et al.*, 2002; Sutherland, 2010). The successful applications of nanoparticles depend upon both the synthetic pathway and the surface modification of the particles. Surface modification can improve the inherent characteristics of the nanoparticles (Wang and Hong, 2010).

Nanoparticles of inorganic semiconductors which are referred to as quantum dots are well suited for the development of novel opto-electronic devices, due to their flexibility and simple processability combined with their excellent optical properties (Gunes *et al.*, 2007). Also the intrinsic electron mobility within nanoparticles is quite high (Zhou *et al.*, 2011). The novel applications of nanomaterials are also as a result of their magnetic, physical and mechanical properties which differ from the bulk materials (Abe *et al.*, 1998). These unique properties are sizes and shapes dependant (Chen *et al.*, 2009). As a result of the strong quantum confinement in nanoparticles, they exhibit photoluminescence with high quantum efficiencies and the emission peak as well as the absorption onset is strongly size-tunable (Guchhait *et al.*, 2010). Remarkably, these unique properties lead researchers to the possibility of being able to engineer band gaps and tailor material properties by simply increasing or decreasing the size of nanoparticles of a particular element or compound. Nanoparticles by virtue of their size

also possess a high fraction of surface atoms with the surface fraction falling gradually with increase in size (Fan *et al.*, 2007). Therefore, nanoparticles have been used to improve the performance of plastic light-emitting diodes to obtain single-photon sources operating at room temperature, and the development of optically pumped laser device (Gunes *et al.*, 2007; Niv *et al.*, 2012). In addition to applications as light emitters, semiconductor nanoparticles have also been used to improve polymer photovoltaic solar cells, based on the bulk or bilayer heterojunction concepts (Ong and Levitsky, 2010). Semiconductor nanocrystals are regarded as useful materials for building hybrid solar cells.

KNUST

1.3.1 Quantum Dots

Semiconducting nanomaterials with all three dimensions in the nanometer ranges are referred to as quantum dots (QDs) (Neeleshwar *et al.*, 2005). The unique properties of particles in this size ranges are due to their large surface-to-volume ratio and their reduced dimensions in relation to the excitonic radius of the bulk material. As the particle size is reduced, the ratio of the surface atoms in relation to those in the crystal lattice increases, thereby increasing the significance of the surface in determining the properties of the material (Ip *et al.*, 2012). The increase in the band gap of the nanocrystalline material with corresponding reduction of particle size is explained by the phenomenon described as the quantum size effect. This effect is a consequence of the confinement of the charge carriers within the dimensions of the quantum dots which results in them being treated quantum mechanically as particles in a box (O'Brien *et al.*, 2005). In this novel state of matter the valence band and conduction band split, giving rise to discrete energy levels rather than a continuous band as observed in the bulk material. The close proximity of the electron-and-hole pair in nanosized

semiconductors makes it impossible to ignore the coulombic interaction between the electron and hole and they consequently assume a higher state of kinetic energy than the bulk material. Experimentally, this increase in energy is observed in the optical spectra, where there is blue shift in the band gap as the particle size decreases (Lewis, 2010).

1.3.2 Lead Sulphide (PbS) Quantum Dots

Among the quantum dots, lead sulphide (PbS) and lead selenide (PbSe) quantum dots possess excellent photosensitivity in the near-infrared spectrum (Zhao *et al.*, 2010). This has enhanced their applications in photonic materials, selective sensors and optoelectric devices, solar absorbers (Boadi *et al.*, 2012; Boxberg and Tulkki, 2008). However, it has long been found that the size and morphology of compound II–VI semiconductors affect strongly their properties and applications. Uniform-shaped PbS quantum dots with different sizes is potentially meaningful in expanding novel potential applications of such kinds of semiconductors (Duan *et al.*, 2007).

1.3.3 Properties of Lead Sulphide (PbS) Quantum Dots

PbS quantum dots are a class of unique materials that are extremely important for both basic scientific research and technological applications (Kang and Wise, 1997). PbS is unique for having the smallest band gap of 0.41 eV in the bulk form at 300K and a large exciton Bohr radius of 18 nm (Zhou *et al.*, 2002). Its high extinction coefficients and absorption onset can be tuned over a large wavelength range from that of bulk PbS (0.41 eV) all the way into the visible region of the electromagnetic spectrum (Leventis *et al.*, 2010). Also, PbS nanoparticles possess extraordinary third order nonlinear optical properties which makes it an advantageous candidate for applications in optical

devices (Akhtar *et al.*, 2010). Since the third-order nonlinear optical response of them is expected to be 30 times larger than that of gallium arsenide (GaAs) and 1000 times larger than that of cadmium selenide (CdSe) materials, the PbS nanocrystals are highly desired for photonic and optical switching device applications (Duan *et al.*, 2007; Li *et al.*, 2007).

The unique properties of quantum dots are as a result of quantum confinement. This is the change in the electronic structure caused by the confinement of the electronic wavefunction to the dimensions of the particle, which is less than the mean free path of electrons. Quantum confinement, in the case of most semiconductor particles, increases the band gap (Malik *et al.*, 2010). The inherent dependence of the degree of quantum confinement on size implies that the electronic properties and thereby other material properties now become a function of the size of a nanoparticle (Fan *et al.*, 2007). Quantum confined materials also have an electron affinity and ionization potential shifted from that found in their bulk counterparts. This allows one to influence the type of heterojunction formed when nanocrystals are brought into contact with other semiconductors (Klem, 2008). PbS has been identified as a material that is both abundant and low in cost, making it suitable for large scale production of photovoltaics, assuming efficiency can be tailored using quantum confinement (Noone *et al.*, 2010). Remarkably, it leads to the possibility of being able to engineer band gaps and tailor material properties by simply increasing or decreasing the size of nanoparticles of a particular element or compound.

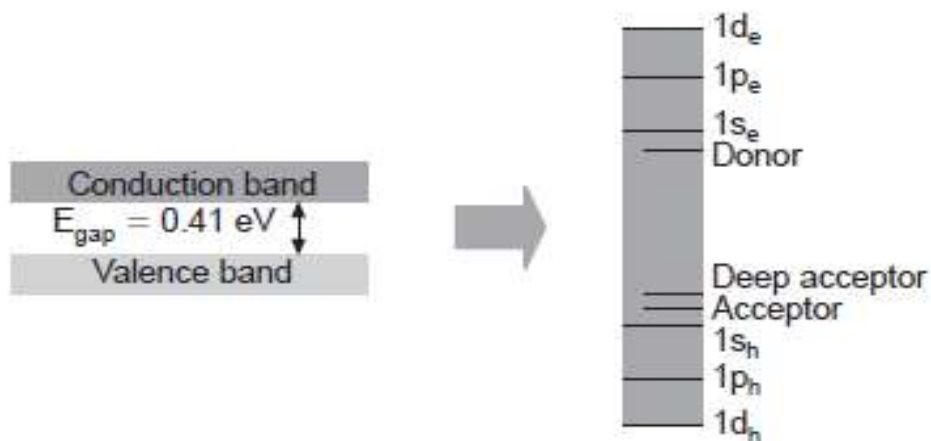


Figure 1: Schematic representation of the energy diagram for the strong quantum-confined PbS colloids

1.3.4 Applications of PbS Quantum Dots

From a technological perspective, PbS quantum dots are extremely promising materials for a large number of applications in the mid- and near-infrared emission and detection range (Bakueva *et al.*, 2004), opto-electronic devices (Schaller *et al.*, 2003), photography, sensors, multiple exciton generation (MEG), solar absorbers (Bisquert, 2010) and light emitting diodes (Akhtar *et al.*, 2010).

1.4 Synthetic Routes to PbS Nanoparticles

Conventionally, PbS was synthesized by the reaction of a dissoluble lead salt and H₂S gas in aqueous media (Lewis, 2010). Based on traditional precipitation techniques, a great deal of research effort has been devoted to developing methods for the synthesis of PbS particles with various sizes in a controllable manner. This led to several routes for the syntheses to PbS. These include solvothermal, gas-phase cation substitution reaction (Jang *et al.*, 2010), the use of strong matrix supports to stabilize the particles, including organic and inorganic polymers, zeolites like other refractories are ceramic materials, in which the particles are embedded in the supporting media forming

nanocomposite structures (Duan *et al.*, 2007). Gas phase synthesis of semiconductor nanoparticles involve atmospheric or low pressure evaporation of either powders of the preformed semiconductor, or the co-evaporation of the two elemental components, for example, from lead metal and sulphur. However, the use of these techniques usually resulted in deposits of particles with larger size distributions, in some cases ranging from 10–200 nm (O'Brien *et al.*, 2005). Also ultrasound and microwave irradiation have been used to synthesize nanocrystalline PbS with a narrow size distribution (Zhao *et al.*, 2004).

More recently, single source precursors approach has attracted much more attention since it is possible to adjust the shape and size distribution of the products by controlling the reaction conditions (Duan *et al.*, 2007). Different single source precursors have also been used as successful candidates for the syntheses of PbS. Among the precursors are dithiocarbamate, dialkyldithiophosphinato complexes and dithiocarbonato complexes (Zhao *et al.*, 2004).

However, lead dithiocarbamates and xanthate are the most commonly used single source precursors for PbS thin films and nanoparticles (Akhtar *et al.*, 2011). The use of the single source precursors result in nanoparticles with highly reactive surfaces. This causes fusion of the smaller particles into larger crystallites (Han *et al.*, 2008). This effect, known as, particle agglomeration is unwanted in the syntheses of nanoparticles. To prevent this agglomeration, protecting groups can be passivated or ‘capped’ to the surface atoms of the nanoparticles (Zhao *et al.*, 2004). Capping agents are compounds that can be covalently bound to surface metal atoms. Typically, a Lewis base or an organic group can be bound directly to the surface, another layer of a different material

cannot be grown onto the surface of the particle. Thus, the organic polymers form a shell around the particle. The capping agents form a ligand shell around a nanocrystal and play the key role of determining the “solubility” of a nanocrystal in a solvent (Fan *et al.*, 2007). Some capping agents that have been widely used are trioctylphosphine oxide (Patla *et al.*, 2007), hexadecylamine (Acharya *et al.*, 2006), oleylamine, trioctylamine (Pradhan *et al.*, 2003) and oleic acid (Chen and Liu, 2006).

Solventless decomposition of single source precursors have been found to be a useful synthetic route for the syntheses of metal nanoparticles, metal oxides, metal chalcogenides (Chen *et al.*, 2007). This solventless decomposition is usually referred to as the “melt method”. This is a quick, less toxic and less expensive method for the syntheses of nanoparticles and thin films because toxic and expensive solvents such as capping agents are not used in the syntheses. Also, simple instrumental setup is employed in this type of synthetic approach. The precursor serves as a source for the metal and chalcogen (Chen *et al.*, 2007).

1.5 Aims and Objectives of the Project

1.5.1 Main Aim

The main aim of this research is to synthesize and characterize PbS nanoparticles from a series of lead xanthate single source precursors using the “melt method”.

1.5.2 Specific Objectives

The specific objectives for this research are as follows:

- (i) to synthesize a series of lead xanthate complexes.
- (ii) to characterize these lead xanthate precursors using mass spectroscopy, infrared spectroscopy, nuclear magnetic resonance, thermogravimetric analysis and differential scanning calorimetry.
- (iii) to synthesize PbS nanoparticles from the lead xanthate single source precursors.
- (iv) to characterize the PbS nanoparticles using scanning electron microscopy, transmission electron microscopy, x-ray diffraction and energy dispersive X-ray spectroscopy.

1.6 Justification of Objectives

The use of single source precursors for the synthesis of metal sulphide nanoparticles have been of interest to many researchers in the past few decades. Lead xanthate single source precursors have been used to produce PbS nanoparticles using different methods. The solventless method provides a low cost, simple and clean PbS nanoparticles using lead xanthate precursors. The as-prepared PbS nanoparticles were characterized using SEM to determine their surface morphology. EDX was also used to determine the percentage elemental composition of the PbS nanoparticles. XRD was used to determine the diffraction pattern of the nanoparticles. PbS nanoparticles have potential application in opto-electronics at relatively low price. For example, PbS nanoparticles can be used as acceptors in hybrid solar cells. These solar cells can solve the major energy problem in Ghana and Africa as a whole. This is possible because of the sufficient sunlight in this part of the world.

CHAPTER TWO

LITERATURE REVIEW

2.1 Single Source Precursors (SSP)

Single source precursors are precursors containing two or more of the constituent elements in a single molecule (Malik *et al.*, 2010). The precursors are of technological importance and also designed to contain the required elements in their correct ratios. Under favourable conditions, the use of a molecular precursor also allows nanocrystal growth under mild conditions with greater synthetic control over dispersity and crystallinity (Davidovich *et al.*, 2010). The use of single source precursors for the syntheses of thin films and nanocrystals has been an area of interest to many researchers (Akhtar *et al.*, 2010; Fan *et al.*, 2007; Lazell and O'Brien, 1999; Malik *et al.*, 2010). Many researches on single source precursors have revealed them as efficient route to high quality, crystalline monodispersed nanoparticles of semiconducting materials (Akhtar *et al.*, 2010; Akhtar *et al.*, 2011). A major role in tailoring material properties reside in a proper choice of the molecular precursors, whose nature strongly affects the composition, the microstructure and the morphology of the final product. In particular, single source precursors containing all the elements to be deposited in a unique molecule can be used conveniently as building blocks for the single-step transformation of molecules into nanomaterials (Barreca *et al.*, 2005).

Single source precursors provide several key advantages over other routes (Fan *et al.*, 2007). These advantages include their appreciable volatility and stability to moisture (Barreca *et al.*, 2005). The existence of preformed bonds can lead to a material with fewer defects and/or better stoichiometry (Ritch *et al.*, 2010). The existence of

performed M-S bonds and the absence of M–C bonds in these precursors lead to the formation of metal (II) sulphide in an inert atmosphere (Barreca *et al.*, 2005; Fan *et al.*, 2007). Several of the single source precursors are also air-stable and are therefore easier to handle and characterize (Akhtar *et al.*, 2010). The use of single source precursors is also motivated by their potential to reduce the environmental impact of material processing. This is as a result of the use of limited solvent in the process (Fan *et al.*, 2007). Thermal decomposition of these precursors result in nanoparticles with high yields (Duan *et al.*, 2007). Furthermore, purification is easier as there is only one precursor involved. The major advantages of the single source approach over conventional metal-organic chemical vapour deposition (MOCVD) using dual sources include limited pre-reactions and good quality films (Davidovich *et al.*, 2010). These single source precursors contain, within a single molecule; the reactants and where possible, the capping agent, reducing the number of materials needed for nanoparticles synthesis and nanoparticles can be produced in ‘one-pot’ syntheses (Singhal *et al.*, 2007).

2.2 Lead Xanthate as a Single Source Precursor for PbS Nanoparticles

The past decade has witnessed the used of lead xanthate as a single source precursor for the synthesis of PbS nanoparticles by many researchers.

2.2.1 Background to Xanthates

There exists quite a considerable range of names used for the class of compounds that are most commonly known as xanthates. These names include O-alkyl dithiocarbonate, carbonic acid dithio, O-alkyl ester salt, carbonodithioic acid, metal alkyl xanthogenate and metal- O-alkyl carbonodithioate. For example, potassium ethyl

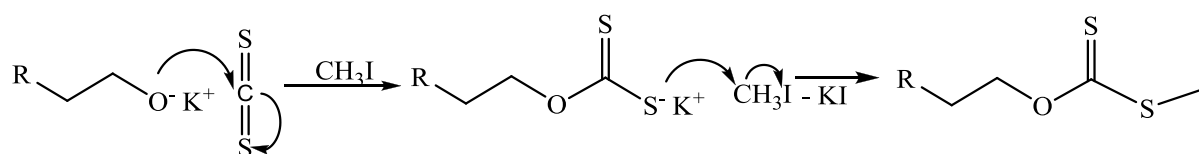
xanthate may be referred to as carbonodithioic acid, O-ethyl ester potassium salt. Of these alternative names, ethyl dithiocarbonate is the name most frequently employed (Sydney, 2005).

Special mention must be made of intermolecular addition of 2-oxoalkyl radicals to olefins that produce xanthate adducts in generally good yields and tolerate many functional groups (Boivin *et al.*, 2003). Xanthate ligands are known to coordinate metal centres in a variety of coordination modes, e.g. monodentate, bidentate, bridging, etc., giving rise to a rich diversity in their structural motifs (Koh *et al.*, 2003). In the last decade, xanthates have been reported as self-capped single source precursors (Sawant *et al.*, 2001). However, xanthates are more prone to form polymeric complexes. This is usually the result of bridging through the bidentate xanthate moiety (M-S-C-S-M bridge) (Matthew, 1990).

2.2.2 Chemical Properties of Xanthates

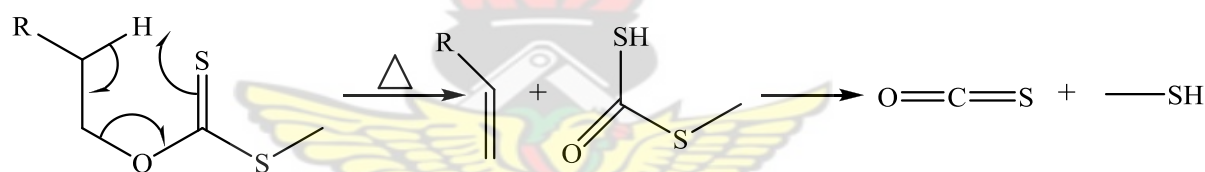
Xanthates ($-S_2COR$) are a class of inorganic compounds which have been successfully used for the syntheses of metal sulphides with deposition temperatures for thin films as low as 250 °C (Alam *et al.*, 2008). Their decomposition pathway is similar to the Chugaev mechanism. The pathway is cleaner than those of other precursors and can occur at considerably lower temperatures than the analogous dithiocarbamates (Clark *et al.*, 2011). In the Chugaev mechanism, an alkene (R-H), OCS and MSH fragments are formed.

In the first step of the mechanism, a potassium xanthate is produced when the alkoxide reacts with carbon disulphide in the presence of methyl iodide.



Scheme 5: Reaction mechanism for the preparation of O-alkylxanthato complexes

The Chugaev elimination typically can occur at 200 °C, an alkene is formed by a syn-elimination, *via* a 6-membered cyclic transition state, the hydrogen atom is moved from the β -C-atom to the sulphur. The side product decomposes to carbonyl sulphide (OCS) and methanethiol.



Scheme 6: Chugaev elimination reaction

This clean elimination which also happens in metal xanthate complexes may be important in chemical vapour deposition (CVD) and other materials processing environments leading to low temperature decomposition (Boadi *et al.*, 2012). The successful growth of PbS thin films on polyimide substrates from $[\text{Pb}(\text{S}_2\text{COBu})_2]$ by aerosol-assisted chemical vapour deposition (AACVD) at temperatures as low as 150 °C has been reported (Akhtar *et al.*, 2011). The crystals structure of lead ethyl xanthate has been reported since 1966 as being monoclinic with $a = 13.267 \pm 0.016$, $b = 4.301 \pm 0.015$, $c = 22.722 \pm 0.016$ Å; $\beta = 109^\circ 16' \pm 5'$ (Hagihara and Yamashita, 1966). The spacing group was $\text{P}2_1/c$ and $Z = 4$. The dithiocarbonic ends of the two xanthate groups

are bonded to the lead atom, at a bond angle of $98.2^\circ \pm 0.9^\circ$. The molecule is not planar, although each xanthate group, ignoring the hydrogen atoms, is almost planar. A geometrical interpretation is given of the asymmetrical molecular structure in terms of the rotations of the molecular segments around Pb-S, C-S and O-S single bonds in the crystalline state. The molecules are bound together through van der Waals forces between double-bonded sulphur atoms and between methyl ends of the alkyl groups. Diffuse reflectance Fourier transform infrared spectroscopy, Hallimond tube flotation cell and microelectrophoresis have been utilized to investigate the reactions involved in the adsorption- abstraction of K-amyloxanthate on finely ground galena (Cases *et al.*, 1990). The method reveals the presence of amyldixanthogen and 1:1 coordinated lead xanthate at submonolayer coverage. For higher surface coverages amyldixanthogen, non-stoichiometric lead xanthate and amylocarbonate disulphide were observed. When the grinding pH is equal to 11.0, a two-stage adsorption process is revealed. During the second stage (for total statistical surface coverage higher than 5.4) mainly amyldixanthogen is formed. Several researchers have investigated into the use of lead dithiocarbonate complexes as single source precursors for the synthesis of PbS nanoparticles. Among these investigations is the use of trioctylamine (TOA), as a liganding solvent in a single step, benchtop low- temperature decomposition (90°C) of lead hexadecylxanthate, producing PbS nanowires. The reaction conditions resulted in crystalline, rocksalt PbS, and the liganding solvent enabled a 1-dimensional growth. The nanowires exhibit a nearly perfect crystal lattice, high width uniformity, and tight side-by-side registry (Patla *et al.*, 2007). An investigation on the synthesis of PbS nanocubes from xanthate precursors in ethylene diamine solution at room temperature has also been reported (Sun *et al.*, 2011). Clark *et al.*, (2011), have synthesized a series of lead xanthate *N*- donor ligands. Their preparation was carried out by adding the

donor ligand to the xanthate in acetone. PbS nanoparticles were produced via AACVD at temperatures up to 200 °C of the xanthate adducts and via thermal decomposition of the xanthate without any ligand at temperatures of up to 350 °C. AACVD produced granular PbS films on a range of surfaces while thermal decomposition produce PbS nanotubes with uniform morphology. The growth of PbS thin films on polyimide (Kapton) substrates by AACVD from $[\text{Pb}(\text{S}_2\text{COBu})_2]$ at temperatures as low as 150 °C has been reported (Akhtar *et al.*, 2011). Pradhan *et al.*, (2003) have synthesized highly crystalline octagonal shaped PbS nanoparticles from hexadecyl lead xanthate at room temperature in air. The structures of the isomers of $[\text{Pb}(\text{S}_2\text{COR})_2]$ (R = methyl, ethyl, phenyl) in gas phase and water have been studied theoretically using density functional B3LYP and PBE functional for heavy atom lead. The theoretical results show that Pb-S bond separation do not change much with changes in R (methyl, ethyl or phenyl) but experimentally, Pb-S bond separation depends on R. The structures of all the complexes were hemidirected. It was observed in the study of the complexes that, the bidentate (ROCS₂) ligand uses either S,O or S,S coordination pattern. The formation energy and relative energy values indicated that S,S coordination shows greater stability over S,O coordination (Fredriksson and Holmgren, 2008).

2.2.3 Uses of Xanthates

Xanthates (usually, the sodium or potassium salts) are predominantly used in the mining industry as ‘flotation’ agents in the collection (recovery) of sulphide minerals, metallic elements (e.g., copper, nickel, silver, gold) and some oxidised minerals of lead and copper, from ore slurries (Marabini *et al.*, 2007). They also play an important role in the removal of heavy metals in aqueous waste streams of many industries, such as metal plating, mining, and tanneries (Buckley *et al.*, 2003). Collectors generally

employed in flotation are surfactants that link to the surface of useful minerals by van der Waals or electrostatic bonds and are active towards whole classes of minerals (for example sulphide minerals) rather than towards an individual mineral (Marabini *et al.*, 2007). Alkali metal xanthates appear to be typical anionic surfactants, with a highly polar end group bonded to a hydrophobic alkyl chain (Hamilton and Melbourne, 1986). The flotation process involves crushing and wet grinding an ore to liberate separate grains of the various valuable minerals and gangue components, pulping the ore particles with additional water, and then selectively rendering hydrophobic the surface of the mineral of interest by interaction with an organic collector species. A stream of air bubbles is passed through the pulp; the bubbles attach to, and levitate, the hydrophobic particles and collect them in a froth layer that flows over the weir of the flotation cell. The chemical composition of the remaining pulp can then be altered to render, in turn, further valuable minerals hydrophobic, and hence floatable (Buckley *et al.*, 2003). Examples of commercially available xanthates are sodium and potassium ethyl xanthate, potassium amyl xanthate and sodium isopropyl and isobutyl xanthate (NICNAS, 2000). Sodium ethyl xanthate is the shortest carbon chain xanthate and the most selective flotation agent. It is used mainly for the separation of copper, lead, gold, nickel and zinc ores. The amount of sodium ethyl xanthate used in this process is very small relative to the quantity of treated ore, being approximately 250 to 350 g (solid) per tonne of ore. Sodium ethyl xanthate has also been used as a defoliant, herbicide and as an additive in the curing and vulcanization of rubber and in high pressure lubricants (NICNAS, 2000). While they provide a means for beneficiation of desired sulphide mineral powders, and play an important role also in the viscose process for artificial silk production, at the same time they are unavoidably major pollutants in wastewaters of these industries (Ayranci and Conway, 2001). Recently dithiocarbonates used in

polymer synthesis have largely gained attraction as these have superior optical and thermal properties and may be useful for optical lenses and fiber (Chauhan *et al.*, 2011). Also, xanthates are among the important solvents used for rechargeable lithium ion batteries. Xanthates have been used in analytical chemistry for the trace analysis of metal ions and analysis of alcohols by high performance liquid chromatography (Sydney, 2005).

In particular, xanthates have been found to be not only convenient precursors for transforming an alcohol into the corresponding alkane but also extremely efficient and versatile sources of radicals (Boivin *et al.*, 2003).

2.3 Other Metal Sulphides from Metal Xanthate Single Source Precursors

Xanthates have been used as a precursor for many metal (II) sulphide nanoparticles.

Cadmium bis (O-alkylxanthates) are potential single-source molecular precursors for the chemical vapour deposition (CVD) of cadmium (II) sulphide (CdS) thin films (Barreca *et al.*, 2005). CdS nanowires have been synthesized in a low temperature, one-step, benchtop decomposition of cadmium hexadecylxanthate using hexadecylamine (HDA), as a liganding solvent (Acharya *et al.*, 2006). CdS nanoparticles capped with tri-n-octylphosphine oxide (TOPO) have been synthesised by a single source route using cadmium ethylxanthate as a precursor. The nanoparticles obtained show quantum size effects in the optical absorption spectra and the photoluminescence shows an emission maximum that is characteristically red shifted in relation to the band edge (Nair *et al.*, 2002). Size tuneable cadmium sulphide nanoparticles have been prepared by thermolysis of a single source precursor of cadmium xanthates with variable carbon chain length $[\text{Cd}(\text{S}_2\text{COR})_2]$, (R = ethyl, buthyl, octyl, dodecyl) in an ammonia solution. The ammonia solution was used to promote the formation of CdS and the degradation

of cadmium alkyl xanthate by providing electrons to excite the disproportionation reaction of the carbon disulfide group. The particle size 'D' calculated from the Scherrer equation for cadmium sulphide from ethyl, butyl, octyl, and dodecyl xanthate were 8.82, 8.73, 8.31, 7.25 nm, respectively. This shows that the size of the synthesized CdS nanoparticles decrease progressively with the increasing length of carbon chain of the precursor (Zhang *et al.*, 2011). However, the researchers gave no reason for the decrease in size with increasing length of the carbon chain of the alkyl group.

Nickel O-n-butylxanthate bis (pyridine) adducts have been used as clean precursors to crystalline NiS thin films under very mild AACVD conditions (Alam *et al.*, 2008).

The syntheses of bis (O-alkyldithiocarbonato) platinum (II) complexes with alkyl groups being methyl, ethyl, propyl, butyl, hexyl, octyl, and decyl have also been reported. These precursors were used in chemotherapy as antitumoral agents. The conclusion was that bis (O-alkyldithiocarbonato) platinum (II) complexes with short n-alkyl chains such as methyl, ethyl, propyl, and butyl were found to have greater antitumoral effect as compared to compounds with long alkyl chains such as hexyl, octyl, and decyl (Friebolin *et al.*, 2004). The researchers attributed the greater antitumoral effect to increasing activity with decreasing length of alkyl chain. The activity apparently correlates with the positive inductive effect (+I effect) of the alkyl group of the corresponding xanthate ligand. Orthorhombic Bi₂S₃ nanorods have been synthesized via hydrothermal treatment from a novel kind of single source precursors, the adducts of [Bi(S₂COR)₃] (R = sec-butyl) with neutral ligands (pyridine [C₅H₅N] or 1,10-phenanthroline [C₁₂H₈N₂]). The decomposition of the complex [Bi(S₂COC₄H₉)₃(C₅H₅N)₂] produced Bi₂S₃ nanorods with diameters in the range of 20-35 nm and lengths of hundreds of nanometers. However, no Bi₂S₃ crystals were

produced when the reaction temperature was lower than 130 °C. Between 150 and 180 °C, crystalline Bi₂S₃ products were obtained (Han *et al.*, 2007). Bismuth sulphide (Bi₂S₃) nanoribbons with uniform size have been prepared by the reaction of bismuth nitrate (Bi(NO₃)₃) and sodium O-isopropylthiocarbonate in N,N-dimethylformamide (DMF) at 80 °C for 24 hours (Sun *et al.*, 2008).

Starting from the molecular precursors, antimony O-ethylthiocarbonate, ultralong Sb₂S₃ nanowires with a diameter in the range of 5–10 nm were easily synthesized at room temperature by employing ethylenediamine both as solvent and a bidentate ligand (Han *et al.*, 2011). An investigation of tungsten(v) dimeric complexes with ethyl xanthate have also been reported (Lozano *et al.*, 1991). Synthesis and characterization of two dinuclear gold(I) xanthate complexes, [Au(μ-S₂COR)₂] (R = ethyl, butyl) have also been reported (Mohamed *et al.*, 2004).

Tzhayik *et al.*, (2002) have studied xanthates of C₈ and C₁₈ and found the xanthates to be very efficient in producing and stabilizing copper colloids even in aqueous solutions. The researchers did not give any reason for the choice of the alkyl chains. Styrene oxide can be polymerized to partially isotactic crystalline polymers by using bis (ethylxanthato)nickel(II) as an initiator in air (Kayatürk *et al.*, 2007). Colin and Allan (1978) have reported on the synthesis of tetraethylammonium (dithiocarbonato-S,S¹)-bis (ethylxanthato) cobaltate (III). Palladium (II) alkylxanthates, [Pd(S₂COR)₂], (R = methyl, ethyl, propyl, iso-propyl, butyl, iso-butyl, tert-butyl, amyl, iso-amyl, hexyl and cyclohexyl), have been prepared and reported (Sceney *et al.*, 1973). They concluded that as the chain length increases, the decomposition rate decreases, however as branching increases the rate of decomposition also increases.

Investigations into the spectrochemical properties of xanthates using voltammetry have been conducted and concluded that xanthates are chemisorbed onto the surfaces of metal electrodes (Buckley *et al.*, 1997; Gardner and Woods, 1977; Hope *et al.*, 2001; Siui *et al.*, 1997; Woods *et al.*, 1994a; Woods *et al.*, 1994b).

2.4. Other Uses of Xanthate Ligand

Work on the adsorption and electro-sorption of potassium ethyl xanthate and sodium thiocyanate on high surface area C-cloth electrodes for the purpose of development of procedures for wastewater purification have also been reported (Ayranci and Conway, 2001). The work of these investigators demonstrated how the UV/visible spectrophotometric method, coupled with kinetics and scanning kinetics techniques, can be effectively used to follow the adsorption behaviour of ions absorbing in the UV region on high-area C-cloth.

An insoluble cellulose xanthate has also been used for the removal of heavy metals from wastewater. The heavy metal binding capacities of the insoluble cellulose xanthate was in the order of $\text{Cd}^{2+} > \text{Pb}^{2+} > \text{Ni}^{2+}$. The reason assigned to the difference in binding capacities of the three heavy metals was that each heavy metal used in this study could undergo both ion exchange and complex formation with the insoluble cellulose xanthate. However, the selectivities for heavy metals were in the order of $\text{Pb}^{2+} > \text{Cd}^{2+} > \text{Ni}^{2+}$. The order for the selectivities was as a result of the slight alkalinity of the insoluble cellulose xanthate before the hydroxyl precipitation started (Kim and Lee, 1999). Introduction of xanthate group onto sugarcane (*Saccharum officinarum*) bagasse has been investigated for the removal of cadmium, lead, nickel, zinc, and copper from their aqueous media. The selectivity order in the removal of heavy metals at pH around

4 follows the order $Pb^{2+} > Cu^{2+} > Ni^{2+} > Cd^{2+} > Zn^{2+}$. Furthermore, the affinity of charred xanthated sugarcane bagasse (CXSB) by the metals followed the order: $Pb^{2+} > Cd^{2+} > Cu^{2+} > Zn^{2+} > Ni^{2+}$. The order for the affinity was as a result of the increase in electronegativity that corresponds to easy adsorption by the bioadsorbent (Homagai *et al.*, 2010). Saboury *et al.*, (2007) have reported the use of alkyl (ethyl, propyl, butyl and hexyl) xanthates for the inhibition of both cresolase and catecholase activities of mushroom tyrosinase and concluded that lower alkyl chain xanthate (ethyl) has greater catecholase inhibition. Potassium ethyl xanthate as corrosion inhibitor for copper in acidic chloride solutions has been ascertained during the gravimetric dissolution of copper (Scendo, 2005). Potassium-n-butyl xanthate has been synthesized and its role as an efficient antioxidant and accelerator in stabilizing rubber has been reported (Rajalingam and Radhakrishnan, 1991).

2.5 Other Single Source Precursors for the Syntheses of PbS Nanoparticles

Several single source precursors have been investigated into for the syntheses of PbS nanoparticles. These include:

- (i) lead dithiocarbamate complexes
- (ii) lead dialkyldithiophosphinato complexes
- (iii) lead dithioimidodiphosphinato complexes

The chemistry of the above single source precursors have been reviewed recently (Boadi *et al.*, 2012).

2.5.1 Lead Dithiocarbamate Complexes

Due to the strong metal binding properties of dithiocarbamates, much work has been carried out in the past few decades on metal-dithiocarbamate complexes (Malik *et al.*,

2010). Trindade and O'Brien, (1997) were the first to report on the use of lead (II) dithiocarbamate complexes $[\text{Pb}(\text{S}_2\text{CNRR}')_2]$ ($\text{R}, \text{R}' = \text{ethyl, butyl, } ^i\text{butyl}$) as single source precursors. They synthesized nanocrystalline PbS by thermolysis of the precursors using trioctylphosphine oxide as capping agents. The gray PbS films deposited in their work showed an even distribution of morphologically uniform crystallites. It was observed that the optical and morphological properties of the PbS nanocrystallites were strongly dependent on the temperature of synthesis and less so on the chemical nature of the precursor. For example, the PbS nanocrystallites synthesized at 100°C were spherical with average diameters of 6.3 nm whereas at 150°C , a mixture consisting of a large fraction of cubic crystallites with average size of about 60 nm and a small fraction of spherical nanoparticles were obtained. Zhang *et al.*, (2005) have reported on the syntheses of shape-controlled PbS nanocrystallites from lead diethyldithiocarbamate under mild conditions through two simple steps. In the first step, the lead diethyldithiocarbamate was prepared directly through the precipitation reaction of lead acetate and sodium diethyldithiocarbamate in distilled water at room temperature. In the second step, without the use of any extra capping agent, pure PbS microcrystallites with irregular polyhedral, cubic, and fish bone, star, and flower-like morphologies were obtained via solvothermal decomposition of the lead diethyldithiocarbamate in three different solvents (including ethanol, ethylene glycol and ethylenediamine) at $150\text{--}180^\circ\text{C}$ for 12 hours. The chemistry of lead dithiocarbamate complexes have been extensively reviewed recently (Boadi *et al.*, 2012).

Dithiocarbamates as single source precursors require higher temperatures for decomposition of the respective metal salt, even in an amine solvent. In addition, and

perhaps related to the necessary higher reaction temperatures, the quality of the particles is inferior to those formed from xanthates (Pradhan *et al.*, 2003).

2.5.2 Lead Dialkyldithiophosphinato Complexes

Dithiophosphinate complexes are known to possess biologically important properties and may also inhibit hydrocarbon oxidation. O-benzyl and O-allyl dithiophosphinates have been used as insecticides and nematocides. Salts of dithiophosphonates are useful as antioxidants in lubricants and plastics (Maspero *et al.*, 2003).

Little has been reported on the use of lead dithiophosphinato complexes as single source precursors for the synthesis of PbS nanoparticles. Duan *et al.*, (2007) have synthesized high quality cubic PbS nanocrystals by the solvothermal decomposition of $[\text{Pb}(\text{S}_2\text{POR})_2]$ (R = butyl, octyl, dodecyl) in oleylamine at 140–180 °C. The average size of PbS nanocrystals was 14.8, 58.5, and 74.5 nm, corresponding to dodecyl, octyl, and butyl respectively. It was clear that, the average size of PbS nanocrystals decreased largely with the increase of the substitute alkyl length of precursors. This may have resulted from the increased capping activity of the precursors with higher alkyl chains.

2.5.3 Lead Dithioimidodiphosphinato Complexes

Imidodiphosphinic acid derivatives $\text{R}_2\text{P}(\text{S})\text{NH}(\text{S})\text{PR}'_2$ (R, R' = CH_3 , C_6H_5); were first prepared by Schmidpeter as reported in a current review (Boadi *et al.*, 2012). The synthetic process has since been adapted and improved by others to make a wide range of derivatives. Although some adducts of lead dithioimidodiphosphinato complexes have been synthesized and characterized (Casas *et al.*, 1994; Rez, 1996), there are only a handful of reports on their use as single source precursors for PbS. Among these handful of reports are the use of $[\text{Pb}(\text{SO}(\text{PPh}_2)\text{N})_2]$ as single source

precursors for the synthesis of cubic PbS by aerosol-assisted and low-pressure chemical vapour deposition techniques (Zhang *et al.*, 2005).

2.6 Routes from Single Source Precursors to Nanomaterials

There are several conventional and non-conventional routes for the exploitation of inorganic complexes as single source precursors. The routes include solution phase thermal decomposition, chemical vapour deposition and deposition at the interface of water–toluene (Fan *et al.*, 2007).

2.6.1 Solution Phase Thermal Decomposition

Nanomaterials are obtained by carrying out the decomposition by injecting a solution of the single source precursors into a hot solvent (at temperatures over 200 °C), typically a mixture of tri-n-octylphosphineoxide (TOPO) and long chain alkylamine such as hexadecylamine (HDA), followed by refluxing for a specific period of time (Fan *et al.*, 2007). The particles are isolated by precipitating the mixture with ethanol or methanol. The diameters of the obtained nanoparticles are dependent on the reaction time, temperature, the ratio of the capping agent and the precursor employed (Fan *et al.*, 2007).

2.6.2 Synthesis of Thin Films at the Water–Toluene Interface

The interface between different phases of matter has been put to various uses in the past (Rao *et al.*, 2005). However, the Langmuir–Blodgett technique for deposition of thin films at an air–liquid interface is perhaps best known (Evyapan *et al.*, 2006). There have been several recent reports on the deposition of nanoparticles and thin films at the interface of two immiscible liquids (Stansfield *et al.*, 2010; Wu *et al.*, 2002). In this

method, a metal precursor dissolved in an organic solvent such as toluene is held in contact with an alkali aqueous layer containing, for example, a reducing agent, sulphiding agent or base at room temperature. The reaction (reduction, sulphidation or hydrolysis) proceeds via the ion transport mediated at the interface. The reduction thus initiated is allowed to proceed without disturbance for several hours (Rao *et al.*, 2005). The products of these reactions are deposited at the interface typically forming thin films or aggregates of nanoparticles. The macroscopic structure of the deposit at the interface is reflective of the structure of the interface. Nanoparticles are highly mobile at the interface and rapidly achieve an equilibrium assembly by reduction in interfacial energy. The three parameters that have been found to influence the energy of the assembly process at the liquid–liquid interface are:

- (i) the nature of the interface,
- (ii) surface modification of the nanoparticles at the interface, and
- (iii) the effective radius of the nanoparticles, smaller nanoparticles adsorbing more weakly to the interface than larger ones (Rao and Kalyanikutty, 2008).

The interface, thus, has a dual role of moderating charge/ion transport and directing the structure of the deposit. This method of interfacial deposition is simple, convenient and an inexpensive route to thin films. Films can be deposited at low temperatures and subsequently transferred to various substrates. The thickness of the deposited layers can be controlled by variation of the deposition parameters such as deposition time. The process is potentially easily adapted to large area processing with low fabrication cost (Fan *et al.*, 2007).

2.6.3 Chemical Vapour Deposition (CVD)

Chemical vapour deposition (CVD) has been used for large scale production of metastable materials. The CVD process involves the thermally induced reaction of the molecular precursors on a heated surface. The process can be divided into seven steps:

- (i) mass transport of reagents to the deposition zone
- (ii) gas phase reactions in the boundary layer to produce film precursors and by-products
- (iii) mass transport of film precursor to surface
- (iv) adsorption of film precursor on surface
- (v) surface diffusion of precursor to growth site
- (vi) surface chemical reactions lead to film deposition and by-product desorption
- (vii) mass transport of by-product out reaction zone (Akhtar *et al.*, 2010).

The two important barriers to the CVD method is finding suitable passivating groups that are used to also functionalise the particles and lack of appropriate equipment (Perex *et al.*, 2005).

Initiation of CVD reactions by different sources of energy rather than thermal energy has led to the development of diverse kinds of CVD methods such as low-pressure metal–organic chemical vapour deposition (LP-MOCVD), metal–organic chemical vapour deposition (MOCVD) and aerosol-assisted chemical vapour deposition (AACVD).

2.6.3.1 Low-Pressure Metal–Organic Chemical Vapour Deposition (LP-MOCVD)

This type of CVD uses metal-organic complexes as precursors rather than the inorganic precursors in the conventional CVD method (Akhtar *et al.*, 2010). The precursors used must be readily volatile at a temperature well below that of its decomposition. The precursor is also required to be stable and have a low degree of toxicity for easy use and storage (Malik *et al.*, 2010). The use of several lead dithiocarbamate $\text{Pb}(\text{S}_2\text{CNRR}')_2$ (R, R' = ethyl, butyl, iso-butyl) have been synthesized and tested by sublimation experiments to check their volatility and suitability for LP-MOCVD growth (Trindade and O'Brien, 1997). The work of the researchers revealed that $\text{Pb}(\text{S}_2\text{CN}^i\text{Bu}_2)_2$ was the most promising precursor for the deposition of PbS.

2.6.3.2 Metal–Organic Chemical Vapour Deposition (MOCVD)

MOCVD most often involves the deposition of films by decomposition of volatile metallo-organic or organometallic precursors in tri-n-octyl phosphine (TOP) at relatively high temperatures (>300 °C) (Akhtar *et al.*, 2011). This is followed by injection into hot tri-n-octyl phosphine oxide (TOPO). The formation of the nanoparticles is driven by the decomposition of the precursor. After the initial injection there is a rapid burst of nucleation, which is followed by Ostwald ripening.

The resultant nanoparticles are 'capped' by TOPO, which prevents agglomeration. The nanoparticles are separated by centrifugation and redispersed in toluene to give an optically clear solution of TOPO-capped nanoparticles (Gubin *et al.*, 2005; O'Brien *et al.*, 2005). Pure PbS microcrystallites with irregular polyhedral, cubic, and fish bone-, star-, and flower-like morphologies have been deposited from diethyldithiocarbamate using this method (Zhang *et al.*, 2005).

However, the difficulties with this method are:

- (i) difficulty to control stoichiometry
 - (ii) impurity incorporation
 - (iii) unwanted side reactions
 - (iv) high processing temperature which may cause inter-diffusion of layers
- (Akhtar *et al.*, 2010).

2.6.3.3 Aerosol-Assisted Chemical Vapour Deposition (AACVD)

In this process, a solution of precursor in high boiling organic solvent (or mixture of solvents) is transformed into finely divided sub-micrometer liquid droplets (aerosol). The droplets are generated using the ultrasonic aerosol generator, electrostatic aerosol generator or electro-spraying method (Akhtar *et al.*, 2010). A fine mist of the precursor solution is mixed with a carrier gas and pyrolyzed as in the traditional vapour deposition process to obtain nanoparticles and thin films (Malik *et al.*, 2010).

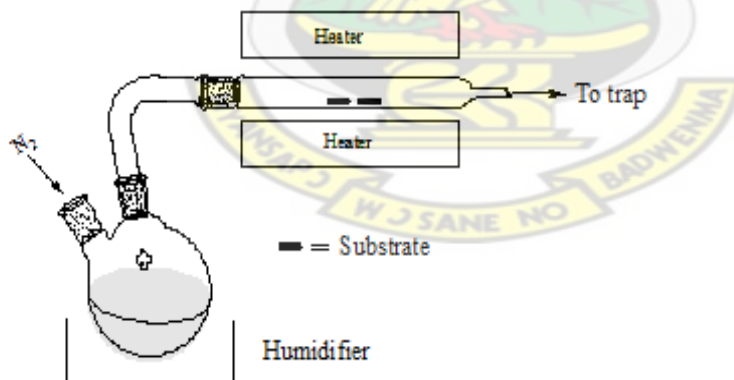


Figure 2: Setup for Aerosol assisted chemical vapour deposition

Due to variations in the precursor transportation modes, AACVD overcomes the limitations of MOCVD. However, this method is expensive due to the extra cost of solvents and instrumentation (Akhtar *et al.*, 2010).

Investigations on the successful growth of PbS thin films on polyimide (Kapton) substrates by AACVD from $[\text{Pb}(\text{S}_2\text{COBu})_2]$ at temperatures as low as 150 °C has been reported (Akhtar *et al.*, 2011). Clark *et al.*, (2011) have synthesized and characterized PbS from N donor - adducts of ethyl and lead butyl xanthate by AACVD at a temperature of 200 °C and an argon carrier gas over two hours.

2.6.4 Solventless Method

The solventless method of synthesis of nanoparticles using the bottom-up approach is also referred to as the melt method (Jung *et al.*, 2010). Solventless thermolysis of precursor metal complexes has been found to be a useful synthetic route for the syntheses of metal nanoparticles, metal oxides, metal chalcogenides (Chen *et al.*, 2007). The solventless method is an outstanding way to produce diverse semiconductors over a wide range of morphologies in that;

- (i) the undesired interparticle collisions/aggregation rarely occur, which leads to size- and shape-monodisperse products
- (ii) the solid-state precursor that separated from the solution can be analyzed by powerful methods, e.g., X-ray powder diffraction (XRD), IR spectra, NMR, which enables one to establish its compositions and crystal structures
- (iii) the nanomaterial is produced from such a well- defined precursor, during which process, the negative effects of the solvent have not been involved, so the shape-control parameters are simplified and the formation mechanism might be relatively easier to access (Larsen *et al.*, 2003).

The precursor serves as the source of the metal, chalcogen, and the capping agent. This makes the route cheap, less toxic and simple (Jung *et al.*, 2010). Thermal

decomposition of a precursor is the key step which produces a thin film and nanoparticles, and ideally the ligands associated with the precursor are cleanly lost into the gas phase. Thermal decomposition allows easier and simpler control of the shapes and sizes of the nanoparticles than other methods (Jung *et al.*, 2010).

Among the various precursors which have been used, xanthates have been found to be efficient molecular precursors for solventless synthesis of nanoparticles (Jung *et al.*, 2010). Such precursors are typically solids at room temperature and nanoparticle synthesis is achieved by heating the precursor in the absence of a solvent, causing the precursor to melt and inducing thermal decomposition (Jung *et al.*, 2010).

This is as a result of the low decomposition pathway. Also the alkyl group from the xanthate serves as a capping agent for the nanoparticles thereby eliminating additional cost for the capping agent (Tzhayik *et al.*, 2002). The products obtained by solventless thermolysis are monodisperse which is due primarily to minimal inter-particle collision (Jose and Jagirdar, 2010). A small body of work also exist on the synthesis of nanoparticles from single source precursors without the use of a solvent.

The first description of self-capping solventless nanoparticle synthesis was the thermal decomposition of the silver carboxylates to form silver nanoparticles (Yang and Aoki, 2005). Abe *et al.*, (1998) heated the silver salts of myristic, stearic, and oleic-acid under a nitrogen atmosphere at 250 °C forming silver nanoparticles capped by alkylate ligands.

The synthesis of monodispersed Cu₂S nanorods by the solventless thermolysis of copper thiolate precursor has been reported (Larsen *et al.*, 2003). Cu₂S was formed by

homolytic cleavage of the thiol and alkyl groups. The sulphur was consequently incorporated into the hexagonal close-packed lattice, while the Cu cations inhabited interstitial space. The thiols (and perhaps the carboxyl ligands) also contribute to the reduction of Cu(II) to Cu(I). The nanorods produced at 148 °C (140 minutes reaction time) were approximately 4 nm in diameter and 12 nm long. Cu₂S undergoes a phase transition from the low-temperature monoclinic crystal structure to the high-temperature hexagonal phase at 104 °C (Larsen *et al.*, 2003).

Silver nanocrystals have been prepared by thermal decomposition of silver salts of fatty acids. The silver nanocrystals were 5–20 nm in diameter and were also surrounded by alkyl moieties with a thickness of 1.4–1.7 nm (Abe *et al.*, 1998). Synthesis of silver nanoparticles by thermal treatment of a silver–aspartame complex under inert atmosphere has been described. Spherical metallic silver nanoparticles with average diameter of 5±2 nm were obtained by thermal treatment of the complex [Ag(C₁₄H₁₇N₂O₅)]·2H₂O at 185 °C. TEM analysis of the particles showed predominance of the spherical shape, but some coalescent and elongated particles were present (Cavicchioli *et al.*, 2005). Monodisperse Ag nanodisks with an aspect ratio of 7 have been successfully synthesized from silver thiolate giving convincing experimental support for a new structure-controlled solventless method under nitrogen atmosphere (Chen *et al.*, 2005).

Bismuth nanofilms with an average thickness of 0.6 nm and monodisperse layered Bi nanorhombuses with an average edge length of 21.5 nm and thickness of 0.9 nm have been successively synthesized by structure controlling solventless thermolysis from a new layered bismuth thiolate precursor. Decomposition for 5 hours generated uniform

rhombuses with layered structural motifs (Chen *et al.*, 2007). Orthorhombic Bi₂S₃ (bismuthinite) nanorods and nanowires have been synthesized by the solventless thermolysis of bismuth alkylthiolate precursors. Reactions carried out in air at ~225 °C in the presence of a capping ligand species, octanoate, produced high aspect ratio (>100) nanowires (Sigman and Korgel, 2005). Through controlled thermolysis of nanoscale molecular clusters [Mn₁₂O₁₂(O₂CR).16(H₂O)₄] (R = phenyl and methyl) in a one-end closed horizontal tube furnace, the successful realization of the solid-state transformation of inorganic core containing molecular clusters (Mn₁₂) into novel MnO nano- and microscale particles in situ without using any reductive or template have been reported (Chen *et al.*, 2009). Product size and morphology was found to depend on the temperature and time of thermolysis as well as the organic ligands employed. Heating of the R = phenyl precursor at 400 °C for 10 hours gave crystalline MnO nanoparticles 70 nm in diameter and spherical in shape. Higher temperatures give larger structures, for example 500 °C for 10 hours yielded pyramid shaped MnO particles 0.12 μm in diameter. Unique PbS nanowires with x-shaped cross sections, having diameters in the range of 300–800 nm with an average of 598 nm ($\sigma \pm 21.7\%$), and lengths of up to several tens of micrometers, have been made by a solventless method. The suitable precursor is obtained from a Pb(NO₃)₂/octanoate/ethylenediamine/dodecanethiol molar ratio of 1:2:1: 1.6, and the PbS nanowires are produced by the thermolysis of such precursors at 280 °C for 1 hour (Chen *et al.*, 2007).

Singhal *et al.*, (2007) have used an allyl-palladium (II) xanthate complex and a palladium (II) xanthate complex as single source precursors for PdS nanoparticle synthesis. The precursors were thermally decomposed by heating in a furnace at 300 °C

under argon atmosphere. XRD showed the products to be crystalline PbS in a tetragonal phase. From the Scherrer equation the particle sizes were estimated to be 32 nm and 16 nm for methyl and iso-propyl derivatives respectively.

The synthesis of PbS, using trioctylamine (TOA), as liganding solvent enables a single step, benchtop low- temperature decomposition of lead hexadecylxanthate, a single precursor, producing PbS nanowires. Reaction conditions resulted in crystalline, rocksalt PbS, and the coordinating solvent TOA enabled one dimensional growth (Patla *et al.*, 2007).

Starting with an alkyl lead xanthate precursor, PbS nanoparticles can be prepared from the melt method. Aside the reproducibility of this method, it is also cheap and simple. Other methods use capping agent which introduces additional cost, toxicity to the process and may hinder technological application of the as-prepared PbS nanoparticles. In addition to their appreciable volatility and stability to air and moisture, the presence of pre-formed Pb-S bonds and the absence of Pb-C bonds in the precursor enable their clean conversion into lead (II) sulphide in an inert atmosphere.

2.7 Application of Nanoparticles in Novel Solar Cells

Nanoparticles have found useful applications as absorbers in novel solar cells. This application is as a result of their relatively small size which is in the nanometer region.

2.7.1 Background to Solar Cells

There is a lot of interest in solar cells with thin active regions that minimize material costs while maintaining high efficiencies (Zhao *et al.*, 2010). Solar cell is a solid state electrical device that converts the energy of sunlight directly into electricity by the photovoltaic effect (Chi *et al.*, 2013). At present, the active materials used for the

fabrication of solar cells are mainly inorganic materials, such as silicon (Si), gallium-arsenide (GaAs), cadmium-telluride (CdTe), and cadmium-indium-selenide (CIS). The power conversion efficiency for these solar cells varies from 8 to 29 % because these cells lose as much as 60 % of the sunlight that falls on them due to transmission. Also these solar cells tend to degrade upon long exposure to sunlight and their efficiency decreases by 10–20 % (Afzaal and O'Brien, 2006). These solar cells rely on high quality materials since the charge carriers generated in the device, after photon absorption, remain in the same material until they are extracted at the selective contact electrodes. This involves the use of sophisticated technologies with high production cost in order to avoid charge carrier recombination prior to their extraction at the contact electrodes (Bisquert, 2010). Due to the high cost of inorganic solar cells, a research into hybrid solar cells, which are third generation solar cells have become the subject of interest to many researchers (Ip *et al.*, 2012).

2.7.2 Hybrid Solar Cells

A typical hybrid solar cell is based on a thin film comprising a blend of inorganic nanoparticles and a semi-conducting polymer sandwiched between two charge collecting electrodes (Dowland *et al.*, 2011). The operation of such devices is based on a photo-induced charge separation reaction at the inorganic–organic semiconductor heterojunction. The resultant photogenerated electrons and holes are subsequently transported through the inorganic and organic semiconductor components respectively and collected at the appropriate device electrodes (Ip *et al.*, 2012).

A hybrid solar cell, consisting of both organic and inorganic materials, combines the unique properties of inorganic semiconductors with the film forming properties of

conjugated polymer (Dowland *et al.*, 2011). Hybrid solar cells have organic materials that consist of conjugated polymers that absorb light as the donor and transport holes. These conjugated polymers provide ease of processing, low cost, physical flexibility and large area coverage (McDonald *et al.*, 2005; Ong and Levitsky, 2010). Polymer photovoltaic devices rely on the introduction of another material for electron transport. The presence of a second material also provides an interface for charge transfer and therefore, small conjugated molecules have been blended with polymers at a concentration that enables the formation of percolation pathways for electron transport (Afzaal and O'Brien, 2006; Ip *et al.*, 2012). These second materials are inorganic materials which are used as the acceptors and electron transporters in the solar cell structure. These inorganic materials have been manufactured as nanoparticles. A hybrid solar cell is more efficient to create an electric field at an interface between two different semiconductor materials, known as a heterojunction (Kamat, 2008). This utility is due to the fact that their optical band can be tuned by both material selection and quantum confinement and because advances in synthesis allow control over nanocrystal size and shape to optimize performance. Other advantages of using structured layers in thin film solar cells are;

- (i) the optical path for photon absorption is more increased than the actual thin film thickness due to multiple reflections and
- (ii) light generated from electrons and holes need to travel over a short path therefore, recombination losses are greatly reduced and consequently, the absorber layer thickness in nano-structured solar cells can be as thin as 150 nm instead of several microns in traditional solar cells (Afzaal and O'Brien, 2006).

The hybrid solar cell is deficient only in efficiency since it is lower than their inorganic counterparts (Wang *et al.*, 2008). In order to improve the efficiency, research into the effect of various nanoparticles with different sizes and shapes has been the interest of many researchers (Fan *et al.*, 2007).

2.7.3 The use of PbS in Hybrid Solar Cells

PbS nanoparticles have found interesting applications in the fabrication of solar cell materials as light absorbers. This is as a result of their narrow band gaps and high extinction coefficients. The absorption onset of PbS nanoparticles can also be tuned over a large wavelength range which is different from that of bulk PbS (Leventis *et al.*, 2010). Such behaviour arises from the strong quantum confinement of charge carriers in the material, which can be several times stronger in lead-based quantum dots than in most III-V or II-VI semiconductors (Arici and Serdar, 2004). Wang *et al.*, (2010) have fabricated a solar cell by using poly[2-methoxy-5-(3,7-dimethyloctyloxy)-1,4-phenylenevinylene] (MDMO-PPV) capped PbS quantum dots as the acceptors in a bulk heterojunction approach. The efficiency of the solar cell was increased by the addition of the quantum dots. This was evident by the absorption spectra which did not only improve in polymer region but also the beyond that region in both the near infrared and ultraviolet ranges. Cells based on lead sulphide quantum dots with organic semiconducting polymers have been reported to show photovoltaic effects (Arici and Serdar, 2004). Çapan *et al.*, (2010) have successfully synthesized a PbS colloidal quantum dot solar cell to exceed 2% air mass (AM) and 1.5 power conversion efficiency (PCE). This was also reported as the first infrared solution-processed solar cell that has achieved stability in air and under solar illumination. Nanocomposite approach in which PbS nanocrystals tuned by the quantum size effect sensitize the

conjugated polymer poly[2-methoxy-5-(2'-ethylhexyloxy-p-phenylenevinylene)] (MEH-PPV). This solution-processed device had a sensitivity far beyond 800 nm, thus harvesting of infrared-photogenerated carriers and demonstrating infrared photovoltaic effect (McDonald *et al.*, 2005).

KNUST



CHAPTER THREE

MATERIALS AND METHODS

3.1 Chemicals

- (i) Sodium hydride (laboratory reagent grade 99 %)
- (ii) Ethanol (laboratory reagent grade 99.8 %)
- (iii) Carbon disulphide (laboratory reagent grade 98 %)
- (iv) Lead acetate (laboratory reagent grade 97 %)
- (v) Hexane (laboratory reagent grade 96 %)
- (vi) Acetonitrile (laboratory reagent grade 97 %)
- (vii) Diethylether (laboratory reagent grade 98 %)
- (viii) Acetone (laboratory reagent grade 98 %)
- (ix) 1-Butanol (laboratory reagent grade 99.8 %)
- (x) 1-Hexanol (laboratory reagent grade 98 %)
- (xi) 1-Octanol (laboratory reagent grade 98 %)

All chemicals were used as received from Sigma Aldrich without any further purification.

3.2 Synthesis of Lead Alkyl Xanthate Precursors

Generally, the lead xanthate precursors were synthesized by a reaction between an alcohol, sodium salt, carbon disulphide and lead salt.

3.2.1 Synthesis of Lead Ethyl Xanthates [Pb(S₂COEt)₂]

In a three necked flask, ethanol (1.842 g, 40 mmol), NaH (0.96 g, 40 mmol) and 50 ml diethylether were stirred at room temperature for two hours. The mixture was then cooled to 0 °C in melting ice. CS₂ (3.046 g, 40 mmol) was added drop-wise and the resulting mixture was stirred at room temperature for one hour. A freshly prepared lead acetate solution containing lead acetate (7.587 g, 20 mmol) was added drop-wise to the

ligand and the resulting mixture was stirred for one hour at room temperature resulting in the formation of a precipitate. The precipitate was then filtered, washed with distilled water and air dried. The crude sample was then recrystallized in cold acetone and precipitated with diethyl ether and dried under vacuum. The mass of product was 5.21 g.

3.2.2 Synthesis of Lead Butyl Xanthates [Pb(S₂COBu)₂]

This was synthesized through the same steps as [Pb(S₂COEt)₂] above with ethanol replaced with n-butanol (2.965 g). The crude sample was then recrystallized in hot acetonitrile and dried under vacuum. The mass of product was 5.68 g.

3.2.3 Synthesis of Lead Hexyl Xanthates [Pb(S₂COHex)₂]

This was synthesized through the same steps as [Pb(S₂COEt)₂] above with ethanol replaced with 1-hexanol (4.087 g). The crude sample was then recrystallized in hot acetonitrile and dried under vacuum. The mass of product was 4.76 g.

3.2.4 Synthesis of lead octyl xanthates [Pb(S₂COOct)₂]

This was synthesized through the same steps as [Pb(S₂COEt)₂] above with ethanol replaced with 1-octanol (5.209 g). The crude sample was then recrystallized by heating in acetone and dried under vacuum. The mass of product was 5.20 g.

3.3 Characterization of Lead Xanthate Precursors

The physical, thermal and chemical properties of the synthesized lead xanthate precursors were investigated and compared to literature.

3.3.1 Nuclear Magnetic Resonance (NMR)

^1H and ^{13}C NMR studies were carried out using Ultrashield Advance Bruker 400Hz NMR. The samples were prepared by dissolving ~3 mg of each of the as-synthesized lead xanthate precursor in chloroform-d at room temperature. An 8” thin walled NMR tube was filled with the precursor solution and which was then analysed. The chemical shifts and splitting patterns of the different hydrogen and carbon atoms were then compared to standard values in literature.

3.3.2 Melting Point

Melting point was determined using Stuart Scientific melting point apparatus. A capillary tube was filled at one end with the sample and inserted into the melting point apparatus. The sample was then monitored as it was heated. The temperatures at which the sample began to melt and completely melted were then recorded. The average of these two temperatures was then recorded as the melting point of the sample.

3.3.3 Infra-red Spectroscopy (IR)

Infrared spectra were obtained on a Perkin Elmer FT-IR spectrophotometer with Bruker detector. The samples were scanned as solids from 4000–400 cm^{-1} . The different wavenumbers of the spectra were compared to literature to determine the different functional groups in the sample.

3.3.4 Micro-elemental Analyses

Micro-elemental analyses were performed using the University of Manchester Micro-analytical facility. The micro-elemental analyses were used to ascertain the purity of synthesized precursors. The theoretical elemental percentages were compared to the

experimental elemental percentages of the different elements in the precursors. The elements analysed were Pb, C, H and S.

3.3.5 Mass Spectroscopy (MS)

Mass spectrometry was performed using the University of Manchester mass spectrometry facility. The samples were dissolved in suitable solvents and analysed using the Electrospray ionization technique due to the polymeric nature of the lead xanthate precursors. The different fragments were then determined and the base and molecular ion peaks identified.

3.3.6 Thermogravimetry Analysis (TGA)

TGA studies were performed using a Perkin Elmer TGA7 analyzer. The samples were heated from 25 to 600 °C under a flow of dry nitrogen gas. The experimental decomposition percentages of PbS was then compared to the theoretical decomposition of PbS in the different lead xanthate precursors.

3.3.7 Differential Scanning Calorimetry (DSC)

DSC studies were performed using a Perkin Elmer Diamond hyper DSC. The samples were heated from -50 to 120 °C and cooled from 120 to -50 °C at a rate of 10 °C per minute under the flow of nitrogen gas. The melting and crystallization temperatures were then determined from the heating and cooling curves respectively.

3.3.8 X-ray Crystallography

X-ray crystallographic measurements were made using graphite monochromated Mo-K α radiation ($\lambda \sim 0.71073 \text{ \AA}$) on a Bruker APEX diffractometer. The structures were

solved by Direct Methods and refined by full-matrix least squares on F^2 (Sheldrick, 2008). All calculations were carried out using the SHELXTL package Version 6.10. Non-hydrogen atoms were refined with anisotropic atomic displacement parameters. Hydrogen atoms were placed in calculated positions, assigned isotropic thermal parameters and allowed to ride on their parent carbon atoms.

3.4 Synthesis of PbS from Lead Xanthate Precursors

Decomposition was carried out in a conventional horizontal tube furnace reactor. First, the powder of lead xanthate precursor (0.3 g) was spread out flat on the bottom of a ceramic boat which was then inserted into the centre of a quartz tube. The quartz tube was then placed inside the tube furnace with one end connected to the argon gas at a flow rate of 160 SCCM (SCCM denotes cubic centimeter per minute). The furnace was then heated for the different temperatures and times. The black product obtained after the decomposition process was then collected and analysed.

3.5 Characterization of PbS Nanoparticles

The diffraction patterns, morphologies and elemental percentages of the as-prepared PbS nanoparticles were determined and compared with literature.

3.5.1 X-ray Diffraction (XRD)

XRD studies were carried out by using a Bruker D8 AXS diffractometer equipped with monochromated Cu-K α radiation. The samples were scanned between 20 and 85 degrees in a step size of 0.070° at a count rate of 10 s at a temperature of 20 °C. The samples were prepared by dispersing the PbS in hexane and spotting on a glass slide.

The particle size 'D' was calculated according to the Scherrer equation: $D = \frac{k\lambda}{b \cos \theta}$;

where b is the full width at half maximum, λ is the wavelength of the radiation, θ is the angle of diffraction and $k = 0.9$ is the Scherrer constant.

3.5.2 Scanning Electron Microscopy (SEM)

SEM was carried out on a Philips XL30 FEG Scanning Electron Microscope. The samples were prepared by dispersing the as-prepared PbS nanoparticles in hexane and spotting on a glass slide. The slides were then carbon coated using Edward's E306A coating system before the SEM analysis. The images were then taken at 50,000x, 20,000x, 10,000x, 5,000x, 2,000x, and 1,000x magnifications.

3.5.3 Energy Dispersive X-ray Spectroscopy (EDX)

EDX was performed on a DX4 equipped to the Philips XL30 FEG Scanning Electron Microscopy. The samples were prepared by dispersing the as-prepared PbS nanoparticles in hexane and spotting on a glass slide. The slides were then carbon coated using Edward's E306A coating system. The elemental composition of the as-prepared nanoparticles were then determined and quantified.

3.5.4 Transmission Electron Microscopy (TEM)

Samples for TEM were prepared by evaporating a dilute hexane solution of the as-prepared PbS nanoparticles on carbon coated copper grids (S163-3, Agar Scientific) and Philips CM200 Transmission Electron Microscope (TEM) was used to obtain micrographs of the nanoparticles. The images were obtained at both low and high magnifications. The images obtained at high magnifications were used to determine the lattice fringes.

CHAPTER FOUR

RESULTS AND DISCUSSIONS

4.1 Physical Appearance of Lead Xanthate Precursors

The as-synthesized lead alkyl xanthates (ethyl, butyl, hexyl and octyl) were mostly yellow coloured as shown in Table 4.1 below. The precursors were stable and easy to handle. Their yields were low ranging from 42.10 - 57.99 %. This could be attributed to the fact that the masses and yields were taken after recrystallization. However, most yields that have been reported for metal xanthates were reported for the crude product and this makes the yield relatively high (Alam *et al.*, 2008; Jain, 2006; Nair *et al.*, 2002).

Table 4.1: Physical appearance of the lead xanthate precursors

Precursor	Colour	Reported colour
Lead ethyl xanthate	Yellow	Yellow (Clark <i>et al.</i> ,2011)
Lead butyl xanthate	Brown	No colour reported
Lead hexyl xanthate	Yellow	No colour reported
Lead octyl xanthate	Yellow	No colour reported

4.2 NMR of Lead Xanthate Precursors

The different types of carbon and hydrogen atoms and their environment in the lead xanthate precursors were also determined.

4.2.1 ^1H NMR

The different types of hydrogen atoms and their environments were determined using ^1H NMR. Since the groups around the Pb in the compounds were symmetrical, only one half was considered (Clark *et al.*, 2011).

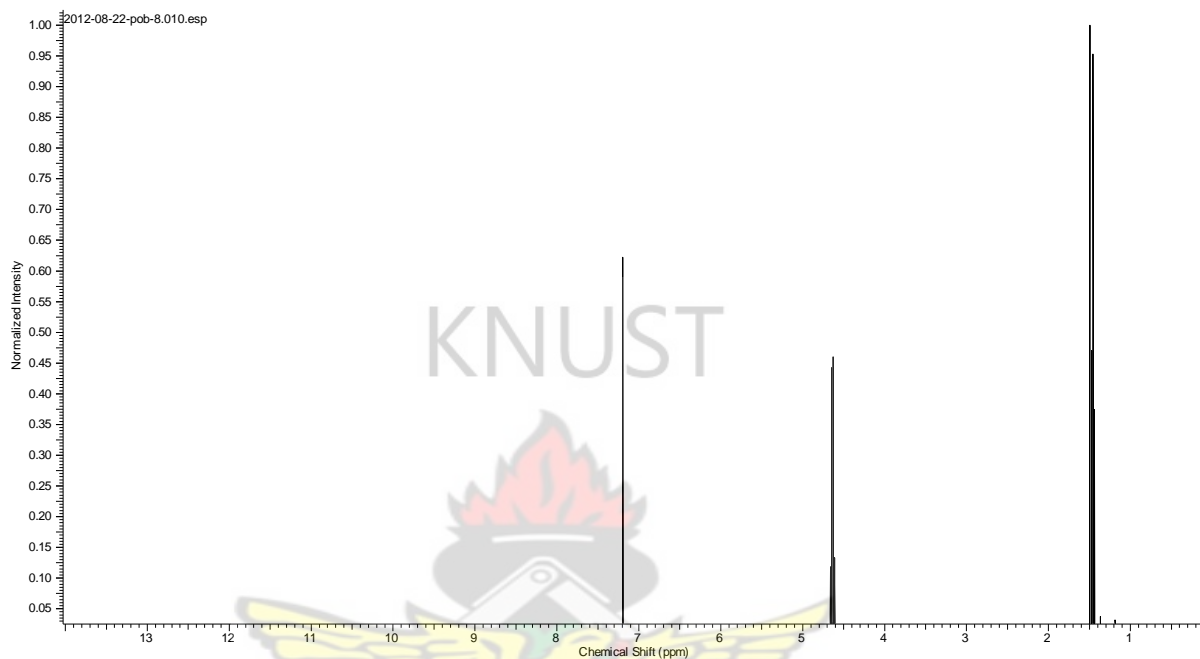


Figure 4.1: ^1H NMR for lead ethyl xanthate (normalized intensity against chemical shift)

For lead ethyl xanthate, the chemical shift (δ) for the methylene hydrogens was observed as a multiplet at 4.63 ppm. The multiplet was as a result of the splitting by the adjacent hydrogens from the CH_3 group. The δ resulted from the attachment to the electronegative oxygen atom. The methyl hydrogens were split by the 2 methylene hydrogens into a triplet at a δ of 1.45 ppm. Although the 1.45 ppm was higher as compared to the methyl protons of the other precursors, this resulted from the short alkyl chain and the fact that the electronegative effect of the oxygen atom was felt on the CH_3 protons (Drake *et al.*, 1991). CDCl_3 showed a singlet at δ of 7.19 ppm in all the

precursors (Drake *et al.*, 1996; Mege *et al.*, 1993; Nyamen *et al.*, 2012; Thammakan and Somsook, 2006).

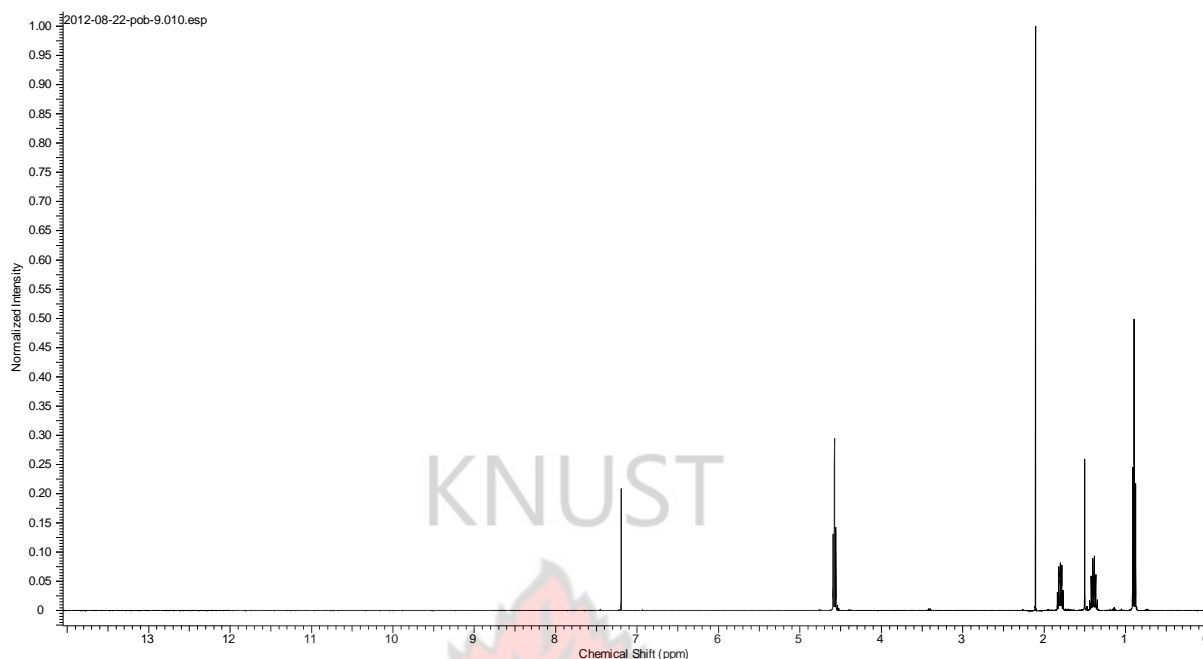


Figure 4.2: ^1H NMR for lead butyl xanthate (normalized intensity against chemical shift)

Lead butyl xanthate had its CH_3 protons split at a δ of 0.89 ppm into a triplet by the adjacent CH_2 group. Both the methylene hydrogens were split into a multiplet by the neighbouring protons at 1.39 and 1.80 ppm. The δ of protons in O-CH_2 occurred at δ of 4.57 ppm which was comparable to that of the lead ethyl xanthate. This shows little effect of the butyl alkyl chain on the chemical shift (Akhtar *et al.*, 2011).

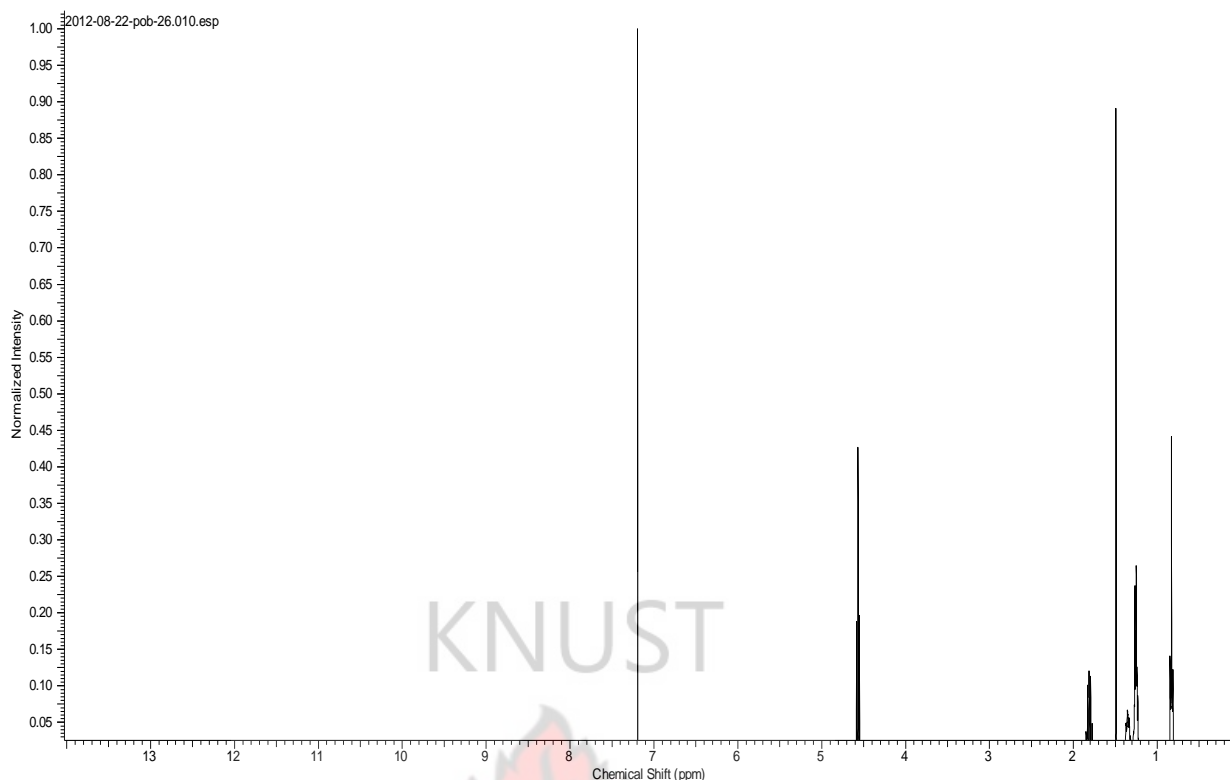


Figure 4.3: ^1H NMR for lead hexyl xanthate (normalized intensity against chemical shift)

Lead hexyl xanthates showed the protons of CH_3 at a δ of 0.82 ppm. However, the protons of the CH_2 in the complex were observed as multiplets caused by the neighbouring CH_2 groups at 1.24, 1.35, and 1.81 ppm depending on their closeness to the methyl group. The least δ value corresponded to the protons of the CH_2 directly attached to the CH_3 group. Also, the O-CH_2 was split into a triplet at 4.56 ppm by the adjacent CH_2 protons. It was observed that as the alkyl chain becomes longer, the δ for the methyl protons move further upfield as compared to the δ of the CH_3 protons of lead ethyl xanthate. This implies that there is little or no effect of the electronegative oxygen atom on the methyl protons.

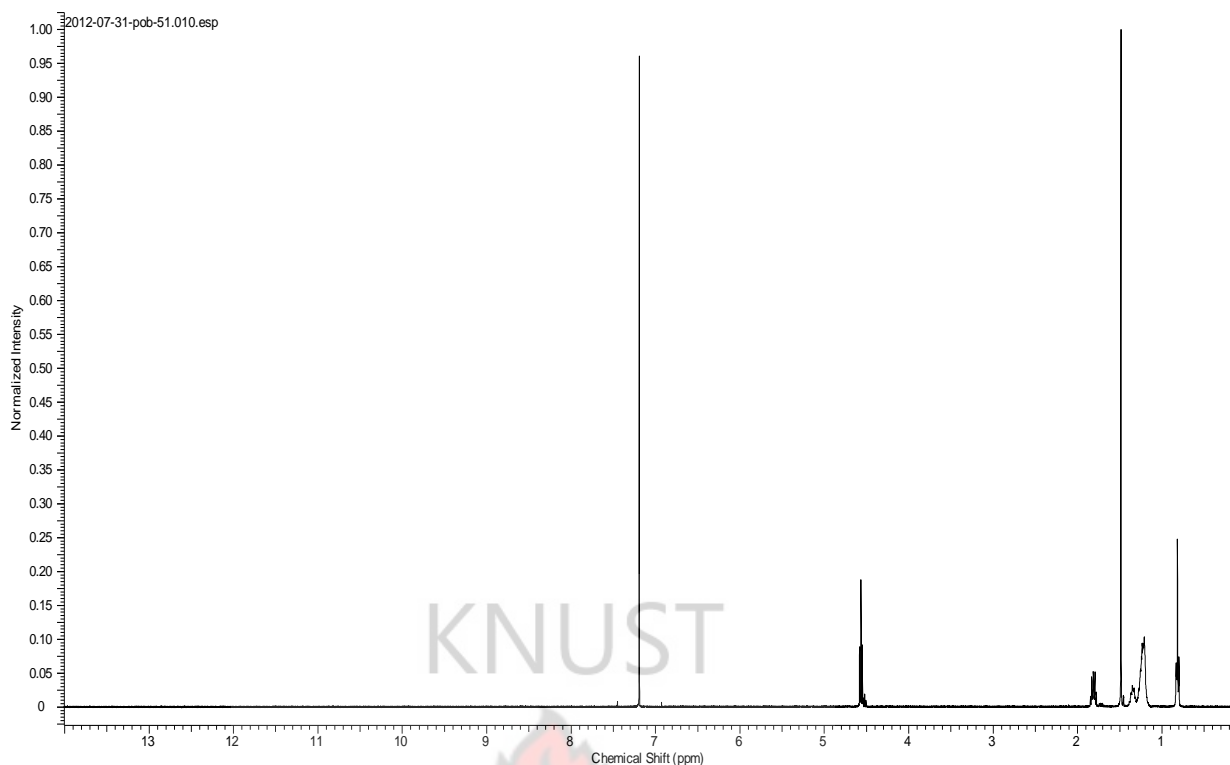


Figure 4.4: ^1H NMR for lead octyl xanthate (normalized intensity against chemical shift)

The splitting pattern of lead octyl xanthate was similar to the splitting pattern of lead hexyl xanthate. The δ for the CH_3 protons occurred at 0.81 ppm. The methylene protons $\text{CH}_3(\text{CH}_2)_6\text{CH}_2\text{-O}$ in the precursor were observed as multiplets at 1.24, 1.35, and 1.81 ppm. The 3 different δ observed for the 6 CH_2 groups implies that some of the protons were in the same environments. Also the protons of O-CH_2 were split into a triplet at 4.56 ppm.

4.2.2 ^{13}C NMR

The different types of carbon atoms and their environments were also determined using ^{13}C NMR. All the peaks were singlets irrespective of the type of precursor used. The triplet in the spectrum was from the C atom in the CDCl_3 solvent used to dissolve the complexes (Bailey *et al.*, 1995; Lazell and O'Brien, 1999; Perepichka *et al.*, 2004).

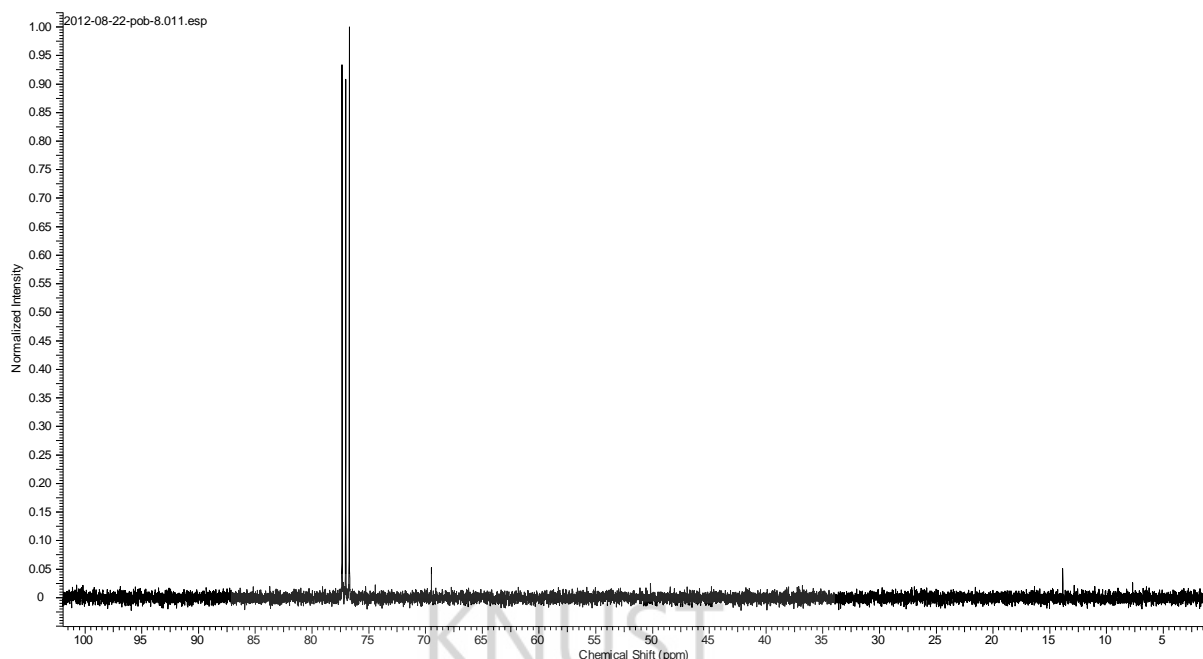


Figure 4.5: ^{13}C NMR for lead ethyl xanthate (normalized intensity against chemical shift)

For the lead ethyl xanthate, two different singlets were observed for the two different C atoms in the precursor as showed in Figure 4.5 above. The observed triplet was the splitting pattern of the C atoms in chloroform-d used to dissolve the precursor (Clark *et al.*, 2011). The C atom of CH_3 appeared at a chemical shift of 13.84 ppm. The chemical shift observed at an upfield was as a result of the CH_2 attached to the CH_3 group. The C atom of the CH_2 which is attached to the oxygen atom of the lead ethyl xanthate was at a chemical shift of 69.47 ppm. This could be attributed to the shorter alkyl chain and the strong effect of the oxygen atom on the C atom.

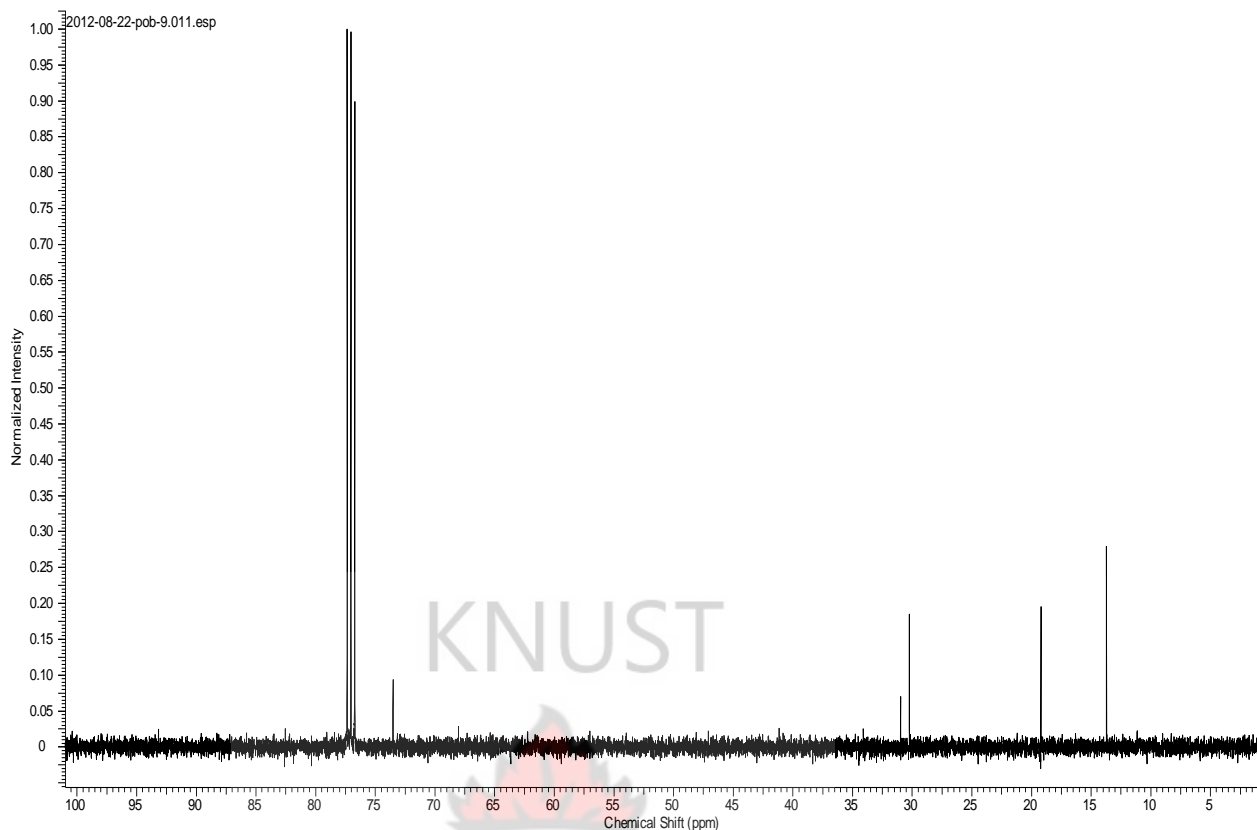


Figure 4.6: ^{13}C NMR for lead butyl xanthate (normalized intensity against chemical shift)

The chemical shifts for lead butyl xanthate were observed at 13.70, 19.20, 30.10 and 73.20 ppm corresponding to carbon atom of CH_3 , CH_3CH_2 , $\text{CH}_2\text{CH}_2\text{CH}_2\text{-O}$ and $\text{CH}_2\text{-O}$ respectively as shown in Figure 4.6 above. The δ of the C atom of the CH_3 in the lead butyl xanthate was comparable to the δ of the C atom in the CH_3 in the lead ethyl xanthate. This resulted from the equivalent environments of the C atoms in the CH_3 groups in the two lead xanthate precursors. The two different CH_3 groups were attached to CH_2 groups in the complexes. The observed triplet was the splitting pattern of the C atoms in chloroform-d used to dissolve the precursor (Clark *et al.*, 2011). The value of the chemical shift at a further downfield resulted from the three electronegative chlorine atoms attached to the C atoms.

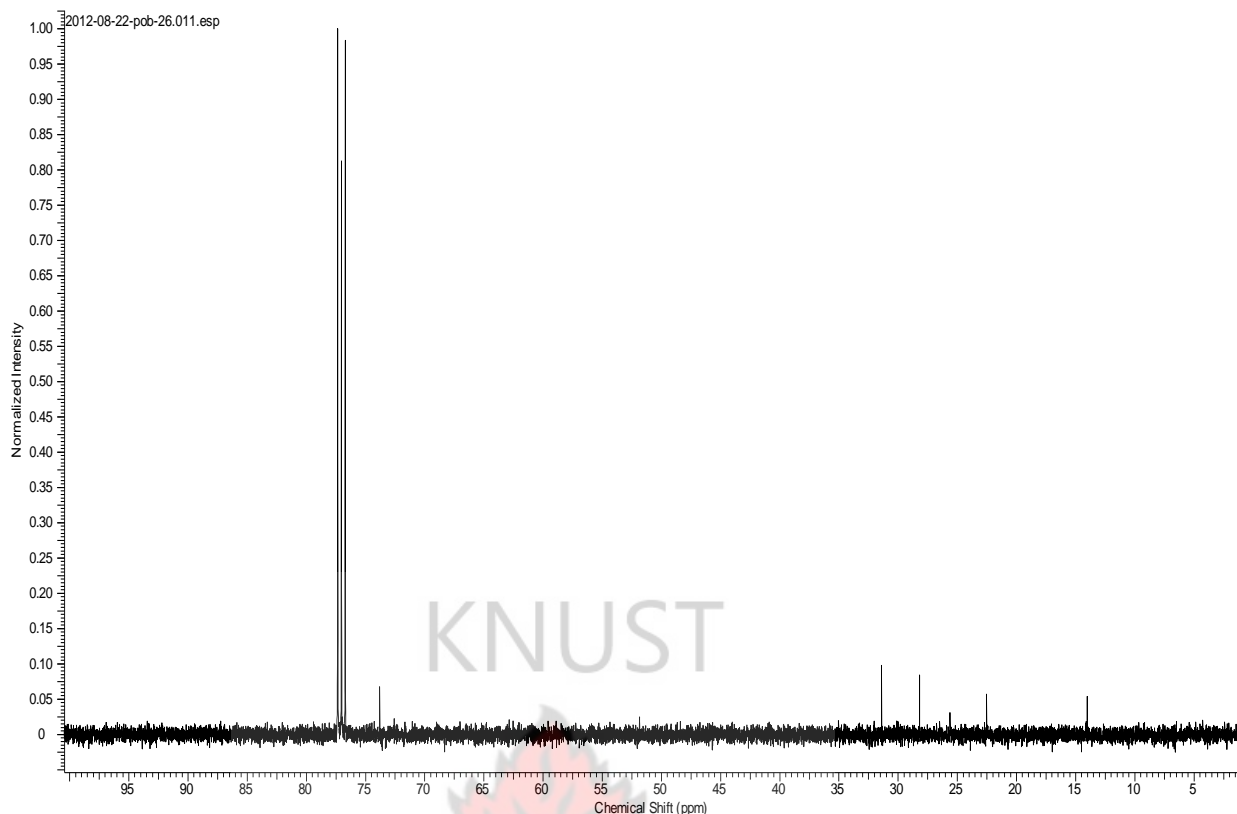


Figure 4.7: ^{13}C NMR for lead hexyl xanthate (normalized intensity against chemical shift)

As shown in Figure 4.7, six different singlet peaks were obtained from the spectrum signifying the six different C atoms in the lead hexyl xanthate complex. Peaks at 14.01, 22.52, 25.61, 28.18, 31.39 and 73.50 ppm were the observed chemical shifts for lead hexyl xanthate. The least δ (14.01 ppm) represented the C atom in the CH_3 whereas 73.50 ppm was from the C atom in $\text{CH}_2\text{-O}$. The chemical shift at a further downfield of 73.50 ppm was as a result of the attachment of the C atom to an electronegative oxygen atom. A triplet peak was observed as the chemical shift of the C atom in the chloroform-d which was used to dissolve the precursor before analysis.

Lead octyl xanthate showed chemical shifts of the C atoms in the six CH_2 carbons in the complexes ranged from 22.61-31.77 ppm as shown in Figure 4.8 above. The values

of the chemical shift of the C atoms were comparable to the chemical shifts of the C atoms in butyl and lead hexyl xanthates except that the number of CH₂ groups increased from 2 to 4 to 6. The singlet peak observed further downfield at a δ of 73.80 ppm was due to the attachment of the C atom to an electronegative O atom in CH₂-O. The C atom in the chloroform-d was observed as a triplet 73.03 ppm (Clark *et al.*, 2011).

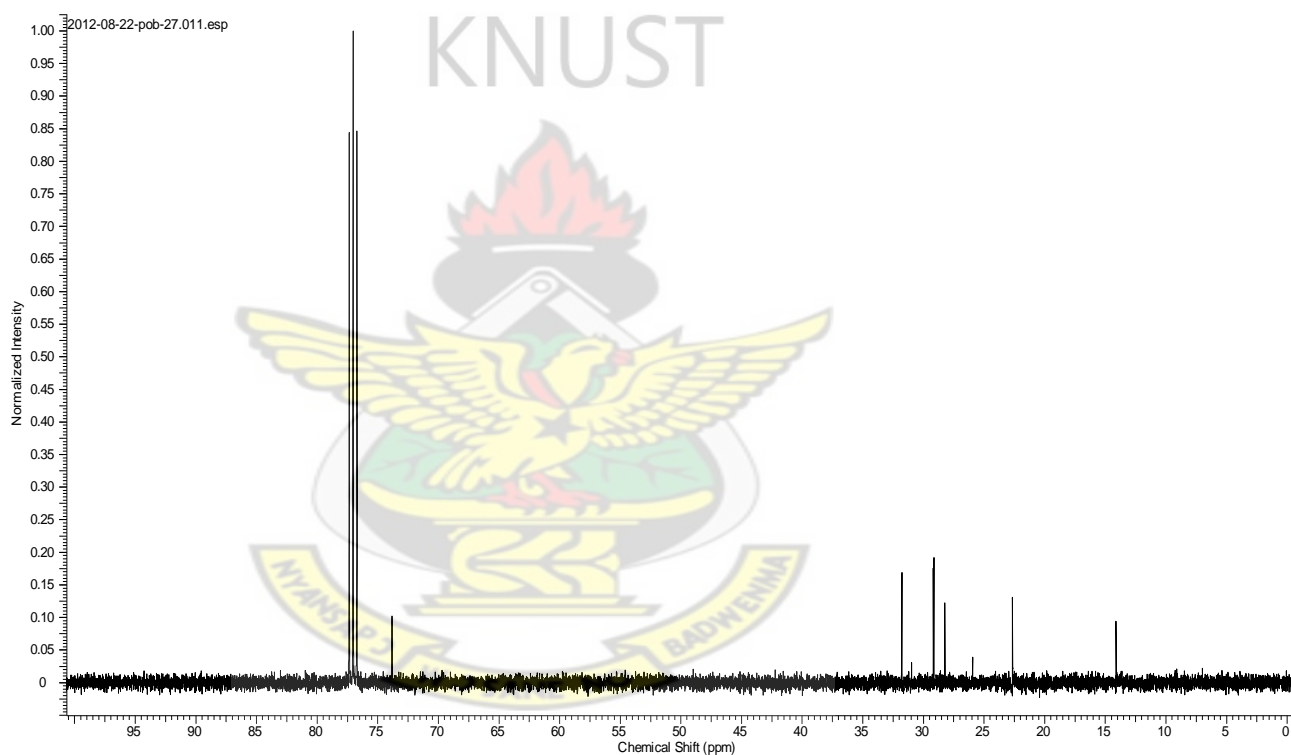


Figure 4.8: ¹³C NMR for lead octyl xanthate (normalized intensity against chemical shift)

4.3 Melting Points of Lead Xanthate Precursors

Table 4.2: Melting points of lead xanthate precursors (average)

Precursor	Melting points/°C
Lead ethyl xanthate	(115) 114-116
Lead butyl xanthate	(85) 84-86
Lead hexyl xanthate	(60.5) 60-61
Lead octyl xanthate	(78) 77-79

The observed melting points of the lead xanthate precursors were relatively sharp. This confirms the purity of the lead xanthate precursors (Clark *et al.*, 2011). Generally, an increase in alkyl chain corresponded to a decrease in melting point. The melting points were observed at 115 °C, 85 °C and 60.5 °C for ethyl, butyl and hexyl lead xanthates respectively. Lead octyl xanthate however, had a melting point of 78 °C which deviated from the general trend. This may have resulted from the polymeric behaviour of xanthates which increases with increasing alkyl chain (Barreca *et al.*, 2005). This could also be attributed to the varying physical properties of the starting alcohols. The low melting points for the precursors made them suitable candidates for thermal decomposition as single source precursors for M – S nanoparticles (Fan *et al.*, 2007). Other single source precursors have relatively high melting points (Shi *et al.*, 2010).

4.4 Infra-red (IR) of Lead Xanthate Precursors

Infrared Spectroscopy provides a valuable means of detecting the presence of organic species at surfaces, identifying the chemical nature of surface compounds, and determining the structure and orientation of the adsorbed entity (Buckley *et al.*, 2003).

The vibrational spectrum of a molecule is considered to be a unique physical property and is characteristic of the molecule. As such, the infrared spectrum can be used as a fingerprint for identification of molecules (Coates and Ed, 2000). The major functional groups of metal xanthate precursors occur in the fingerprint region (Clark *et al.*, 2011).

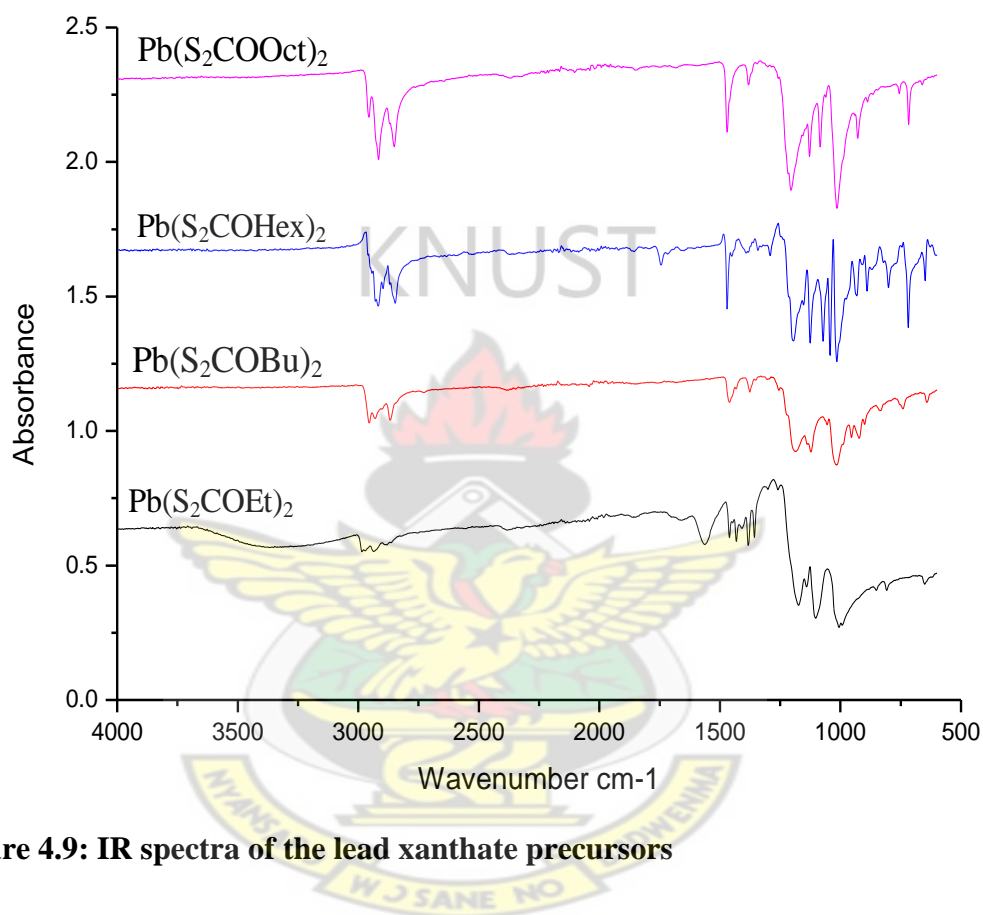


Figure 4.9: IR spectra of the lead xanthate precursors

Strong absorption bands which appeared in the region 1011 – 1045 and 1056 – 1098 cm⁻¹ were due to vibrations of the C = S bond in the C - O stretching of xanthate moiety respectively (Cases *et al.*, 1990; Chauhan *et al.*, 2011; Homagai *et al.*, 2010). The C-S vibrations are lower than the C-O vibrations (Leppinen and Rastas, 1986; Sydney, 2005). Other vibrations observed were the C – C, C - H bending, symmetric and anti symmetric stretches. The C – C ranged between 1121 and 1138 cm⁻¹. C – H bending vibrations were observed at 1459 – 1460 cm⁻¹. Anti symmetric CH stretch of

the methyl and methylene groups $2916 - 2969 \text{ cm}^{-1}$ occurred at slightly higher frequency than symmetric vibrations 2847 and 2867 cm^{-1} , respectively (Coates and Ed, 2000; Hope *et al.*, 2001; Liang *et al.*, 2009). Generally, as the chain length of the alkyl group increases the vibrational frequencies also increase. This can be due to the greater electron-releasing tendency as the alkyl group increases (Shankaranarayana and Patel, 1961).

4.5 Micro-elemental Analyses of Lead Xanthate Precursors

Table 4.3: Micro-elemental analyses for the lead ethyl xanthate

	% Elements	Expected	Found
Lead ethyl xanthate ($\text{C}_6\text{H}_{10}\text{O}_2\text{PbS}_4$)	C	16.03	16.51
	H	2.24	2.36
	S	28.47	28.52
	Pb	46.13	43.09

Table 4.4: Micro-elemental analyses for lead butyl xanthate

	% Elements	Expected	Found
Lead butyl xanthate ($\text{C}_{10}\text{H}_{18}\text{O}_2\text{PbS}_4$)	C	23.75	20.80
	H	3.59	3.32
	S	25.31	24.48
	Pb	41.01	48.75

Table 4.5: Micro-elemental analyses for lead hexyl xanthate

	% Elements	Expected	Found
Lead hexyl xanthate (C ₁₄ H ₂₆ O ₂ PbS ₄)	C	29.93	30.31
	H	4.67	4.53
	S	22.79	22.72
	Pb	36.92	35.37

Table 4.6: Micro-elemental analyses for lead octyl xanthate

	% Elements	Expected	Found
Lead octyl xanthate (C ₁₈ H ₃₄ O ₂ PbS ₄)	C	34.99	34.85
	H	5.55	5.56
	S	20.72	20.50
	Pb	33.56	33.45

The purity of the lead xanthate precursors were determined using micro–elemental analysis. This reveals the relative percentage of each element in the complex. The closeness of the theoretical (calculated) elemental percentages to the experimentally determined is used to assess the purity of the analysed complexes. The theoretical percentages of the prepared complexes were comparable to the results from the experiment. As can be seen from the results in Tables 4.3 - 4.6, all the lead xanthate precursors are relatively pure. The obtained results were also comparable to the work of other researches on xanthate precursors (Alam *et al.*, 2008; Barreca *et al.*, 2005; Clark *et al.*, 2011).

4.6 Mass Spectrometric (MS) Analyses of Lead Xanthate Precursors

In order to further characterize the structure of alkyl lead xanthates, mass spectrometric analyses were undertaken using positive and negative Electro Spray Ionisation (ESI) which is a ‘soft’ ionization technique in accordance with the literature (Barreca *et al.*, 2005).

Table 4.7: Mass spectra of lead xanthate precursors

Precursor	Electrospray ionization(positive)		Electrospray ionization(negative)	
	Base peak	Molecular ion peak	Base peak	Molecular ion peak
Lead ethyl xanthate	$2\text{CS}_2\text{Pb}^+$ (571)	$\text{C}_6\text{H}_{10}\text{O}_2\text{PbS}_4^+$ (450)	OCSPbCl^- (570)	-
Lead butyl xanthate	$2\text{OCS}_2\text{PbS}_2\text{COC}_2\text{H}_4\text{Na}^+$ (862)	-	$2\text{HC}_2\text{H}_4\text{OCS}_2\text{Pb}$ - (655)	$\text{C}_{10}\text{H}_{18}\text{O}_2\text{PbS}_4^+$ (506)
Lead hexyl xanthate	PbS_2CNa^+ (305)	$\text{C}_{14}\text{H}_{26}\text{O}_2\text{PbS}_4^+$ (562)	$\text{PbS}_2\text{COC}_5\text{H}_{10}^-$ (739)	-
Lead octyl xanthate	$2\text{OCSPbSCOC}_6\text{H}_{12}^+$ (823)	-	$\text{C}_8\text{H}_{17}\text{OC}^+$ (165)	$\text{C}_{18}\text{H}_{34}\text{O}_2\text{PbS}_4^+$ (618)

The fragments identified for the various alkyl lead xanthate precursors are shown in Table 4.7 above. The molecular ion peaks of the ethyl (450) and hexyl (562) lead xanthates appeared in the positive while those of butyl (506) and octyl (618) lead xanthates appeared in the negative ESI spectra. The appearance of dimers as base peaks confirms the polymeric nature of the xanthate precursors. The positive ESI had Na^+ as part of the base peak of the butyl and lead hexyl xanthate whereas Cl^- was observed in the base peak of lead ethyl xanthate (Fenn *et al.*, 1989). ESI ionization technique can activate several decomposition pathways in bis (O-alkylxanthate) compounds, due to

both ionization mechanisms and interaction with solvent that make the Pb–S bond weaker than in the solid or gas phase. This hypothesis was corroborated by the fact that preliminary decomposition experiments in an inert atmosphere from metal xanthate yielded the formation of M-S films at relatively low substrate temperatures of 0 °C, showing that the core structure of the precursor effectively represents the building-block for the solid- state structure of M-S (Barreca *et al.*, 2005). On this basis, it might be concluded that M–S moieties were relatively stable in the gas phase, thus indicating the suitability of metal xanthates as single-source precursors for M-S (Nair *et al.*, 2002).

KNUST

4.7 Thermogravimetric Analyses (TGA) of Lead Xanthate Precursors

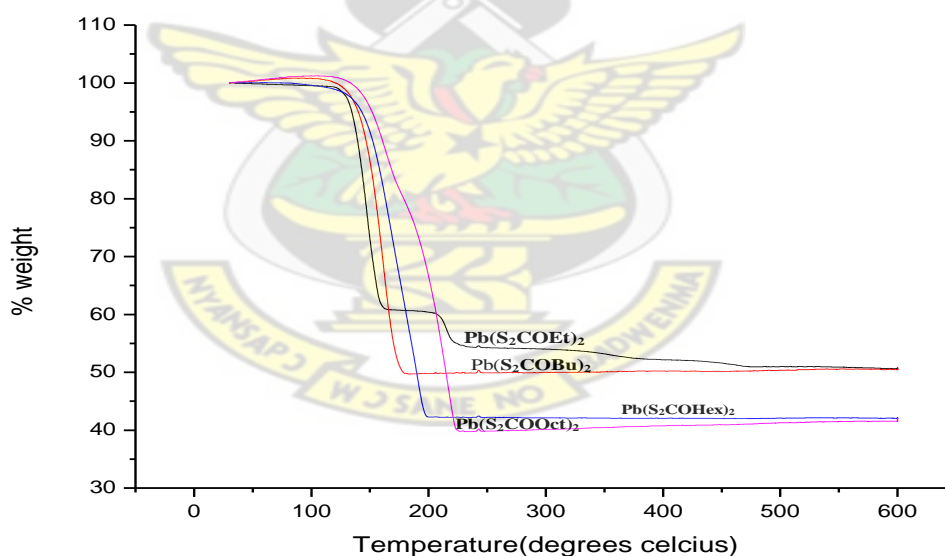


Figure 4.10: TGA graphs of lead xanthate precursors

The thermogravimetric curves that were recorded under nitrogen flow displayed a qualitatively similar trend for the different lead alkyl xanthate precursors. Nitrogen was used as the inert gas because of its availability and also the fact that decomposition

steps are not significantly influenced by the surrounding gaseous atmosphere employed (Pandey, 1988).

Thermogravimetric analysis (TGA) curves of the dialkyldithiocarbonatolead(II) are shown in Figure 4.10 above. The TGA results revealed that butyl, hexyl and lead octyl xanthate showed clean, one-step decomposition. The two step decomposition pathway observed in lead ethyl xanthate could be attributed to the relatively short alkyl chain (Clark *et al.*, 2011). Decomposition temperature and observed final residue along with onset and offset temperatures are given in Table 4.8 below. All experimental and calculated values are in good agreement with the formation of PbS. Generally, an increase in alkyl group caused an increase in the offset temperature. Also the low decomposition temperatures make metal xanthates suitable single source precursors for the melt method. Higher experimental residue percentages were observed for butyl and octyl lead xanthates whereas the lower experimental residue percentages were observed for ethyl and hexyl lead xanthates (Clark *et al.*, 2011). The differences in theoretical and experimental percentages of the PbS were acceptable based on literature (Akhtar *et al.*, 2011; Clark *et al.*, 2011).

Table 4.8: TGA data for lead xanthate precursors

Precursor	% PbS residue (calculated)	% PbS residue (found)
Ethyl lead xanthate	53.21	50.20
Lead butyl xanthate	47.30	50.34
Lead hexyl xanthate	42.58	42.02
Lead octyl xanthate	38.71	42.37

4.8 Differential Scanning Calorimetry (DSC) of Lead Xanthate Precursors

Information about the physical and chemical changes that involves endothermic and exothermic changes in heat capacity was determined using differential scanning calorimetry (DSC). DSC monitors heat effects associated with phase transitions and chemical reactions as a function of temperature. In a DSC the difference in heat flow to the sample and a reference at the same temperature, is recorded as a function of temperature. The reference is an inert material such as alumina, or just an empty aluminium pan. The temperature of both the sample and reference are increased at a constant rate (Cooper, 2000; Tip, 2000). The maximum temperature was chosen based on the TGA plots of the lead alkyl xanthates

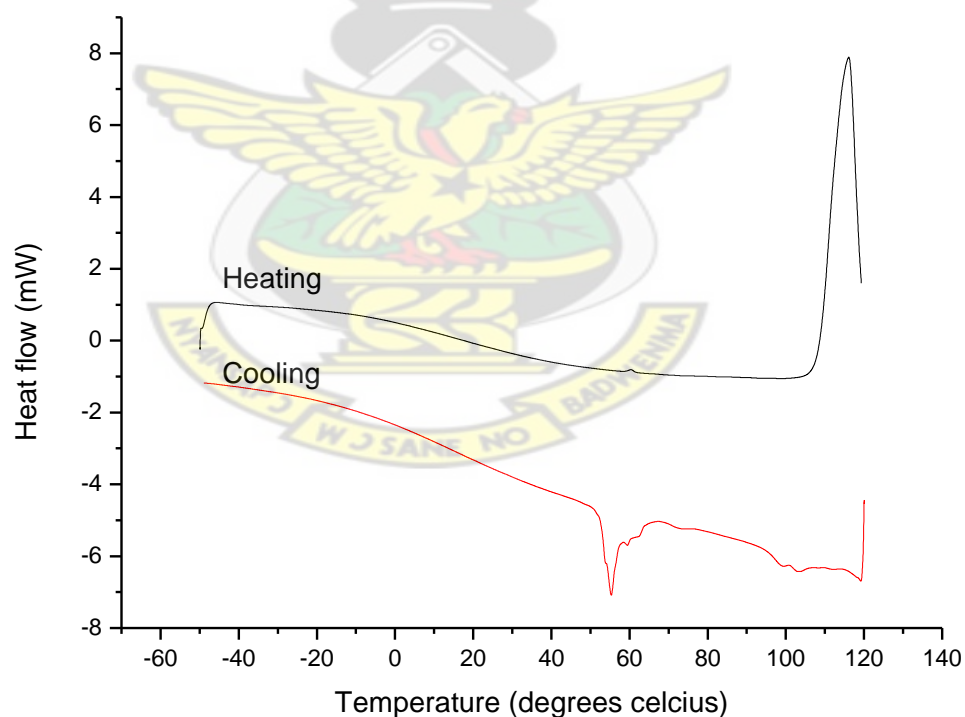


Figure 4.11: DSC of lead ethyl xanthate

The exothermic curve for lead ethyl xanthate revealed a single peak. This peak was the melting temperature (T_m) at 116 °C. At this temperature, the sample changes phase

from the solid state into an amorphous state. The enthalpy of the process is given by the area under the peak (Cooper, 2000). From the thermogram, the enthalpy of fusion of lead ethyl xanthate was found to be 33.35 J/g. The sample crystallized at 55.31 °C at an enthalpy of -11.34 J/g as calculated from the cooling or endothermic curve.

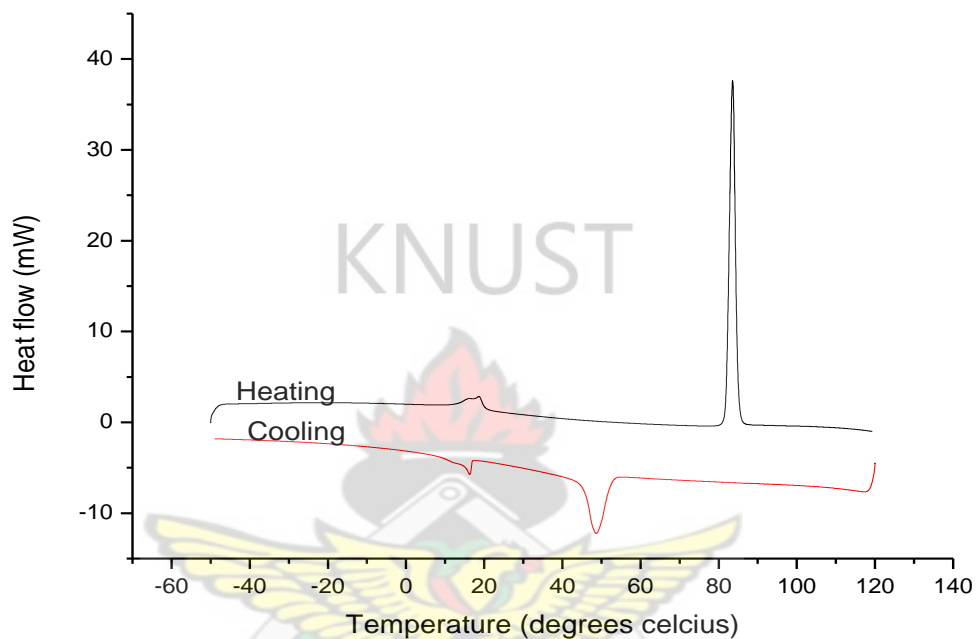


Figure 4.12: DSC of lead butyl xanthate

The exothermic curve of lead butyl xanthate showed two thermal transitions. These are the glass transition (T_g) and melting temperature (T_m). The first peak can be the T_g whereas the second peak is the T_m . The T_m occurred at 83.55 °C at an enthalpy of 35.308 J/g. The cross linking and T_c occurred at 48.68 °C and 16.30 °C corresponding to enthalpies of -14.986 J/g and 1.816 J/g respectively.

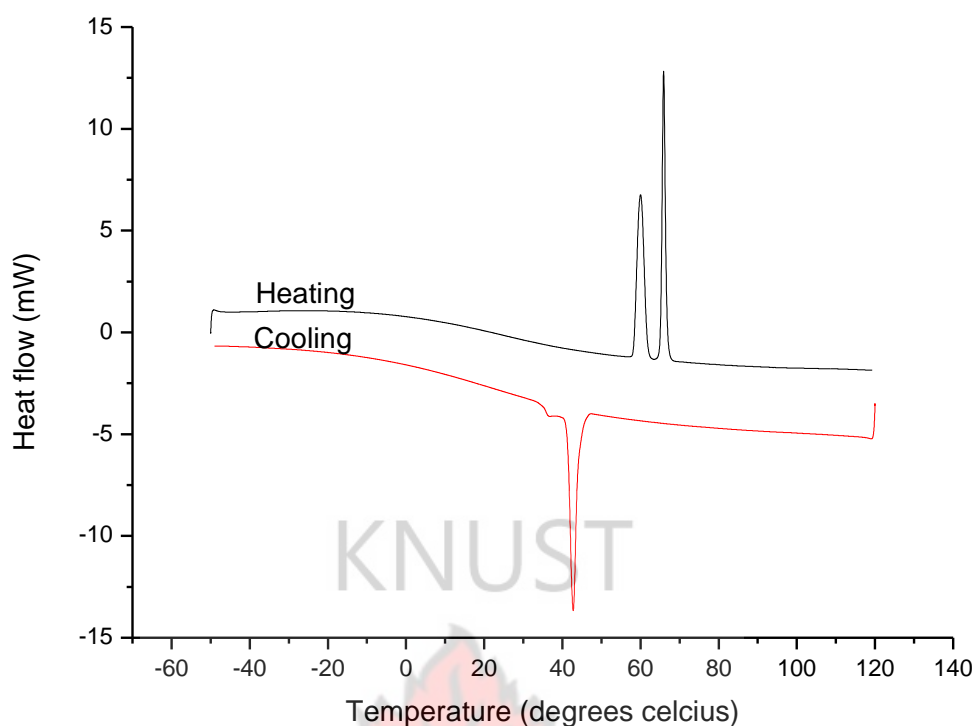


Figure 4.13: DSC of lead hexyl xanthate

Lead hexyl xanthate showed two sharp peaks for T_m at $60.01\text{ }^\circ\text{C}$ and $65.91\text{ }^\circ\text{C}$ in the exothermic curve. The first peak appears as an apparent melting at the glass transition temperature. This peak may have resulted from stresses built in the precursor as a result of processing, handling or thermal history released when it was heated through its T_g . The reason this occurred at the T_g is that the precursor went from a rigid to flexible structure and thus can move to release the stress (Thomas, 2000). The corresponding enthalpies were 35.163 and 30.025 J/g respectively. However the sample crystallized at $42.78\text{ }^\circ\text{C}$ with an enthalpy of -47.634 J/g .

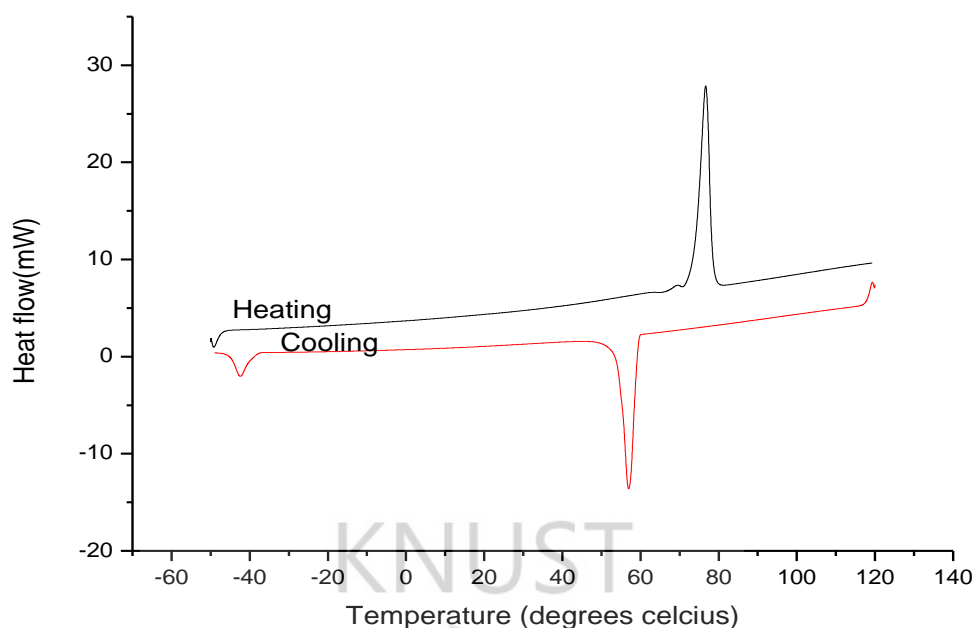


Figure 4.14: DSC of lead octyl xanthate

At 66.68 °C, lead octyl xanthate showed T_g at a heat capacity of 0.748 J/g°C. Below the glass transition temperature, the polymer exists in a hard, rigid, brittle, glassy state in which the molecules are held together tightly by intermolecular forces and the motion of the polymer molecules is restricted to molecular vibrations. As the polymer is heated the molecules acquire thermal energy. At the glass transition temperature, T_g, the molecules have enough energy to partially overcome the intermolecular forces, and they have more freedom of movement. The amorphous region now becomes rubbery, and the polymer becomes soft and flexible. The T_m occurred at 76.69 °C with a sharp peak with enthalpy of 63.0718 J/g. The melt crystallized out at 56.95 °C. The appearance of T_g in lead octyl xanthate confirms the polymeric nature of metal xanthates (Nair *et al.*, 2002).

4.9 Crystal Structure of Lead Hexyl Xanthate ([Pb(S₂COHex)₂])

Crystals of [Pb(S₂COHex)₂] suitable for X-ray crystallographic studies were obtained by slow diffusion of diethylether into an acetone solution of the precursor at room temperature. The molecular structure of the compound is shown in Figure 4.15 below, and selected bond lengths and angles are given in Table 4.9 below. The crystalline phase of the compounds belongs to the monoclinic space group with Cc. Apart from the differing alkyl constituents of the molecules, the crystal structure core is similar to those reported in the literature for ethyl and lead butyl xanthates (Hagihara and Yamashita, 1966; Hagihara, *et al.*, 1968). Each lead atom is surrounded by four sulphur atoms, two from each chelating xanthate ligands. The structure can be described as based on a distorted square pyramidal with the four sulphur atoms forming the base of the square and the lone pair occupying the pyramidal position. The bond distances between the Pb and the 4 S atoms are not very different as depicted in Table 4.10.

4.9.1 Crystal Structure Data for [Pb(S₂COHex)₂]

Table 4.9: Crystal data for Pb(S₂COHex)₂]

Chem formula	C ₁₄ H ₂₆ O ₂ PbS ₄
Formula wt	561.78
Cryst syst	Monoclinic
Space group	Cc
a(Å)	44.540(3)
b(Å)	4.1956(3)
c(Å)	10.8338(7)
α(deg)	90
β(deg)	101.752(3)
γ(deg)	90
V(Å ³)	1982.1(2)
Z	4
D _{calcd} (mg m ⁻³)	1.883
μ(Mo Kα) (mm ⁻¹)	20.496
R1 (I>2σ(I)) ^b	0.1176
wR2 (all data)	0.2807
GOF on F ²	1.416

Table 4.10: Selected bond lengths (Å) and bond angles (°) from the single crystal structure of [Pb(S₂COHex)₂]

C(1)-S(1)	1.728(17)
C(1)-S(2)	1.654(19)
Pb(1)- S(2)	2.847(4)
Pb(1)- S(1)	2.811(5)
Pb(1)-S(4)	2.799(4)
Pb(1)-S(3)	3.020(5)
C(8)- S(4)	1.685(19)
C(8)- S(3)	1.63(2)
O(1)-C(1)-S(2)	117.0(13)
O(1)-C(1)-S(1)	118.4(14)
S(2)-C(1)-S(1)	124.4(10)
S(3)-C(8)-S(4)	128.6(11)
S(4)-Pb(1)-S(2)	81.70(12)
S(1)-Pb(1)-S(3)	91.61(13)
S(2)-Pb(1)-S(3)	132.93(14)
S(4)-Pb(1)-S(1)	98.04(13)
S(4)-Pb(1)-S(3)	61.64(12)
S(1)-Pb(1)-S(4)	63.84(12)
O(2)-C(8)-S(3)	119.8(14)
O(2)-C(8)-S(4)	111.3(14)

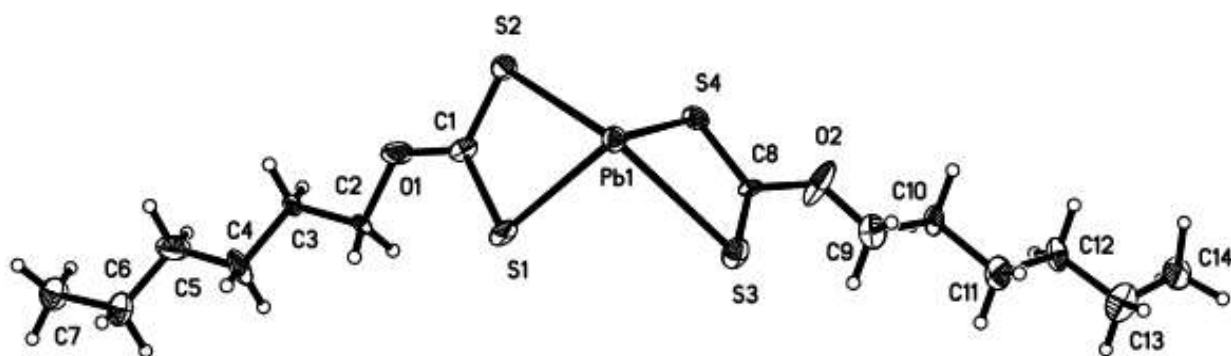


Figure 4.15: Crystal structure of lead hexyl xanthate

4.10 X-ray Diffraction (XRD) of the as-prepared PbS Nanoparticles

X-ray diffraction (XRD) showed several diffraction peaks at 2θ values of 25.90, 30.09, 43.08, 51.00, 53.39, 62.56, 68.91, 70.97 and 78.97. These were assigned to the diffraction lines produced by (1 1 1), (2 0 0), (2 2 0), (3 1 1), (2 2 2), (4 0 0), (3 3 1), (4 2 0) and (4 2 2) planes of the face-centered cubic (fcc) structure of PbS (ICDD No. 01-077-0244 and 01-078-1901). The cubic PbS from xanthates confirms the reports in literature (Akhtar *et al.*, 2011; Liu *et al.*, 2005; Sun *et al.*, 2011). The as-prepared PbS had a rock salt structure. The dominant and sharp peaks indicated that PbS nanocrystals were highly crystalline (Barote *et al.*, 2011). The strong (2 0 0) peak suggests (100) oriented growth.

Since the major factors that control the growth of nanoparticles using self-capped single source precursors are time and temperature, this research sought to exploit both factors.

4.10.1 Effect of Temperature on the as-prepared PbS Nanoparticles

The effect of temperature was monitored by performing the melt experiment at constant time and varying temperature from 150, 175, 200 °C for each of the four lead xanthate single source precursors. The temperature was varied based on the degradation pattern of the thermogravimetric analyses results.

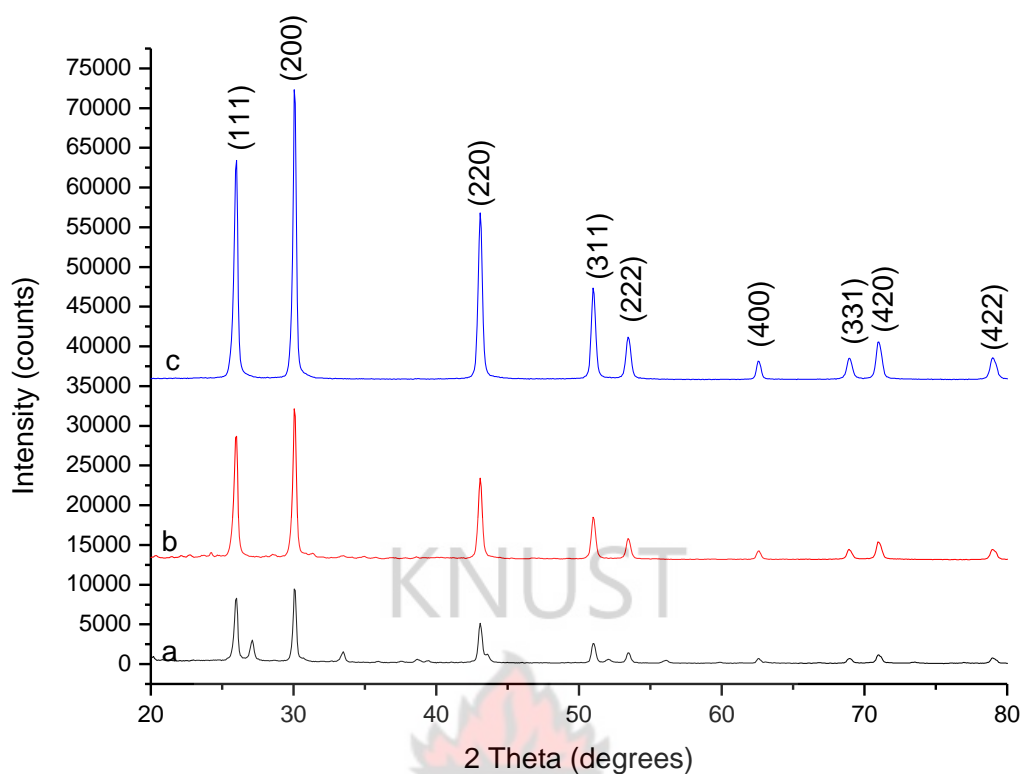


Figure 4.16: XRD patterns of PbS nanoparticles obtained from the decomposition of lead ethyl xanthate at (a) 150, (b) 175 and (c) 200 °C.

The XRD pattern of lead ethyl xanthate is showed in Figure 4.16 above. At 150 °C although the XRD pattern showed a cubic PbS phase there were other peaks from the precursor due do incomplete decomposition. This proves that 150 °C was a low temperature for the decomposition of lead ethyl xanthate to yield PbS nanoparticles. However, increasing the temperature from 150 to 175 °C produced a pure cubic PbS phase. This resulted from the crystal sinter getting bigger and some defects on the crystal plane (100) which have low coordination and hence diffuse into a more stable plane. Increasing the temperature further to 200 °C increased the intensity of the peaks thereby increasing the size of the nanoparticles. The most intense phase for the three different temperatures was the (2 0 0) phase whereas the least intense peak was the (4 0 0) phase. Increase in intensity implies an increase in the number of particles along

that plane. The calculated particle sizes at 175 and 200 °C were 26.43 and 27.03 nm respectively. This makes 175 °C the optimum temperature for growth of cubic PbS from lead ethyl xanthate using the solventless method although the calculated particle size is similar to that of 200 °C. Clark *et al.*, (2011) have successfully synthesised PbS nanocubes with size of 200 nm from lead ethyl xanthate using AACVD at 350 °C. The size of 200 nm may have resulted from the relatively high temperature since nanoparticles tend to agglomerate at high temperatures. Also the time for synthesis might have contributed to the size since the time was not mentioned in the report of the researchers. On the contrary, the melt method can be used in place of AACVD at temperatures as low as 175 °C.

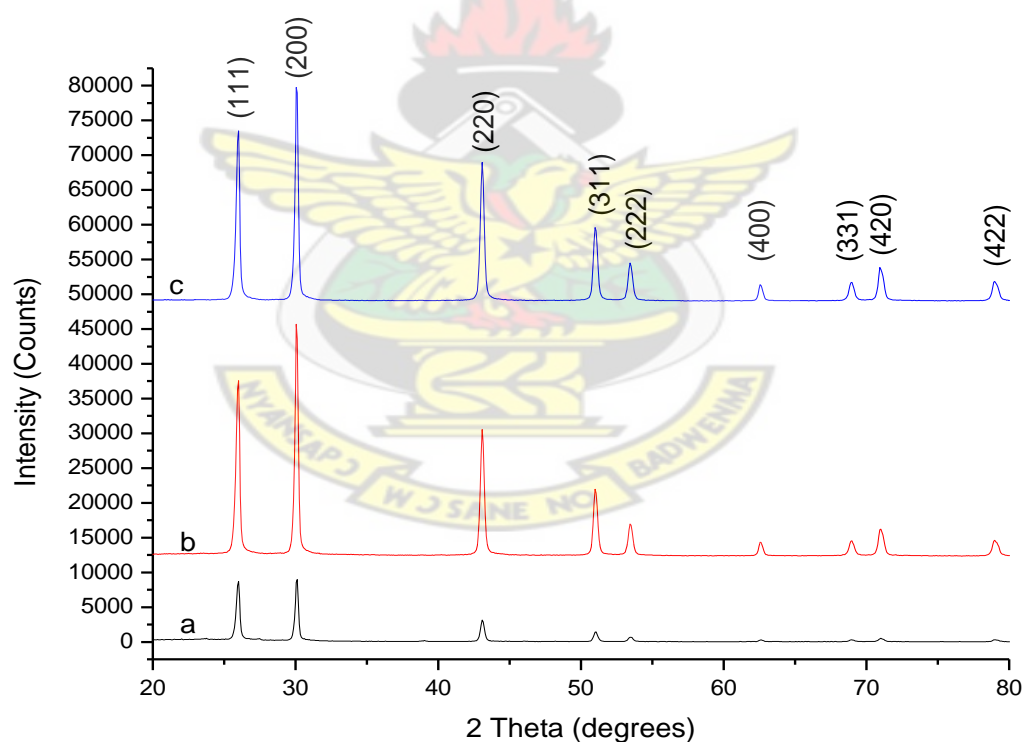


Figure 4.17: XRD patterns of PbS nanoparticles obtained from the decomposition of lead butyl xanthate at (a) 150, (b) 175 and (c) 200 °C.

Lead butyl xanthate decomposed at 150 °C and showed a pure cubic PbS phase. The intensities of the (1 1 1) and the (2 0 0) were almost similar. However, decomposition

at 175 and 200 °C, yielded peaks with bigger particle sizes as evident in the nature of the peaks. The peaks at these two temperatures were similar. Both temperatures had (2 0 0) and (4 0 0) phases as the most and least intense peaks in the pattern respectively. This analysis also confirms 150 °C as the optimum temperature for the synthesis of PbS from lead butyl xanthate using the melt method.

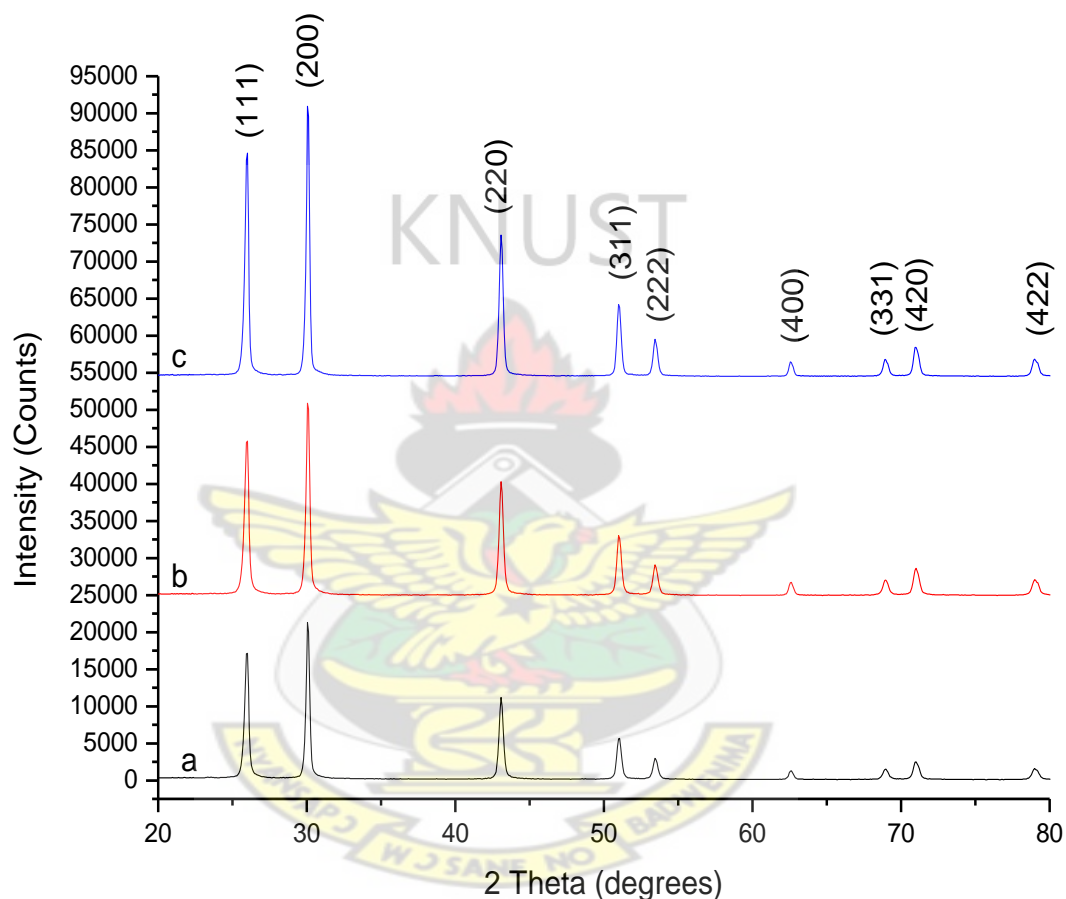


Figure 4.18: XRD patterns of PbS nanoparticles obtained from the decomposition of lead hexyl xanthate at (a) 150, (b) 175 and (c) 200 °C.

An increase in alkyl group of self-capped single source precursors increases the capping efficiency of the precursor. Lead hexyl xanthate decomposed at the three temperatures to produce pure cubic PbS phases without any impurities from the precursor or phases with low coordination. The difference between the three peaks was

in the intensity of the (2 0 0) peaks. As the temperature increased from 150 to 200 °C most of the nanoparticles were aligned on the (2 0 0) plane making it the most prominent phase.

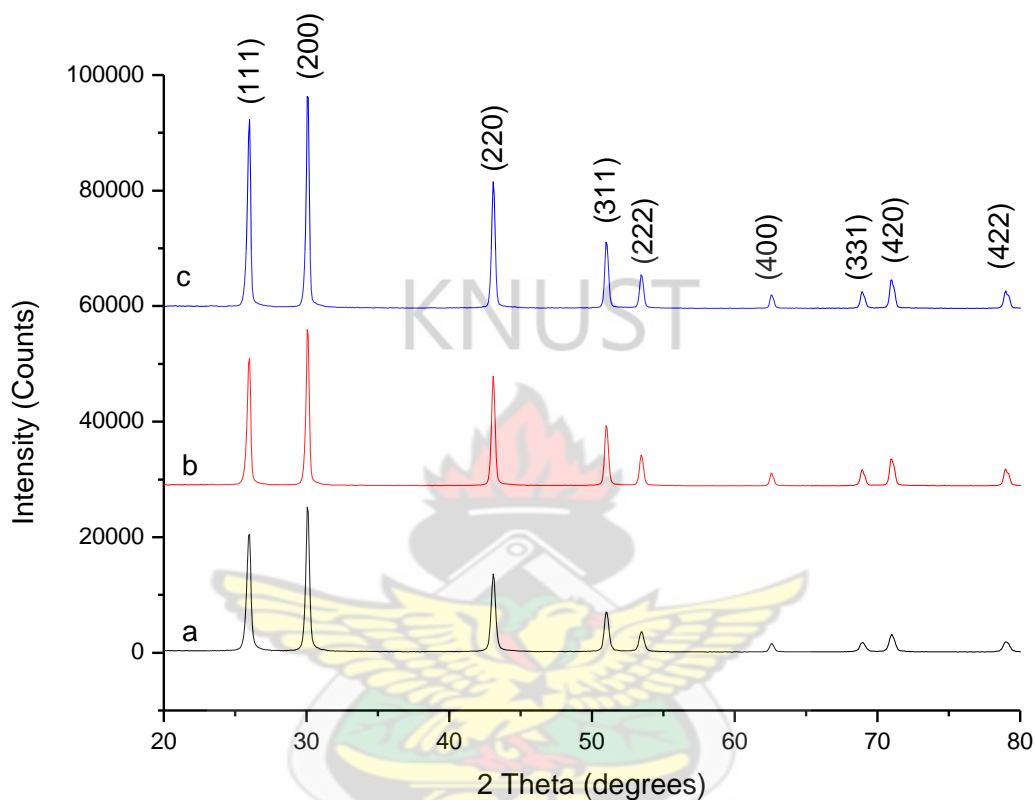


Figure 4.19: XRD patterns of PbS nanoparticles obtained from the decomposition of lead octyl xanthate at (a) 150, (b) 175 and (c) 200 °C.

Lead octyl xanthate also produced clean peaks corresponding to a pure cubic PbS phase. The (2 0 0) phase was the most intense phase and this proves that the as-prepared nanoparticles were highly crystalline. 150 °C was the optimum temperature for the synthesis of PbS from lead octyl xanthate single source precursors. The size of the PbS nanoparticles at this temperature was 23.32 nm. The size increased to 23.36 and 23.92 nm with the corresponding increase in temperature to 175 and 200 °C. Although increasing the temperature causes agglomeration in the synthesis of

nanoparticles, there was not much significant change in the particle size due to the efficient capping activity of the octyl alkyl group.

4.10.2 Effect of Time on the as-prepared PbS Nanoparticles

Effect of time was monitored by performing the melt experiment at a constant temperature of 175 °C at 5, 15, 30 and 60 minutes. 175 °C was chosen as a temperature to monitor the effect of time because it was the optimum temperature for the formation of particles with required sizes and phase characteristics for all the lead xanthate precursors.

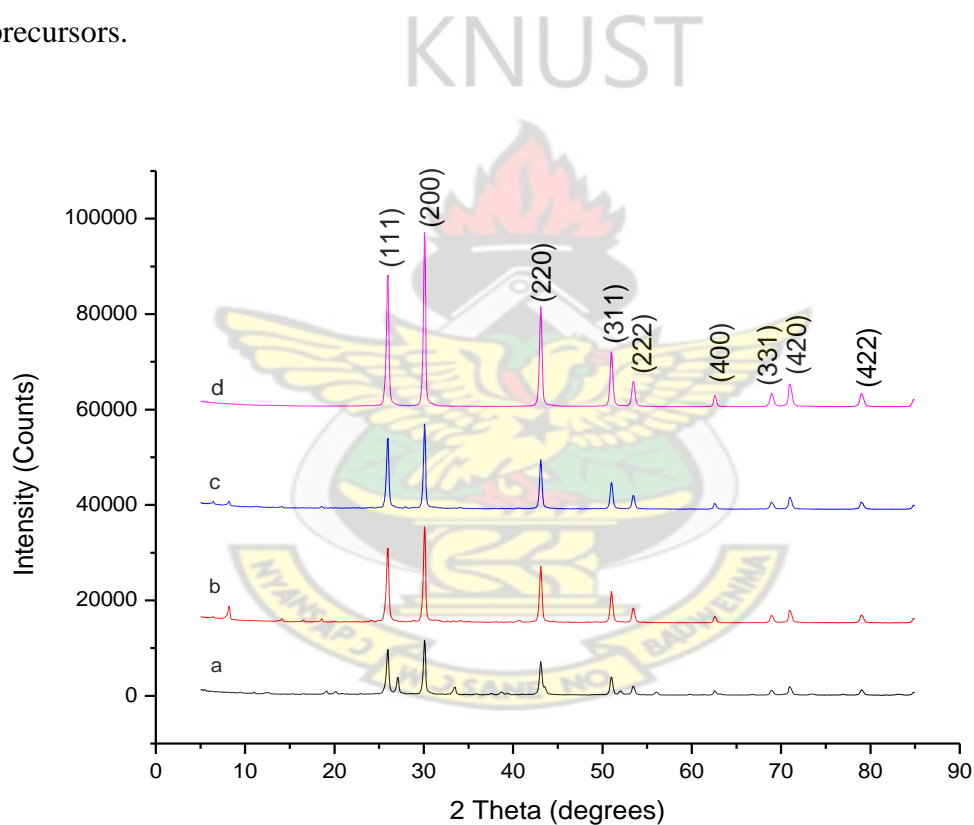


Figure 4.20: XRD patterns of PbS nanoparticles obtained from the decomposition of lead ethyl xanthate at 175 °C at (a) 5, (b) 15, (c) 30 and (d) 60 minutes.

The XRD patterns of the black precipitate obtained after the melt experiment showed predominantly cubic PbS peaks. At 5 minutes reaction time, two peaks appeared at 2 theta values of ~26 and 33 which may have resulted from incomplete decomposition of

the lead ethyl xanthate precursor. These two peaks disappeared at 15 minutes reaction time. Increasing the time further to 30 and 60 minutes resulted in a clean and pure cubic PbS phase. The intensity of the (2 0 0) and (2 2 0) phase peaks at 30 minutes reaction time almost doubled at 60 minutes reaction time as shown in Figure 4.20 above.

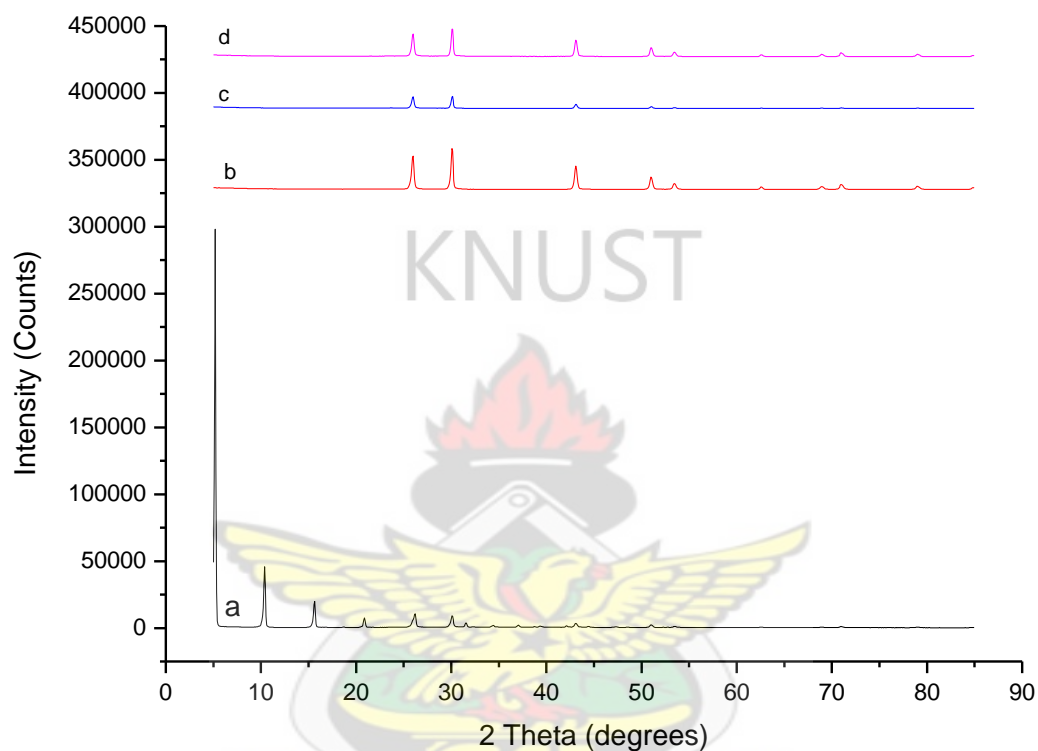


Figure 4.21: XRD patterns of PbS nanoparticles obtained from the decomposition of lead butyl xanthate at 175 °C at (a) 5, (b) 15, (c) 30 and (d) 60 minutes.

Lead butyl xanthate decomposed at 15, 30 and 60 minutes reaction time at 175 °C showed pure PbS peaks without any interference of precursor peaks as depicted in Figure 4.21. However, at 5 minutes, different peak patterns were observed. These peaks may have resulted from incomplete decomposition of the precursor at that temperature.

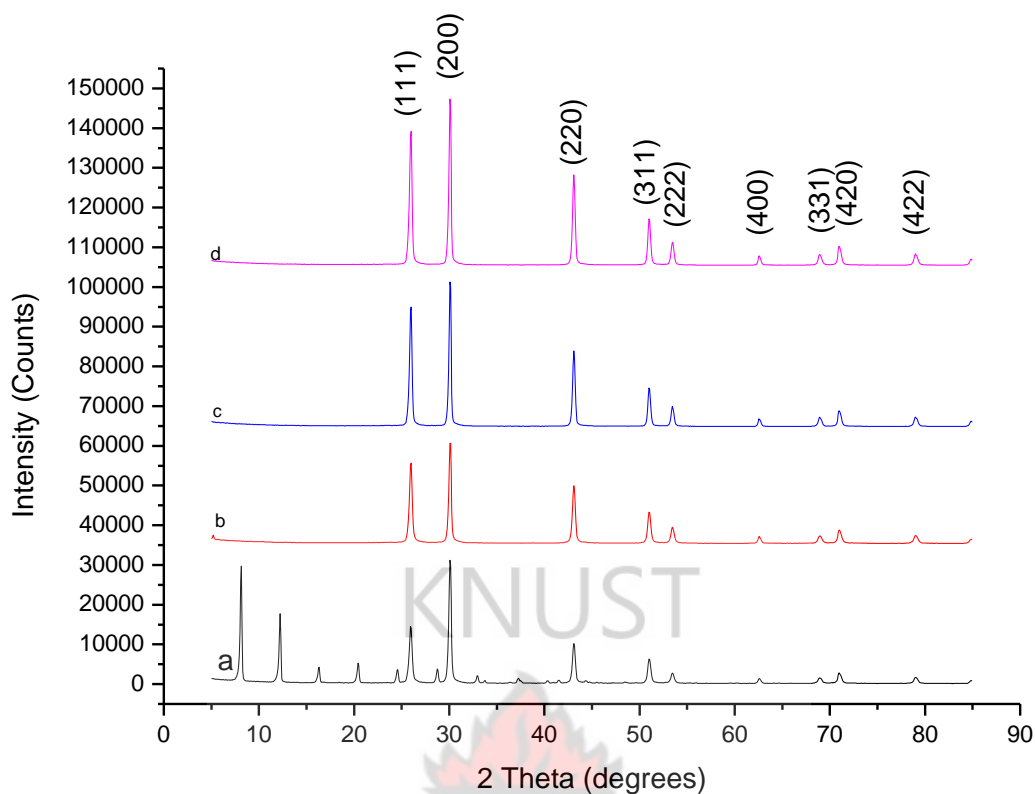


Figure 4.22: XRD patterns of PbS nanoparticles obtained from the decomposition of lead hexyl xanthate at 175 °C at (a) 5, (b) 15, (c) 30 and (d) 60 minutes.

Although lead hexyl xanthate decomposed at 5 minutes showed peaks corresponding cubic PbS, there were a lot of precursor peaks as a result of incomplete decomposition. This makes 5 minutes an unfavourable time for the decomposition of lead hexyl xanthate at 175 °C using the melt method as shown in Figure 4.22. At 15 minutes reaction time, there was complete decomposition resulting in a pure cubic PbS phase. Increasing the time further from 30 minutes through to 60 minutes only increased the intensity of the peaks with the (2 0 0) becoming the most prominent phase.

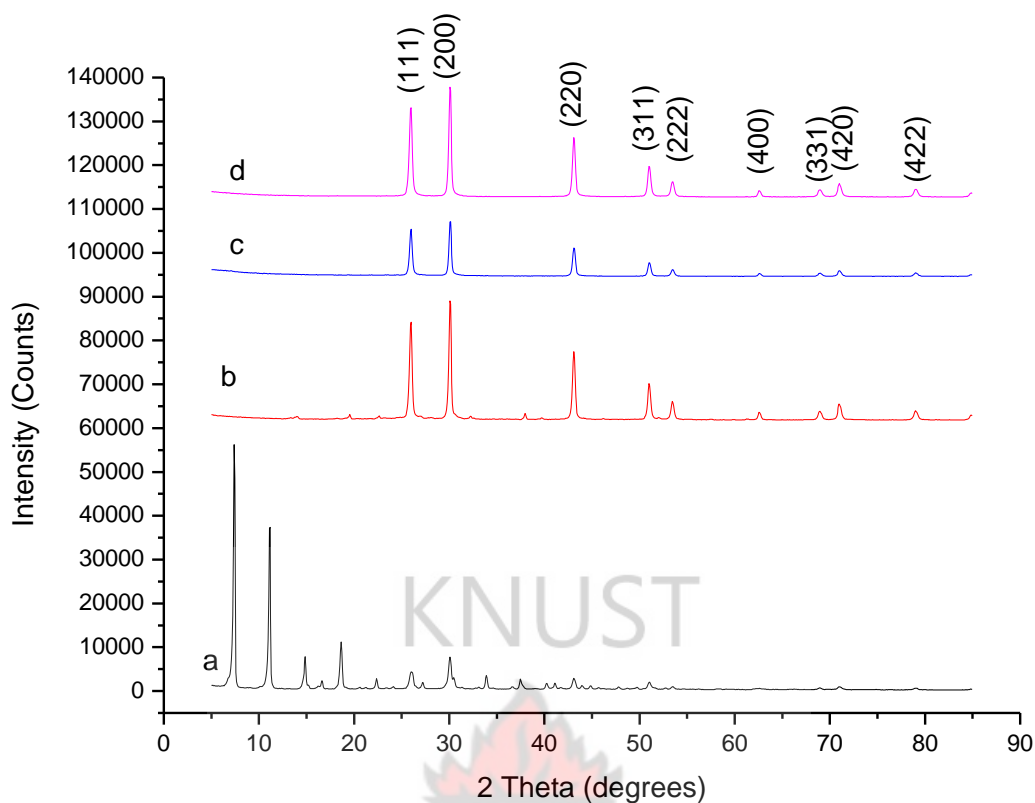


Figure 4.23: XRD patterns of PbS nanoparticles obtained from the decomposition of lead octyl xanthate at 175 °C at (a) 5, (b) 15, (c) 30 and (d) 60 minutes.

Lead octyl xanthate decomposed at 5 minutes yielded peaks which were not similar to PbS but rather to incomplete decomposed precursor as shown in Figure 4.23. At 15 minutes of reaction time, the observed peaks were predominantly PbS peaks however there small additional peaks from the precursor. Decomposing the precursor further to 30 minutes resulted in a pure cubic PbS peaks with no additional peaks. At 60 minutes, there was only an increase in intensity of the (2 0 0) phase. This implies that increasing time at a constant temperature only results in most of the particles aligning on the (2 0 0) plane.

4. 11 Scanning Electron Microscopy (SEM) of the as-prepared PbS Nanoparticles

A scanning electron microscope (SEM) is a type of electron microscope that produces images of a sample by scanning it with a focused beam of electrons. The electrons interact with electrons in the sample, producing different signals that can be detected and that contain information about the sample's surface topography and composition.

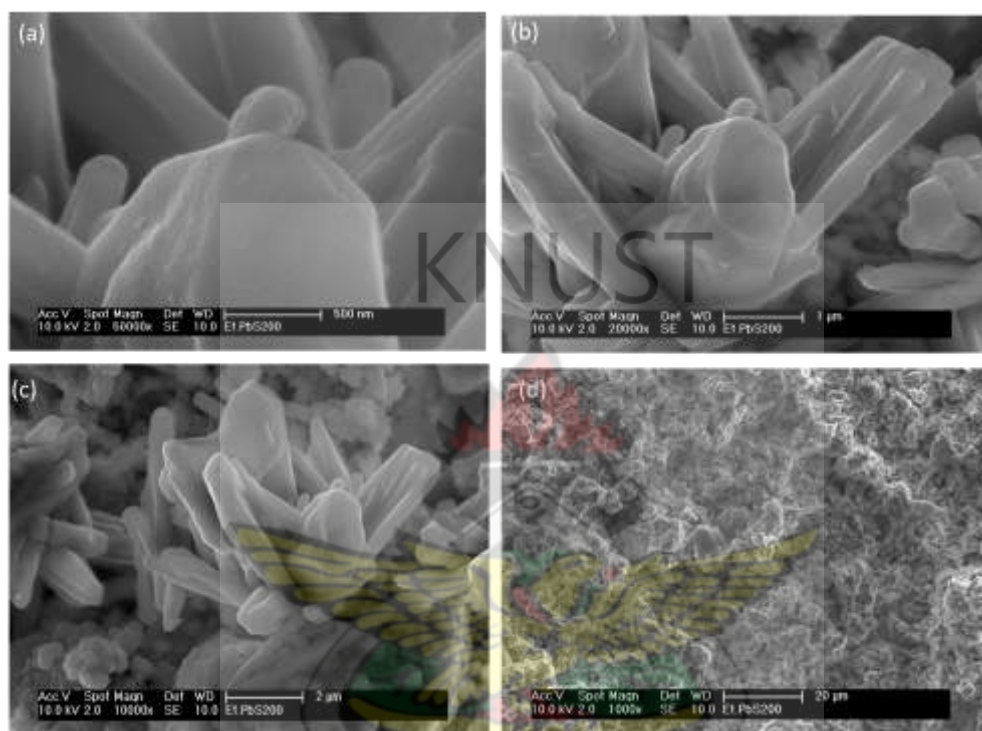


Figure 4.24: SEM images of PbS obtained from lead ethyl xanthate at (a) 50,000 (b) 20,000 (c) 10,000 and (d) 1,000 X magnifications

The surface morphology of the as-prepared PbS nanoparticles from lead ethyl xanthate decomposed at 200 °C was determined by scanning electron microscopy are shown in Figure 4.24 above.

The micrographs were obtained at 50,000, 20,000, 10,000 and 1,000 x magnifications. The growth of the nanoparticles was observed to be a rosette-like structure. Clark *et al.*, (2011) have reported on the synthesis of PbS from lead ethyl xanthate using AACVD at

350 °C. SEM micrographs revealed a growth towards cubic PbS. The factors that affect the morphology of nanoparticles are:

- (i) Temperature
- (ii) Time
- (iii) Capping agent
- (iv) Method for synthesis

The growth towards rosette-like morphology can be partially justified by the nucleation of fresh PbS particles during the growth process (Barote *et al.*, 2011). Also the relatively short alkyl chain could contribute to the different morphology since the alkyl group served as the capping agent. The temperature (200 °C) can contribute to the morphology since increase in temperature can result in different morphologies. The solventless approach to PbS nanoparticles have been reported to reveal strikingly unique morphologies (Chen *et al.*, 2007)

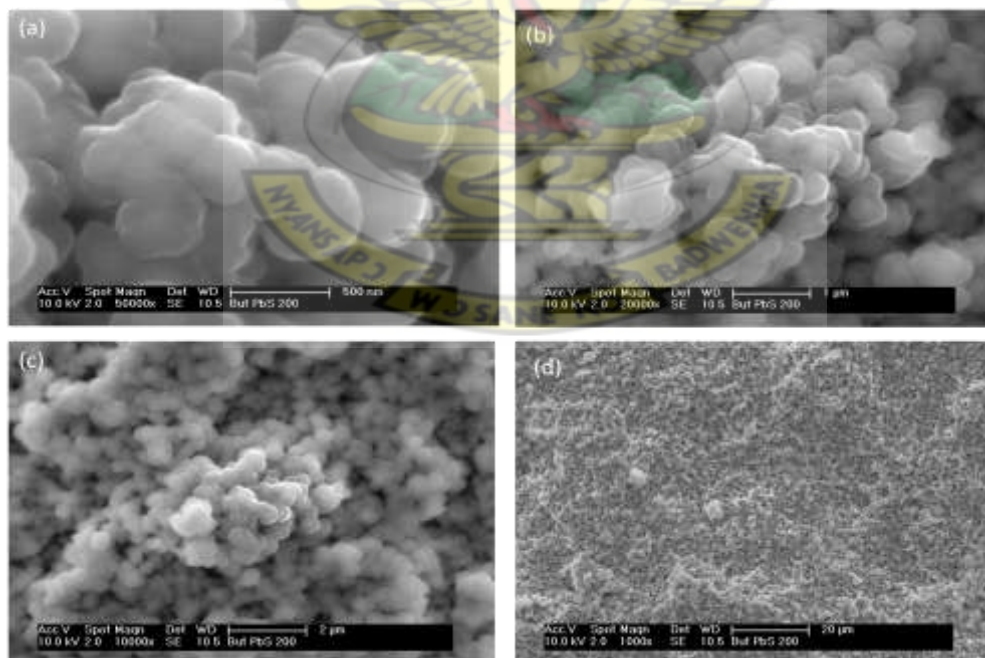


Figure 4.25: SEM images of PbS obtained from lead butyl xanthate at (a) 50,000 (b) 20,000 (c) 10,000 and (d) 1,000 X magnifications

The micrographs from the decomposition of lead butyl xanthate revealed a closed packed spherical morphology. The different morphology from the PbS obtained from lead ethyl xanthate could result from the difference in the starting alcohols. The precursors are self-capped hence the difference in starting materials results in differences in capping activities.

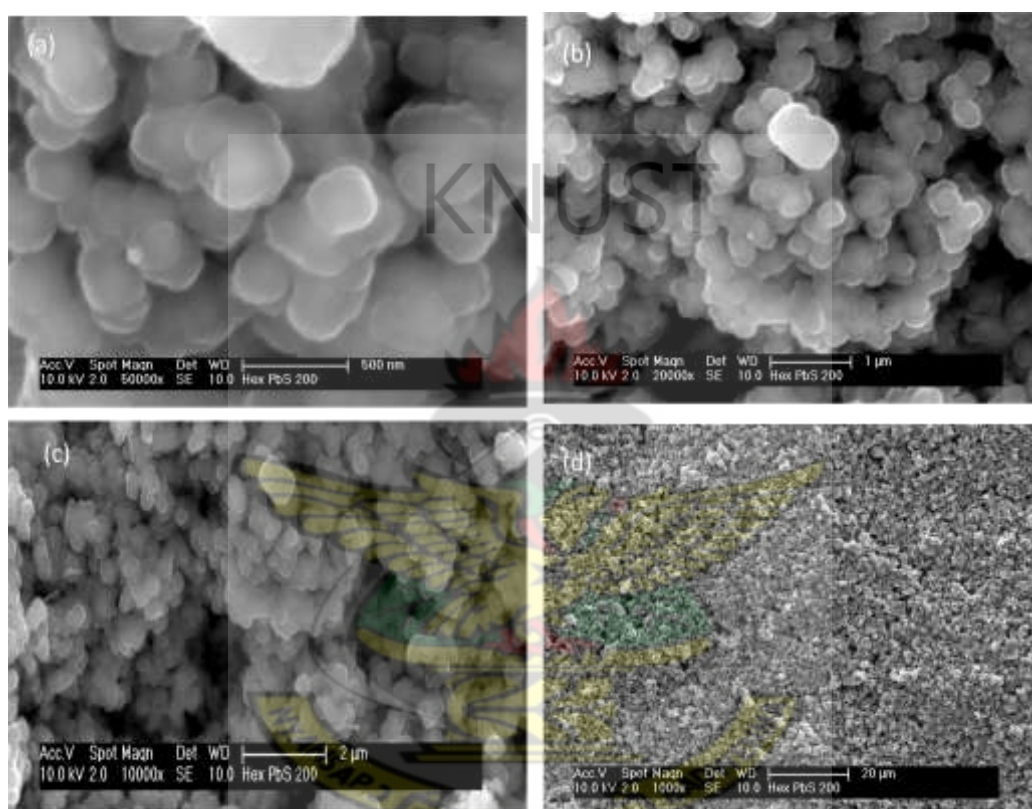


Figure 4.26: SEM images of PbS obtained from lead hexyl xanthate at (a) 50,000 (b) 20,000 (c) 10,000 and (d) 1,000 X magnifications

Increasing the alkyl chain length for the starting alcohol to hexanol yielded densely packed spherical morphology of the as-prepared PbS nanoparticles as shown in Figure 4.26.

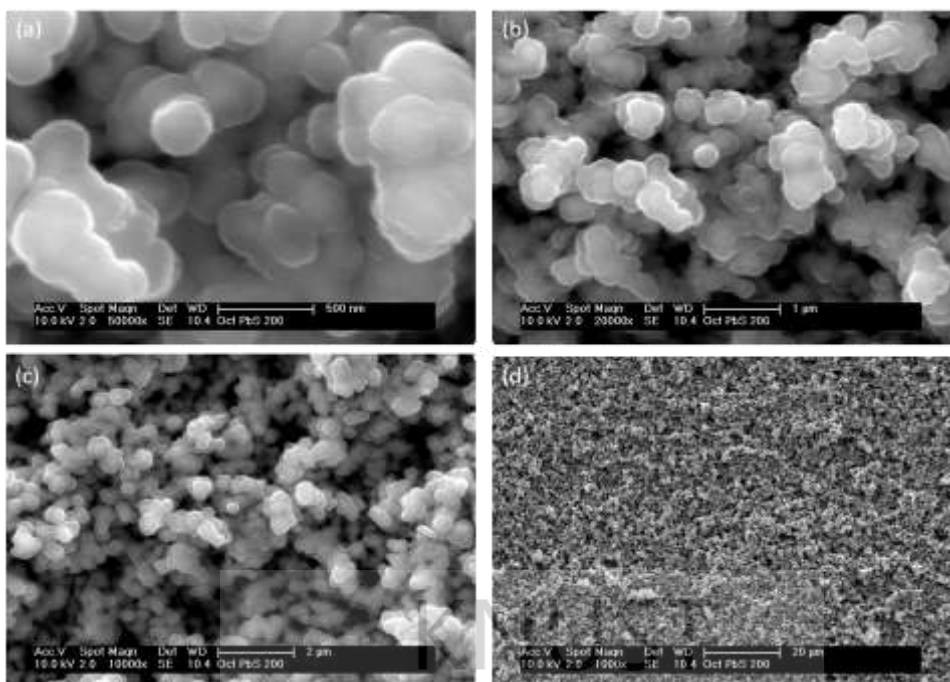


Figure 4.27: SEM images of PbS obtained from lead octyl xanthate at (a) 50,000 (b) 20,000 (c) 10,000 and (d) 1,000 X magnifications

Changing the starting alcohol to octanol also resulted in closely packed spherical morphology. As the alkyl chain increases from butyl to octyl, there is little or no effect of capping agent on the morphology using self-capped precursors in the solventless method.

4.12 Energy Dispersive X-ray (EDX) of the as-prepared PbS Nanoparticles

The associated analytical facility of Energy Dispersive X-Ray (EDX) analysis was used to identify and quantify the elemental composition of the as-prepared nanoparticles. EDX examinations of these residues also provided evidence for the purity of the samples and revealed emission due exclusively to lead and sulphur atoms within the detection limits of the equipment.

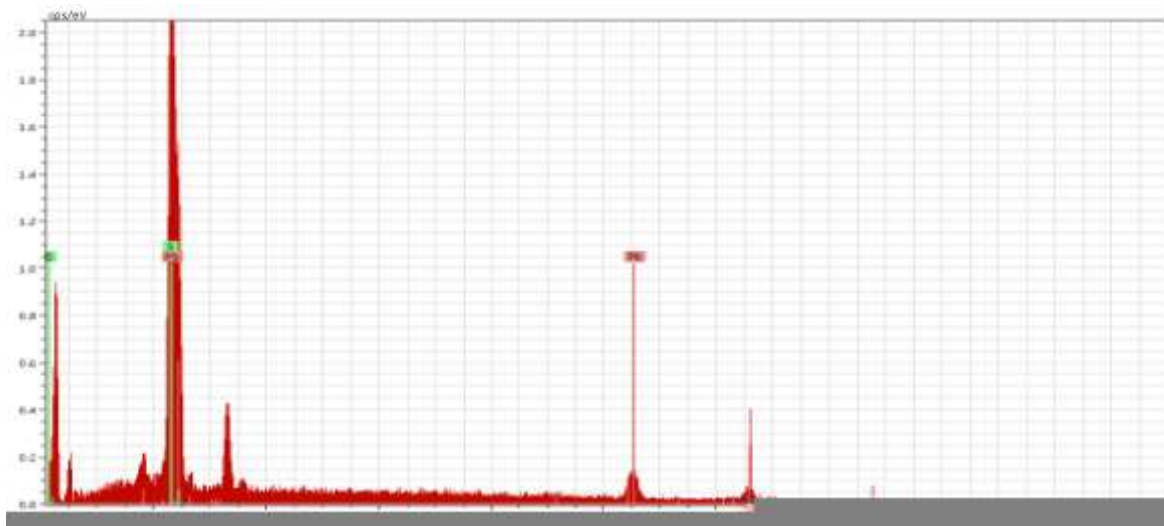


Figure 4.28: EDX for PbS obtained from lead ethyl xanthate

The elemental composition of the black product obtained from the decomposition of lead ethyl xanthate comprised of Pb and S atoms of 49.94 % and 50.06 % respectively.

The ratio of Pb:S was approximately equal to the literature stoichiometry.

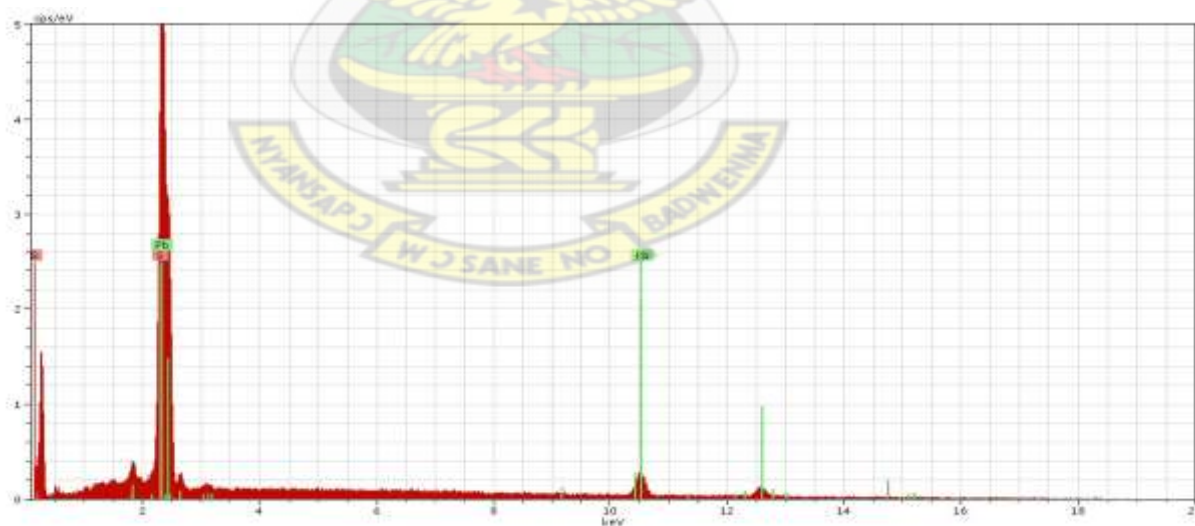


Figure 4.29: EDX for PbS obtained from lead butyl xanthate

The quantification of the Pb and S atoms from the decomposed product from lead butyl xanthate was 53.27 % and 46.73 % respectively. The decomposed product was slightly

Pb-rich. This might have resulted in the lost of some volatile sulphides during the decomposition process.

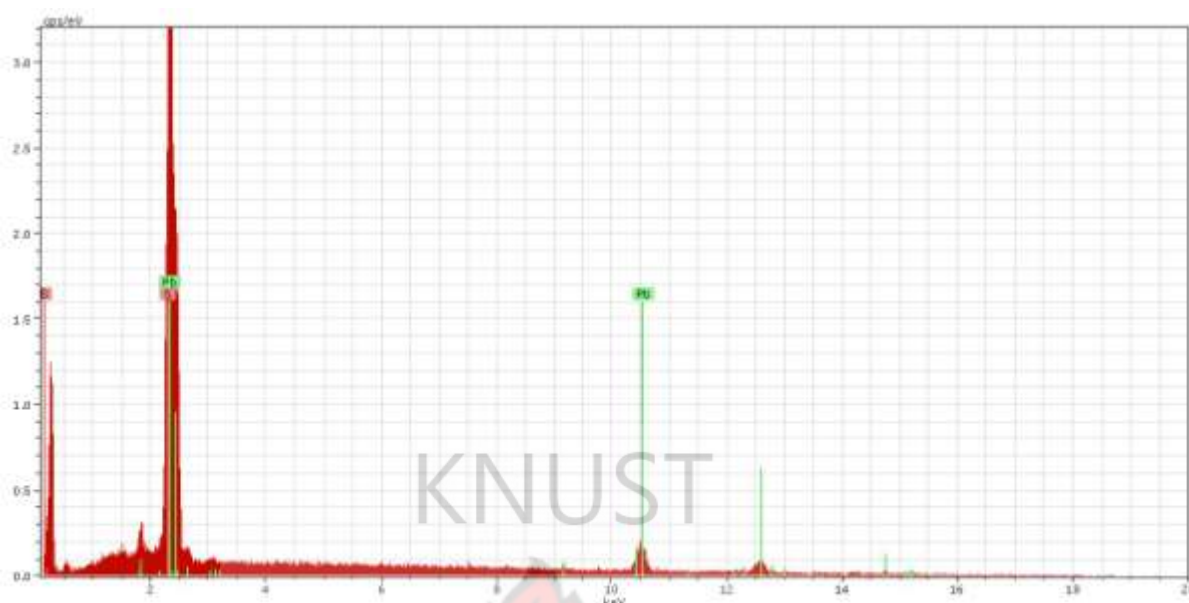


Figure 4.30: EDX for PbS obtained from lead hexyl xanthate

Increasing the alkyl chain to hexyl produced a Pb-rich growth at percentages of 53.27 and 46.73 for Pb and S respectively.

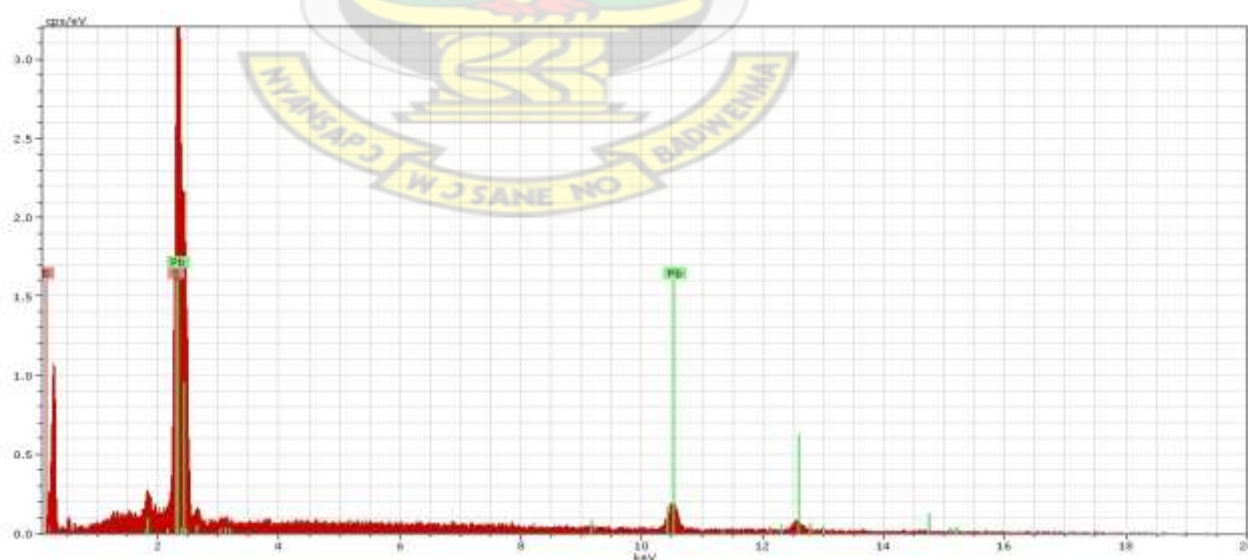


Figure 4.31: EDX for PbS obtained from lead octyl xanthate

Changing the precursor to lead octyl xanthate produced PbS nanoparticles with Pb having 54.05% and S at 45.95 %. Increasing the alkyl group from butyl demonstrated a growth towards Pb-rich nanoparticles. It confirms that the films are lead (Pb) rich (Barote *et al.*, 2011).

4.13 Transmission Electron Microscopy (TEM) of the as-prepared PbS Nanoparticles

Nanoparticles

Further investigations into the morphology of the as-prepared PbS nanoparticles were examined using TEM.

TEMs are capable of imaging at a significantly higher resolution than light microscopes, owing to the small de Broglie wavelength of electrons. The higher alkyl xanthates were selected for TEM analyses based on their increased polymeric behaviour (Barreca *et al.*, 2005).

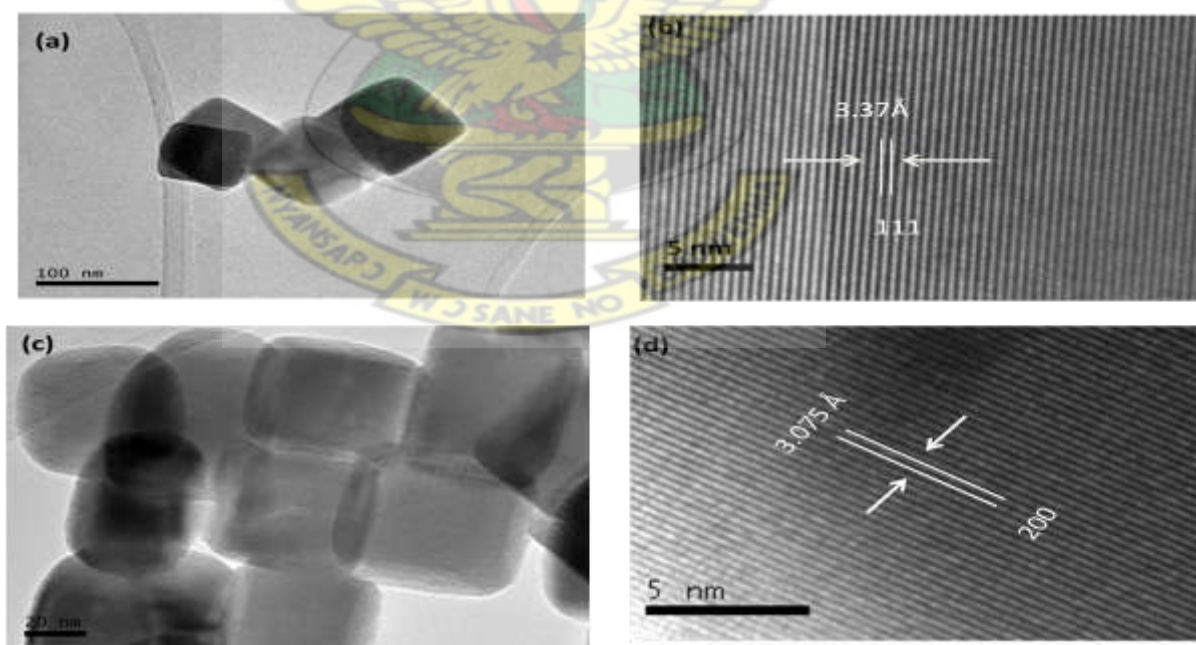
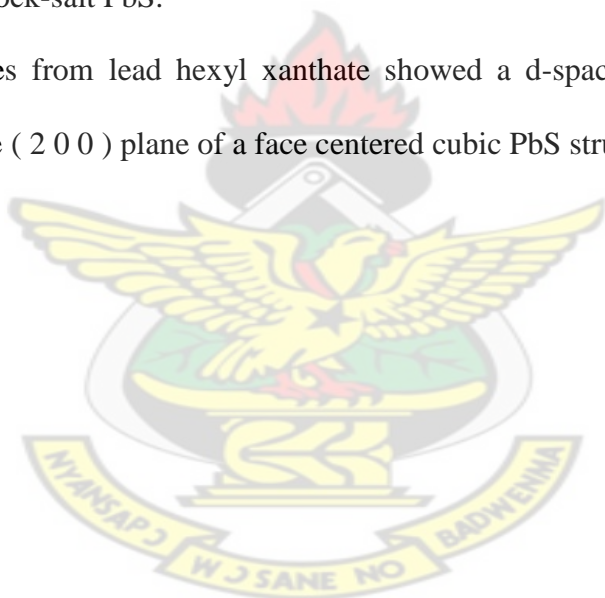


Figure 4.32: TEM images of PbS obtained from (a) lead octyl xanthate (b) HR-TEM of (a), (c) lead hexyl xanthate and (d) HR-TEM of (c)

TEM images of the PbS obtained from the decomposition of octyl and hexyl lead xanthate at 175°C and 30 minutes reaction time as shown in Figures 4.32a and 4.32c above respectively. The micrographs showed uniform PbS nanocubes confirming the cubic patterns from the XRD. However, the difference in the scales resulted from selecting the cluster to be analyzed. The smaller particle sizes observed in the XRD as opposed in the TEM resulted from the XRD giving the average of the different particle sizes.

HRTEM of PbS from lead octyl xanthate shows well-resolved lattice fringes with an inter-planar distance (spacing) of 3.37 Å, which matches with the spacing between the (1 1 1) plane of rock-salt PbS.

PbS nanoparticles from lead hexyl xanthate showed a d-spacing of 3.075 Å which correspond to the (2 0 0) plane of a face centered cubic PbS structure.



CHAPTER FIVE

CONCLUSIONS AND RECOMMENDATIONS

5.1 Conclusions

A series of alkyl lead xanthates have been synthesized (R = ethyl, butyl, hexyl and octyl) and characterised. In view of their potential application as single-source precursors for PbS, their structure–property relationships were analyzed by means of a multi-technique approach, both in the solid state using FT-IR and in solution using NMR. In addition, thermogravimetric analysis (TGA) and mass spectrometry (MS) were used to investigate the thermal behaviour and fragmentation pattern of the above compounds. The thermal analysis indicated the possibility of obtaining PbS by thermal decomposition of lead xanthate precursors in an inert atmosphere. The influence of the alkyl group on the sizes was also observed. The major findings were:

- (i) All the as-prepared nanoparticles indicated the growth of cubic PbS regardless of the starting lead xanthate precursor, temperature and time of decomposition based on the XRD.
- (ii) The crystal structure of lead hexyl xanthate has been determined
- (iii) Also, a solventless method for the syntheses of nanoparticles have been demonstrated as an efficient method since the EDX confirmed the presence of only Pb and S atoms after the decomposition of the lead xanthate precursors.

5.2 Recommendations

There exists a continuing interest in the use of the solventless method for the synthesis of M-S nanoparticles from single source precursors. Further work on other metals using this method should be investigated.

Further investigations into the use of these nanoparticles in hybrid solar cell should also be exploited.



REFERENCES

- Abe, K., Hanada, T., Yoshida, Y., Tanigaki, N., Takiguchi, H., Nagasawa, H., Nakamoto, M., Yamaguchi, T. and Yase, K. (1998). Two-dimensional array of silver nanoparticles. *Thin Solid Films*, 327(329), 524–527.
- Acharya, S., Patla, I., Kost, J., Efrima, S. and Golan, Y. (2006). Switchable assembly of ultra narrow CdS nanowires and nanorods. *Journal of the American Chemical Society*, 128(29), 9294–9295.
- Afzaal, M., and O'Brien, P. (2006). Recent developments in II-VI and III-VI semiconductors and their applications in solar cells. *Journal of Materials Chemistry*, 16(17), 1597-1602.
- Akhtar, J., Afzaal, M., Vincent, M. A., Burton, N. A., Hillier, I. H. and O'Brien, P. (2011). Low temperature CVD growth of PbS films on plastic substrates. *Chemical Communications (Cambridge, England)*, 47(7), 1991–1993.
- Akhtar, J., Afzaal, M., Vincent, M. A., Burton, N. A., Raftery, J., Hillier, I. H. and O'Brien, P. (2011). Understanding the decomposition pathways of mixed sulfur/selenium lead phosphinato complexes explaining the formation of lead selenide. *The Journal of Physical Chemistry C*, 115(34), 16904–16909.
- Akhtar, J., Malik, M. A., O'Brien, P. and Helliwell, M. (2010). Controlled synthesis of PbS nanoparticles and the deposition of thin films by Aerosol-Assisted Chemical Vapour Deposition (AACVD). *Journal of Materials Chemistry*, 20(29), 6116-6124.
- Alam, N., Hill, M. S., Kociok-ko, G., Zeller, M., Mazhar, M. and Molloy, K. C. (2008). Pyridine adducts of nickel (II) xanthates as single-source precursors for the aerosol-assisted chemical vapour deposition of nickel sulfide. *Chemistry of Materials*, 20, 6157–6162.

- Arici, E. and Serdar, N. (2004). Hybrid solar cells. *Encyclopedia of Nanoscience and Nanotechnology*, 3, 929–944.
- Ayranci, E. and Conway, B. E. (2001). Adsorption and electrosorption of ethyl xanthate and thiocyanate anions at high-area carbon-cloth electrodes studied by in situ UV spectroscopy: Development of procedures for wastewater purification. *Analytical Chemistry*, 73(6), 1181–1189.
- Bailey, J. H. E., Drake, J. E., Khasrou, L. N. and Yang, J. (1995). Synthesis and spectroscopic characterization. *Inorganic Chemistry*, 2(12), 124–133.
- Bakueva, L., Konstantatos, G., Levina, L., Musikhin, S. and Sargent, E. H. (2004). Luminescence from processible quantum dot-polymer light emitters 1100–1600 nm: Tailoring spectral width and shape. *Applied Physics Letters*, 84(18), 3459–3461.
- Barote, M. A., Yadav, A. A., Chavan, T. V and Masumdar, E. U. (2011). Characterization and photoelectrochemical properties of chemical bath deposited n-PbS thin films. *Digest Journal of Nanomaterials and Biostructures*, 6(3), 979–990.
- Barreca, D., Gasparotto, A., Maragno, C., Seraglia, R., Tondello, E., Venzo, A. and Krishnan, V. (2005). Cadmium O-alkylxanthates as CVD precursors of CdS: a chemical characterization. *Applied Organometallic Chemistry*, 19(1), 59–67.
- Bisquert, J. (2010). Breakthroughs in the development of semiconductor-sensitized solar cells. *The Journal of Physical Chemistry Letters*, 1, 3046–3052.
- Boadi, N. O., Malik, M. A., O'Brien, P. and Awudza, J. A. M. (2012). Single source molecular precursor routes to lead chalcogenides. *Dalton Transactions (Cambridge, England:2003)* doi:10.1039/c2dt30849e.

- Boivin, J., Jrad, R. and Nguyen, V. T. (2003). On the reduction of S-alkylthionocarbonates (Xanthates) with phosphorus compounds. *Optical Letters*, 5(10), 1645–1648.
- Boxberg, F. and Tulkki, J. (2008). Quantum dots: Phenomenology, photonic and electronic properties. *Modeling and Technology*, 107–118.
- Buckley, A. N., Parks, T. J., Vassallo, A. M. and Woods, R. (1997). Verification by surface-enhanced raman spectroscopy of the integrity of xanthate chemisorbed on silver. *International Journal of Mineral Processing*, 51(97), 303–313.
- Buckley, A. N., Hope, G. A. and Woods, R. (2003). Metals from sulfide minerals: The role of adsorption of organic reagents in processing technologies. *Solid-Liquid Interfaces*, 85, 61–98.
- Çapan, R., Brzozowski, L., Barkhouse, D. A. R., Wang, X., Debnath, R., Wolowiec, R. and Palmiano, E., (2010). Quantum dot photovoltaics in the extreme quantum confinement regime: The surface-chemical origins of exceptional air- and light-stability. *Ascnano*, 4(2), 869–878.
- Casas, S., Castireiras, A., Haiduc, I., Agusth, S. and Vazquez-lpez, E. M. (1994). Crystal and molecular structure of spirobicyclic bis(tetraphenyldithioimidodiphosphinato) lead (II), [Pb{(sppb and N)},], containing a new inorganic (carbon-free) PbS_2P_{2n} chelate ring and Pb (+ C and) interactions. *Polyhedron*, 13(20), 2873–2879.
- Cases, J. M., Kongolo, M., Donato, P. D. E., Michot, L. and Erre, R. (1990). Interaction of finely ground galena and potassium amylxanthate in flotation: Influence of alkaline grinding. *International Journal of Mineral Processing*, 28, 313–337.
- Cavicchioli, M., Varanda, L. C., Massabni, A. C. and Melnikov, P. (2005). Silver nanoparticles synthesized by thermal reduction of a silver(I)–aspartame complex in inert atmosphere. *Materials Letters*, 59(28), 3585–3589.

- Chauhan, H. P. S., Bakshi, A. and Bhatiya, S. (2011). Spectrochimica Acta Part A: Molecular and biomolecular spectroscopy synthesis, spectroscopic characterization and antibacterial activity of antimony (III) bis (dialkyldithiocarbamate) alkyldithiocarbonates. *Spectrochimica Acta Part A: Molecular and Biomolecular Spectroscopy*, 81(1), 417–423.
- Chen, J., Chen, L. and Wu, L. M. (2007). The solventless syntheses of unique PbS nanowires of X-shaped cross sections and the cooperative effects of ethylenediamine and a second salt. *Inorganic Chemistry*, 46(19), 8038–8043.
- Chen, J., Wu, L. M. and Chen, L. (2007). Syntheses and characterizations of bismuth nanofilms and nanorhombuses by the structure-controlling solventless method. *Inorganic Chemistry*, 46(2), 586–591.
- Chen, L., Xing, H., Shen, Y., Bai, J. and Jiang, G. (2009). Solid-state thermolysis of $[\text{MnO}]_{12}$ containing molecular clusters into novel MnO nano- and microparticles. *Journal of Solid State Chemistry*, 182(6), 1387–1395.
- Chen, S. and Liu, W. (2006). Oleic acid capped PbS nanoparticles: Synthesis, characterization and tribological properties. *Materials Chemistry and Physics*, 98(1), 183–189.
- Chen, Y. B., Chen, L. and Wu, L. M. (2005). Structure-controlled solventless thermolytic synthesis of uniform silver nanodisks. *Inorganic Chemistry*, 44(26), 9817–9822.
- Chi, L., Chen, H., Hung, W., Hsu, Y., Feng, P. and Chou, S. (2013). Donor-acceptor small molecule with coplanar and rigid p-bridge for efficient organic solar cells. *Solar Energy Materials and Solar Cells*, 109, 33–39.
- Clark, J. M., Kociok-Köhn, G., Harnett, N. J., Hill, M. S., Hill, R., Molloy, K. C. and Saponia, H. (2011). Formation of PbS materials from lead xanthate precursors. *Dalton Transactions (Cambridge, England: 2003)*, 40(26), 6893–6900.

- Coates, J. and Ed, R. A. M. (2000). Interpretation of infrared spectra, a practical approach interpretation of infrared spectra, *A Practical Approach*, 10815–10837.
- Colin, L. and Allan, H. (1978). Synthesis and structure of tetraethylammonium (dithiocarbonato-S,S¹) -bis (ethylxanthato) cabaltate(III). *Australian Journal of Chemistry*, 31, 291-296.
- Cooper, A. (2000). Differential scanning microcalorimetry, 1–35.
- Davidovich, R. L., Stavila, V. and Whitmire, K. H. (2010). Stereochemistry of lead(II) complexes containing sulfur and selenium donor atom ligands. *Coordination Chemistry Reviews*, 254(17-18), 2193–2226.
- Dowland, S., Lutz, T., Ward, A., King, S. P., Sudlow, A., Hill, M. S. and Molloy, K. C. (2011). Direct growth of metal sulfide nanoparticle networks in solid-state polymer films for hybrid inorganic-organic solar cells. *Advanced Materials (Deerfield Beach, Fla.)*, 23(24), 2739–2744.
- Drake, J. E., Drake, R. J., Khasrou, L. N. and Ratnani, R. (1996). Synthesis and spectroscopic characterization of halodimethyl (O-alkyl dithiocarbonato) tellurium (IV) compounds. Crystal structures of Me₂TeCl[S₂COEt] and Me₂TeI[S₂CO(i-Pr)]. *Inorganic Chemistry*, 1669(4), 2831–2840.
- Drake, J. E., Sarkar, A. B. and Wong, M. L. Y. (1991). O-methyl and O-ethyl dithiocarbonate (Xanthate) derivatives. *Inorganic Chemistry*, (15), 785–788.
- Duan, T., Lou, W., Wang, X. and Xue, Q. (2007). Size-controlled synthesis of orderly organized cube-shaped lead sulfide nanocrystals via a solvothermal single-source precursor method. *Physicochemical Engineering Aspects*, 310, 86–93.
- Evyapan, M., Çapan, R., Namlı, H., Turhan, O. and Stanciu, G. A. (2006). Formation of Langmuir – Blodgett thin film of a novel N-dodecylphthalimide. *Materials Letters*, 60, 2371–2374.

- Fan, D., Afzaal, M., Mallik, M. A., Nguyen, C. Q., O'Brien, P. and Thomas, J. (2007). Using coordination chemistry to develop new routes to semiconductor and other materials. *Coordination Chemistry Reviews*, 251(13-14), 1878–1888.
- Fenn, J. B., Mann, M., Meng, C. K. A. I., Wong, S. F. and Whitehouse, C. M. (1989). Electrospray ionization for mass spectrometry of large biomolecules. *Journal of Physical Chemistry*, 246(6), 64–70.
- Fredriksson, A. and Holmgren, A. (2008). An in situ ATR-FTIR investigation of adsorption and orientation of heptyl xanthate at the lead sulphide/aqueous solution interface. *Minerals Engineering*, 21(12-14), 1000–1004.
- Friebolin, W., Schilling, G., Zo, M. and Amtmann, E. (2004). Synthesis and structure-activity relationship of novel antitumoral platinum xanthate complexes. *Journal of Medicinal Chemistry*, 47, 2256–2263.
- Gardner, J. and Woods, R. (1977). Electrochemical investigation of contact angle and of flotation in the presence of alkylxanthates. II. Galena and pyrite surfaces. *Australian Journal of Chemistry*, 30(5), 981-991.
- Garje, S. S. and Jain, V. K. (2003). Chemistry of arsenic, antimony and bismuth compounds derived from xanthate, dithiocarbamate and phosphorus based ligands. *Coordination Chemistry Review*, 236, 35-56.
- Gunes, S., Fritz, K. P., Neugebauer, H., Serdar, N., Kumar, S. and Scholes, G. D. (2007). Hybrid solar cells using PbS nanoparticles. *Solar Energy Materials and Solar cells*, 91, 420–423.
- Gubin, S. P., Kataeva, N. A. and Khomutov, G. B. (2005). Promising avenues of research in nanoscience: chemistry of semiconductor nanoparticles. *Russian Chemical Bulletin*, 54(4), 827–852.

- Guchhait, A., Rath, A. K. and Pal, A. J. (2010). Near-IR activity of hybrid solar cells: Enhancement of efficiency by dissociating excitons generated in PbS nanoparticles. *Applied Physical Letters*, 96, 2–4.
- Güler, T. (2005). Dithiophosphinate – pyrite interaction: Voltammetry and DRIFT spectroscopy investigations at oxidizing potentials. *Journal of Colloid and Interface Science*, 288, 2005-2012.
- Hagihara, H., Watanabe, Y. and Yamashita, S. (1968). The crystal structure of lead n-butylxanthate . I . Disordered structure. *Acta Crystallographica*, 24, 960-968.
- Hagihara, H. and Yamashita, S. (1966). The crystal structure of lead ethylxanthate. *Acta Crystallographica*, 21, 350–358.
- Hamilton, I. C. and Melbourne, P. (1986). Surfactant property of alkyl xanthates. *International Journal of Mineral Processing*, 17, 113–120 .
- Han, Q., Chen, J., Yang, X., Lu, L., and Wang, X. (2007). Preparation of uniform Bi₂S₃ nanorods using xanthate complexes of bismuth (III), *Journal of Physical Chemistry C* 111, 14072–14077.
- Han, Q., Sun, S., Sun, D., Zhu, J. and Wang, X. (2011). Room-temperature synthesis from molecular precursors and photocatalytic activities of ultralong Sb₂S₃ nanowires. *RSC Advances*, 1, 1364–1369.
- Han, W., Yi, L., Zhao, N., Tang, A., Gao, M. and Tang, Z. (2008). Synthesis and shape-tailoring of copper sulfide/indium sulfide-based nanocrystals. *Journal of the American Chemical Society*, 130, 13152–13161.
- Homagai, P. L., Ghimire, K. N. and Inoue, K. (2010). Preparation and characterization of charred xanthated sugarcane bagasse for the separation of heavy metals from aqueous solutions. *Separation Science and Technology*, 46(2), 330–339.

- Hope, G. ., Watling, K. and Woods, R. (2001). A SERS spectroelectrochemical investigation of the interaction of isopropyl, isobutyl and isoamyl xanthates with silver. *Colloids and Surfaces A: Physicochemical and Engineering Aspects*, 178(1-3), 157–166.
- Ip, A. H., Thon, S. M., Hoogland, S., Voznyy, O., Zhitomirsky, D., Debnath, R. and Levina, L. (2012). Hybrid passivated colloidal quantum dot solids. *Nature Nanotechnology*, 127(10), 1–6.
- Jain, V. K. (2006). Synthesis and characterization of single-source molecular precursors for the preparation of metal chalcogenides. *Journal of Chemical Science*, 118(6), 547–552.
- Jang, S. Y., Song, Y. M., Kim, H. S., Cho, Y. J., Seo, Y. S., Jung, G. B. and Lee, C. (2010). Three synthetic routes to single-crystalline PbS nanowires with with controlled growth direction and their electrical transport properties. *American Chemical Society*, 4(4), 2391–2401.
- Jose, D. and Jagirdar, B. R. (2010). Synthesis and characterization of Pd(0), PdS, and Pd@PdO core–shell nanoparticles by solventless thermolysis of a Pd–thiolate cluster. *Journal of Solid State Chemistry*, 183(9), 2059–2067.
- Jung, Y. K., Kim, J. I. and Lee, J. K. (2010). Thermal decomposition mechanism of single-molecule precursors forming metal sulfide nanoparticles. *Journal of the American Chemical Society*, 132(1), 178–184.
- Kamat, P. V. (2008). Quantum dot solar cells: Semiconductor nanocrystals as light harvesters. *The Journal of Physical Chemistry C*, 112(48), 18737–18753.
- Kang, I. and Wise, F. W. (1997). Electronic structure and optical properties of PbS and PbSe quantum dots. *Journal of the Optical Society of America B*, 14(7), 1632-1647.

- Kayatürk, N., Usanmaz, A. and Önal, A. M. (2007). Polymerization by bis (ethylxanthato)-nickel(II) as an initiator. I. Polymerization of styrene oxide. *Journal of Macromolecular Science, Part A: Pure and Applied Chemistry*, 36(1), 115–135.
- Kim, H. and Lee, K. (1999). Application of insoluble cellulose xanthate for the removal of heavy metals from aqueous solution. *Korean Journal of Chemical Engineering*, 16(3), 298–302.
- Klem, E. J. D. (2008). Infrared sensitive solution-processed quantum dot photovoltaics in a nanoporous architecture. 1-151.
- Koh, Y. W., Lai, C. S., Du, A. Y., Tiekink, E. R. T. and Loh, K. P. (2003). Growth of bismuth sulfide nanowire using bismuth trisxanthate single source precursors. *Chemistry of Materials*, 14(16), 4544–4554.
- Larsen, T. H., Sigman, M., Ghezelbash, A., Doty, R. C. and Korgel, B. A. (2003). Solventless synthesis of copper sulfide nanorods by thermolysis of a single source thiolate-derived precursor. *Journal of the American Chemical Society*, 125(19), 5638–5639.
- Lazell, M. and O'Brien, P. (1999). A novel single source precursor route to self capping CdS quantum dots. *Coordination Chemistry Reviews*, 254, 2041–2042.
- Lee, S.-M., Jun, Y., Cho, S.-N. and Cheon, J. (2002). Single-crystalline star-shaped nanocrystals and their evolution: Programming the geometry of nano-building blocks. *Journal of the American Chemical Society*, 124(38), 11244–11245.
- Leppinen, J. O. and Rastas, J. K. (1986). The interaction between ethyl xanthate ion and lead sulfide surface. *Colloids and Surfaces*, 20(3), 221–237.

- Leventis, H. C., Mahony, F. O., Akhtar, J., Afzaal, M., O'Brien, P. and Haque, S. A. (2010). Transient optical studies of interfacial charge transfer at nanostructured metal oxide/ PbS quantum dot/organic hole conductor heterojunctions. *Journal of the American Chemical Society*, 11, 2743–2750.
- Lewis, A. E. (2010). Hydrometallurgy review of metal sulphide precipitation. *Hydrometallurgy*, 104(2), 222–234.
- Li, D., Liang, C., Liu, Y. and Qian, S. (2007). Femtosecond nonlinear optical properties of PbS nanoparticles. *Journal of Luminescence*, 123, 549–551.
- Liang, S., Guo, X., Feng, N. and Tian, Q. (2009). Application of orange peel xanthate for the adsorption of Pb^{2+} from aqueous solutions. *Journal of Hazardous Materials*, 170(1), 425–429.
- Liu, Q., Ni, Y., Yin, G., Hong, J. and Xu, Z. (2005). High yield synthesis of PbS nanocubes using one-step solid-state reaction in the presence of an anionic surfactant. *Materials Chemistry and Physics*, 89(2-3), 379–382.
- Lozano, R., Roman, J., Jesus, F. D. and Alarcon, E. (1991). Tungsten (V) dimeric complexes with ethyl xanthate. *Polyhedron*, 10(19), 2235–2239.
- Malik, M. A., Afzaal, M. and O'Brien, P. (2010). Precursor chemistry for main group elements in semiconducting materials. *Chemical Reviews*, 110(7), 4417–4446.
- Marabini, A. M., Ciriachi, M., Plescia, P. and Barbaro, M. (2007). Chelating reagents for flotation. *Minerals Engineering*, 20(10), 1014–1025.
- Maspero, A., Kani, I., Mohamed, A. A., Omary, M. A., Staples, R. J., Fackler, J. P. and Chimiche, S. (2003). Syntheses and structures of dinuclear gold (I) dithiophosphonate complexes and the reaction of the dithiophosphonate complexes with phosphines: diverse coordination types. *Inorganic Chemistry*, 42(17), 5311-5319.

- Matthew, E. J. (1990). Studies on some metal complexes of dithio ligands. *Thesis submitted to the Cochin University of Science and Technology*. 1-171.
- Mcdonald, S. A., Konstantatos, G., Zhang, S., Cyr, P. W., Klem, E. J. D., Levina, L. and Sargent, E. H. (2005). Solution-processed PbS quantum dot infrared photodetectors and photovoltaics. *Nature Materials*, *4*, 138-144.
- Mege, S., Osocs, P. and Drake, E. (1993). Synthesis and characterization of dithiocarbonate derivatives of various methyl-, t-butyl- and n-butylgermanes. Crystal structures of MeGe [S₂COEt]. *Inorganica Chimica Acta*, *211*, 37-46.
- Mohamed, A. A., Kani, I., Ramirez, A. O. and Fackler, J. P. (2004). Synthesis, characterization, and luminescent properties of dinuclear gold (I) xanthate complexes: X-ray structure of [Au₂(n Bu-xanthate)₂], *Inorganic Chemistry* *43*(13), 3833-3839.
- Nair, P. S., Radhakrishnan, T., Revaprasadu, N., Kolawole, G. and O'Brien, P. (2002). Cadmium ethylxanthate: A novel single-source precursor for the preparation of CdS nanoparticles. *Journal of Materials Chemistry*, *12*(9), 2722-2725.
- Neeleshwar, S., Chen, C. L., Tsai, C. B., and Chen, Y. Y. (2005). Size-dependent properties of CdSe quantum dots. *Physical Review B*, *71*, 6-9.
- NICNAS. (2000). Chemical assesment of sodium ethyl xanthate. 1-85.
- Niv, A., Gharghi, M., Gladden, C., Miller, O. D. and Zhang, X. (2012). Near-field electromagnetic theory for thin solar cells. *Physical Review Letters*, *109*, 138701-138705.
- Noone, K. M., Strein, E., Anderson, N. C., Wu, P., Jenekhe, S. A. and Ginger, D. S. (2010). Solution-processed quantum dots. *Nano Letters*, *10*, 2635-2639.
- Nyamekye, G. A. (1991). Classification of flotation reagents. *Innovations in Mineral Processing*, *1*, 336-342.

- Nyamen, L. D., Rajasekhar, V. S., Nejo, A. A., Ndifon, P., Warner, J. H. and Revaprasadu, N. (2012). Synthesis of anisotropic PbS nanoparticles using heterocyclic Q1 dithiocarbamate complexes. *Dalton Transactions*, 1, 1-6.
- O'Brien, P., Malik, M. A. and Revaprasadu, N. (2005). Phosphorus, sulfur, and silicon and the related elements precursor routes to semiconductor quantum dots. *Taylor and Francis Int*, 180(3-4), 37-41.
- Ong, P. and Levitsky, I. A. (2010). Organic (IV, III-V) semiconductor hybrid solar cells. *Energies*, 313-334.
- Pandey, O. P. (1988). Chemistry and mechanism of thermal degradation reactions of zirconium (IV) alkyl xanthate complexes. *Thermochromtica Acta*, 127, 193-199.
- Patla, I., Acharya, S., Zeiri, L., Israelachvili, J., Efrima, S. and Golan, Y. (2007). Synthesis, two-dimensional assembly, and surface pressure-induced coalescence of ultranarrow PbS nanowires. *Nano Letters*, 7(6), 1459-1462.
- Perepichka, D. F., Perepichka, I. F., Meng, H., Wudl, F. and Perepichka, P. D. F. (2004). Light emitting polymers. 1, 1-219.
- Perex, J., Bax, L. and Escolano, C. (2005). Roadmap report on nanoparticles 1-57.
- Pradhan, N., Katz, B. and Efrima, S. (2003). Synthesis of high-quality metal sulfide nanoparticles from alkyl xanthate single precursors in alkylamine solvents. *The Journal of Physical Chemistry B*, 107(50), 13843-13854.
- Rajalingam, P. and Radhakrishnan, G. (1991). Potassium-n-butyl xanthate as a new antioxidant for natural rubber. *Polymer-plastic Technology Engineering*, 30(4), 405-411.

- Rao, C. N. R., Kulkarni, G. U., Varun, V., Gautam, U. K. and Ghosh, M. (2005). Use of the liquid – liquid interface for generating ultrathin nanocrystalline films of metals, chalcogenides, and oxides. *Journal of Colloid and Interface Science*, 289, 305–318.
- Rao, C. N. R. and Kalyanikutty, K. P. (2008). The liquid – liquid interface as a medium to generate nanocrystalline films of inorganic. *Accounts of Chemical Research*, 41(4), 489–499.
- Rez, G. E. (1996). Bis (tetraphenylimidothioxodiphosphate-S,O) lead(II)“benzene, [Pb{SO(PPh₂)~N}]₂”C₆H₆: A new asymmetric chelate compound exhibiting dimeric association through intermolecular Pb-S interactions. *Polyhedron*, 15(5), 2–7.
- Ritch, J. S., Chivers, T., Ahmad, K., Afzaal, M. and O’Brien, P. (2010). Synthesis, structures, and multinuclear NMR spectra of tin(II) and lead(II) complexes of tellurium-containing imidodiphosphate ligands: preparation of two morphologies of phase-pure PbTe from a single-source precursor. *Inorganic Chemistry*, 49(3), 1198–2005.
- Saboury, A. A., Alijanianzadeh, M. and Mansoori-Torshizi, H. (2007). The role of alkyl chain length in the inhibitory effect n-alkyl xanthates on mushroom tyrosinase activities. *Acta Biochimica Polonica*, 54(1), 183–191.
- Sawant, P., Kovalev, E., Klug, J. T. and Efrima, S. (2001). Alkyl xanthates: New capping agents for metal colloids. Capping of platinum nanoparticles. *Langmuir*, 17(13), 2913–2917.
- Scendo, M. (2005). Potassium ethyl xanthate as corrosion inhibitor for copper in acidic chloride solutions. *Corrosion Science*, 47(7), 1738–1749.
- Sceney, C. G., Hill, J. O. and R, M. J. (1973). Thermal studies on palladium alkyl xanthates. *Thermochimica Acta*, 6, 111–117.

- Schaller, R. D., Petruska, M. A. and Klimov, V. I. (2003). Tunable near-infrared optical gain and amplified spontaneous emission using PbSe nanocrystals. *The Journal of Physical Chemistry B*, 107(50), 13765–13768.
- Shankaranarayana, M. L. and Patel, C. C. (1961). Infrared spectra and the structures of xanthates and dixanthogens. *Canadian Journal of Chemistry*, 39, 1633–1637.
- Sharma, A. K. (1986). Thermal behaviour of metal-dithiocarbamates. *Thermochimica Acta*, 104, 339–372.
- Sheldrick, G. M. (2008). A short history of SHELX. *Acta crystallographica. Section A, Foundations of Crystallography*, 64(1), 112–222.
- Shi, W., Hughes, R. W., Denholme, S. J. and Gregory, D. H. (2010). Synthesis design strategies to anisotropic chalcogenide nanostructures. *Crystal Engineering Communications*, 12(3), 641-661.
- Sigman, M. B. and Korgel, B. A. (2005). Solventless synthesis of Bi₂S₃ (Bismuthinite) nanorods, nanowires, and nanofabric. *Nano Letters*, 3(7), 1655–1660.
- Singhal, A., Dutta, D. P., Tyagi, A. K., Mobin, S. M., Mathur, P. and Lieberwirth, I. (2007). Palladium(II)/allylpalladium(II) complexes with xanthate ligands: Single-source precursors for the generation of palladium sulfide nanocrystals. *Journal of Organometallic Chemistry*, 692(23), 5285–5294.
- Siui, P., Buckley, A. N. and Woods, R. (1997). Chemisorption the thermodynamically favoured process in the interaction of thiol collectors with sulphide minerals. *International Journal of Mineral Processing*, 51, 15–26.
- Soppimath, K. S., Aminabhavi, T. M., Kulkarni, A. R. and Rudzinski, W. E. (2001). Biodegradable polymeric nanoparticles as drug delivery devices. *Journal of the Controlled Release Society*, 70(1-2), 1–20.

- Stansfield, G. L., Vanitha, P. V, Johnston, H. M., Fan, D., Alqahtani, H., Hague, L. and Grell, M. (2010). Growth of nanocrystals and thin films at the water – oil interface growth of nanocrystals and thin films at the water – oil interface. *Philosophical Transactions*, 368,4313-4330.
- Sun, S., Han, Q., Wu, X., Zhu, J. and Wang, X. (2011). The facile synthesis of PbS cubes and Bi₂S₃ nanoflowers from molecular precursors at room temperature. *Materials Letters*, 65(21-22), 3344–3347.
- Sun, Y., Han, Q., Lu, J., Yang, X., Lu, L. and Wang, X. (2008). Preparation of uniform Bi₂S₃ nanoribbons at a low temperature. *Materials Letters*, 62(21-22), 3730–3732.
- Sutherland, D. (2010). Fabrication Methods. 1–21.
- Sydney, W. (2005). The ultra - trace level analysis of xanthates by high performance liquid chromatography. 1-25.
- Thammakan, N. and Somsook, E. (2006). Synthesis and thermal decomposition of cadmium dithiocarbamate complexes. *Materials Letters*, 60(9-10), 1161–1165.
- Thomas, L. C. (2000). Interpreting unexpected events and transitions in DSC results. *Thermal Analysis and Rheology*, 39, 1–11.
- Tip, T. A. (2000). Interpreting DSC curves. *Article*, 1–6.
- Trindade, B. T. and O'Brien, P. (1997). Lead (II) dithiocarbamate complexes as precursors for the LP-MOCVD of lead sulphide. *Chemical Communications*, 2, 75–77.
- Tzhayik, O., Sawant, P., Efrima, S., Kovalev, E. and Klug, J. T. (2002). Xanthate capping of silver, copper, and gold colloids. *Langmuir*, 18(8), 3364–3369.
- Wang, L. S. and Hong, R. Y. (2010). Synthesis, surface modification and characterisation of nanoparticles. *Advances in Nanocomposites*, 289-322.

- Woods, R., Basilio, C., Kim, D. and Yoon, R.-H. (1994a). Chemisorption of ethyl xanthate on copper electrodes. *International Journal of Mineral Processing*, 42(3-4), 215–223.
- Woods, R., Basilio, C. I., Kim, D. S. and Yoon, R. (1994b). Chemisorption of ethyl xanthate on silver-gold alloys. *International Journal of Mineral Processing*, 42(83), 215–223.
- Wu, P. W., Gao, L. and Guo, J. K. (2002). Formation of disk-like aggregates of cadmium sulfide nanocrystals at the oil – water interface. *Thin Solid Films*, 408, 132–135.
- Yang, N. and Aoki, K. (2005). Molecular numbers in core and shell: Structural dependence of reactivity of alkylcarboxylate-stabilized silver nanoparticles. *Journal of Physical Chemistry B*, 109(8), 23911–23917.
- Zhang, W. M., Sun, Z. X., Hao, W., Su, D. W. and Vaughan, D. J. (2011). Synthesis of size tuneable cadmium sulphide nanoparticles from a single source precursor using ammonia as the solvent. *Materials Research Bulletin*, 46(12), 2266–2270.
- Zhang, Y. C., Qiao, T., Hu, X. Y., Wang, G. Y. and Wu, X. (2005). Shape-controlled synthesis of PbS microcrystallites by mild solvothermal decomposition of a single-source molecular precursor. *Journal of Crystal Growth*, 277(1-4), 518–523.
- Zhao, N., Osedach, T. P., Chang, L., Geyer, S. M., Wanger, D., Binda, M. T. and Arango, A. C. (2010). Colloidal PbS quantum dot solar cells with high fill factor. *American Chemical Society*, 102(11), 1–9.
- Zhao, Y., Liao, X., Hong, J. and Zhu, J. (2004). Synthesis of lead sulfide nanocrystals via microwave and sonochemical methods. *Materials Chemistry and Physics*, 87, 149–153.

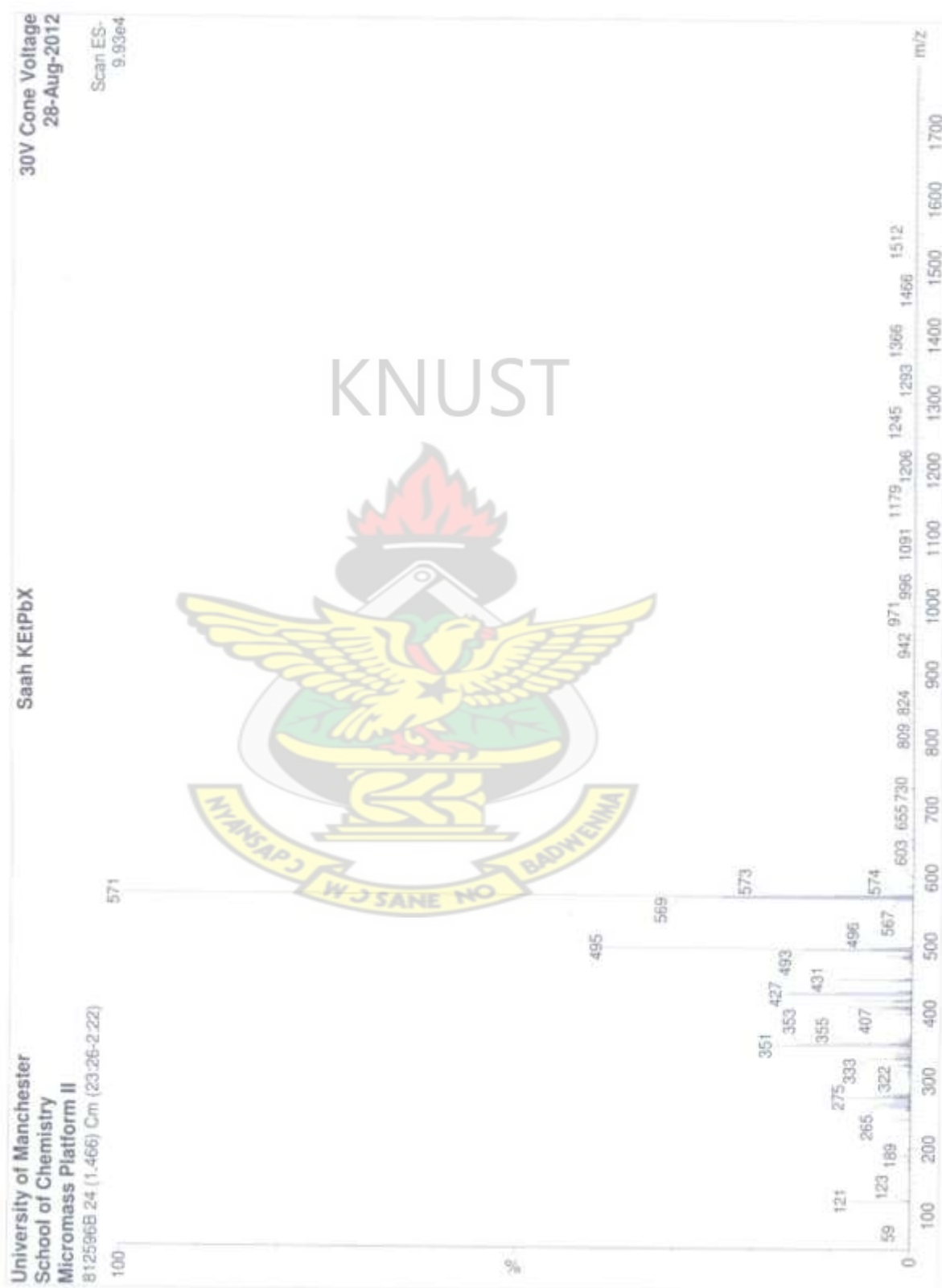
Zhou, Y., Itoh, H., Uemura, T., Naka, K. and Chujo, Y. (2002). Preparation, optical spectroscopy, and electrochemical studies of novel π -conjugated polymer-protected stable PbS colloidal nanoparticles in a nonaqueous solution. *Langmuir*, 20, 5287–5292.

Zhou, Y., Eck, M., Men, C., Rauscher, F., Niyamakom, P., Yilmaz, S. and Dumsch, I. (2011). Efficient polymer nanocrystal hybrid solar cells by improved nanocrystal composition. *Solar Energy Materials and Solar Cells*, 95, 3227–3232.

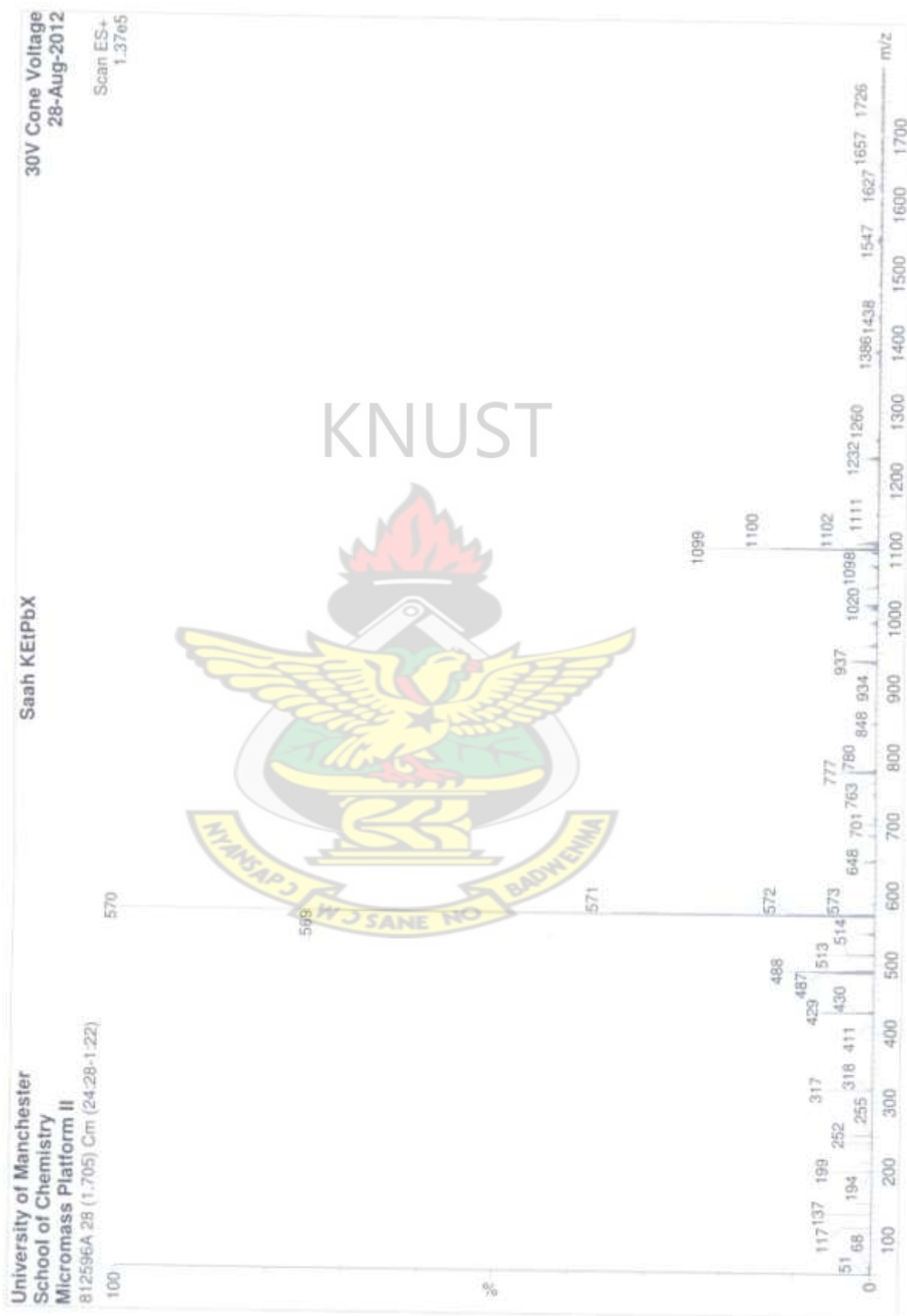


APPENDICES

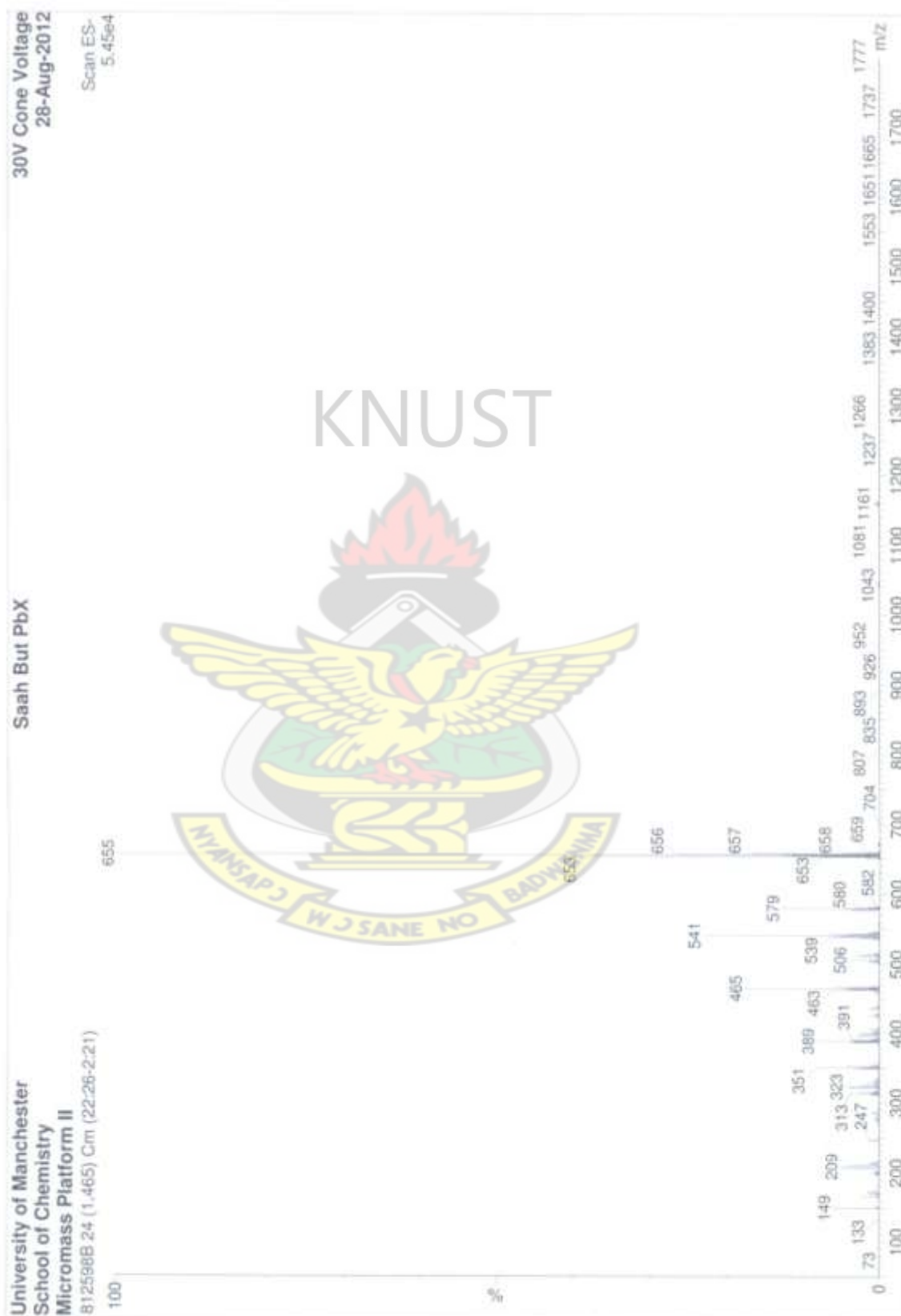
Appendix 1: ESI for lead ethyl xanthate



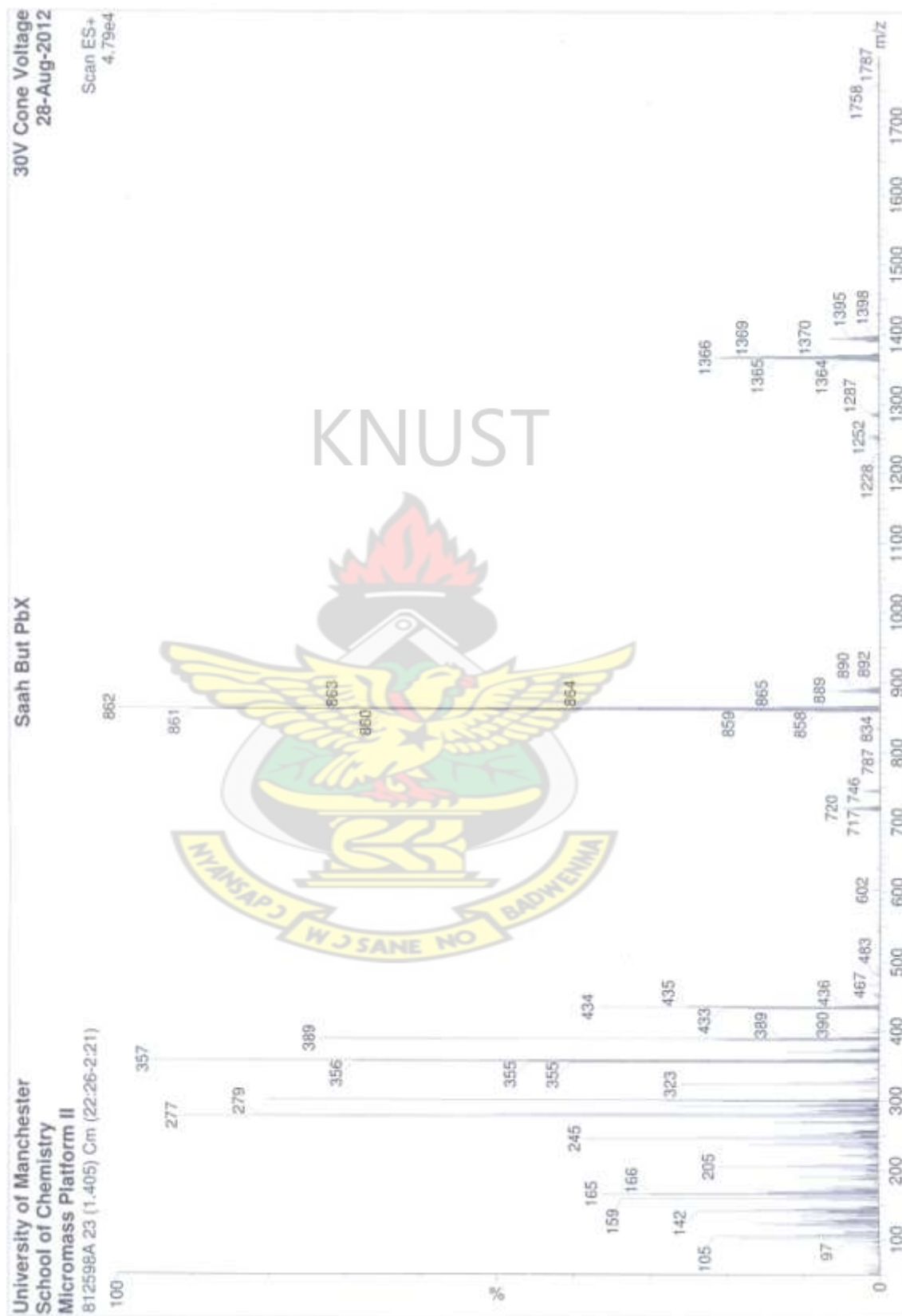
Appendix 2: ESI⁺ for lead ethyl xanthate



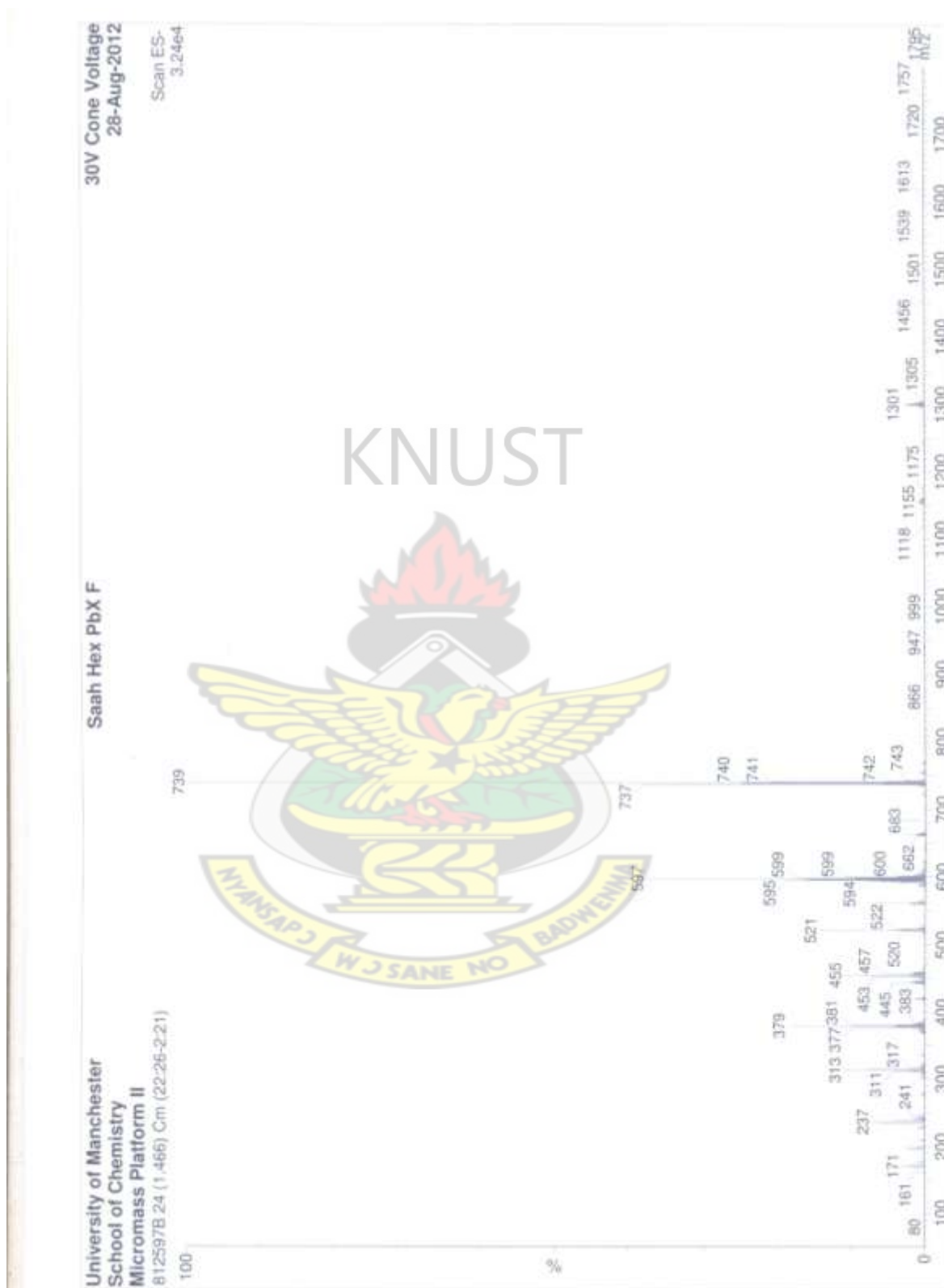
Appendix 3: ESI for lead butyl xanthate



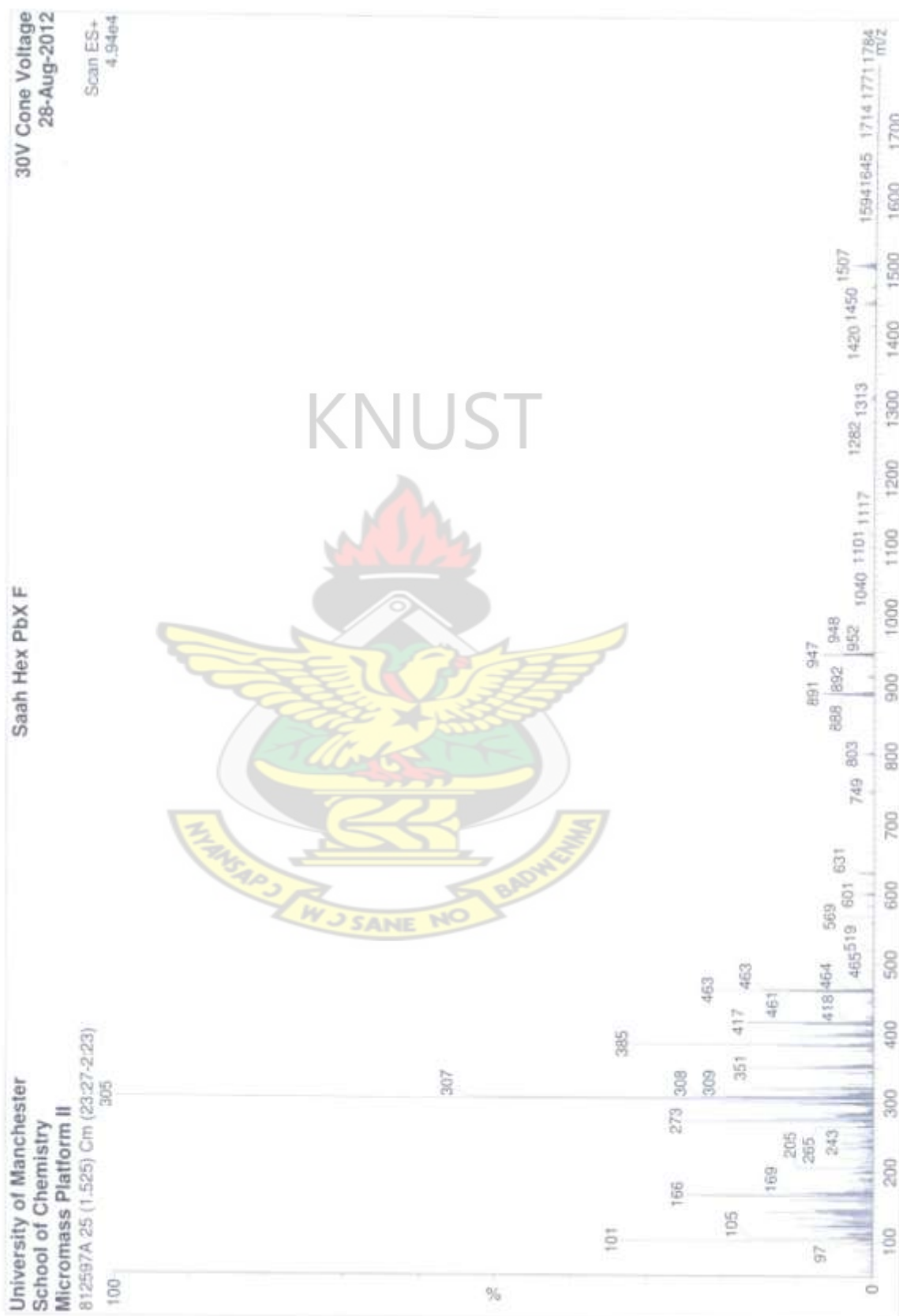
Appendix 4: ESI⁺ for lead butyl xanthate



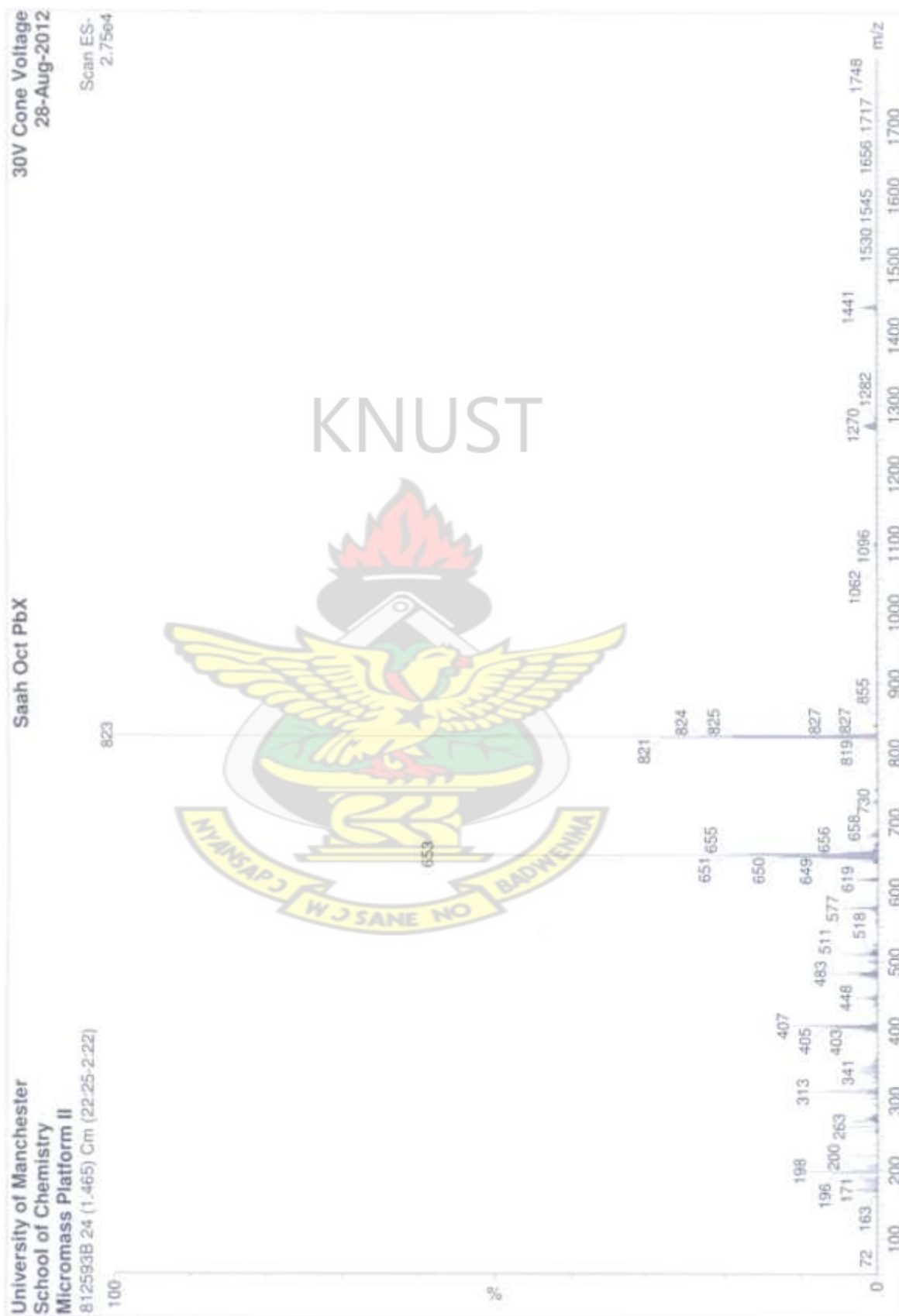
Appendix 5: ESI for lead hexyl xanthate



Appendix 6: ESI⁺ for lead hexyl xanthate



Appendix 7: ESI for lead octyl xanthate



Appendix 8: ESI⁺ for lead octyl xanthate

